AMERICAN UNIVERSITY OF BEIRUT

CONTROLLED DEFECTS IN METAL-ORGANIC
FRAMEWORKS FOR ENHANCED ADSORPTION AND
CATALYTIC PROPERTIES.

by
NISRINE ALI ASSAAD

A thesis
submitted in partial fulfillment of the requirements
for the degree of Master of Science
to the Department of Chemistry
of the Faculty of Arts and Sciences
at the American University of Beirut

Beirut, Lebanon
February 2020

AMERICAN UNIVERSITY OF BEIRUT

CONTROLLED DEFECTS IN METAL-ORGANIC FRAMEWORKS FOR ENHANCED ADSORPTION AND CATALYTIC PROPERTIES.

by
NISRINE ALI ASSAAD

Approved by:

Mohamad HMADEH

_____

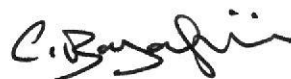Dr. Mohamad Hmadeh, Assistant Professor   Advisor
Chemistry

_____

Dr. Tarek Gaddar, Professor   Member of Committee
Chemistry

_____

Dr. Cassia Boyadjian, Assistant Professor   Member of Committee
Chemical engineering

Date of thesis defense: February 3, 2020

AMERICAN UNIVERSITY OF BEIRUT

THESIS, DISSERTATION, PROJECT RELEASE FORM

Student Name: __Assaad_____Nisrine_____Ali_____
                    Last   First   Middle

☒ Master's Thesis   ◯ Master's Project   ◯ Doctoral Dissertation

☐ I authorize the American University of Beirut to: (a) reproduce hard or electronic copies of my thesis, dissertation, or project; (b) include such copies in the archives and digital repositories of the University; and (c) make freely available such copies to third parties for research or educational purposes.

☒ I authorize the American University of Beirut, to: (a) reproduce hard or electronic copies of it; (b) include such copies in the archives and digital repositories of the University; and (c) make freely available such copies to third parties for research or educational purposes
after:
  One --- year from the date of submission of my thesis, dissertation, or project.
  Two --- years from the date of submission of my thesis, dissertation, or project.
  Three X years from the date of submission of my thesis, dissertation, or project.

_Nis_____   _heBruary, 3, 2020_____
Signature   Date

ACKNOWLEDGEMENTS

First and foremost, I would like to extend my utmost gratitude to my supervisor Dr. Mohamad Hmadeh , who have never failed to provide me with continuous support and guidance throughout my master.

I would like to express my gratefulness to the committee members Dr. Tarek Gaddar and Dr. Cassia Boyadjian .

I am also grateful to the faculty members of the Department of Chemistry especially Dr. Mazen Al Ghoul for their valuable help and support in this venture.

Mentioning the CRSL members is also an absolute necessity. I would especially like to thank Juan and Rania for their immense technical assistance.

Finally, I would like to thank my family and friends for all of the moral support over the years. I couldn't have done it without all of you.

AN ABSTRACT OF THE THESIS

Nisrine Ali Assaad   for Master of Science
                                   Major: Chemistry

Title: CONTROLLED DEFECTS IN METAL-ORGANIC FRAMEWORKS FOR
ENHANCED ADSORPTION AND CATALYTIC PROPERTIES.

Metal organic frameworks (MOFs) are a new class of crystalline, hybrid and porous materials formed by linking metal clusters and organic ligands via strong bonds. Due to their high porosity, large surface areas, and high versatility, MOFs are widely used in gas storage, adsorption, catalysis, drug delivery and sensing. Because of its strong chemical bonding and high coordination number, the Zr-based cluster, $Zr_6O_4(OH)_4(CO_2)_{12}$, found in UiO-66 $(Zr_6O_4(OH)_4(BDC)_6$; (BDC benzene dicarboxylate) is one of the most stable inorganic clusters and therefore is extensively employed as a platform for the construction of thermally and chemically stable MOFs. Recently, it has been shown that modulated synthesis routes by using monocarboxylate linkers such as formic acid, acetic acid and trifluoro-acetic acid promote the formation of defects within the MOF structure. These defects affect the textural features, the stability and the activity of UiO-66. In this work, we aim to control the defects in UiO-66 structure and to study their effects on Arsenic adsorption. To this end, different defected UiO-66 are synthesized using two distinct modulators acetic acid and trifluoro-acetic acid. The amount of these modulators is varied and the obtained MOFs are characterized using powder X-ray diffraction (PXRD), scanning electron microscopy (SEM), Brunauer, Emmett and Teller (BET) and thermogravimetric analysis (TGA). The obtained MOF structures are used as adsorbents for arsenic removal from water. In addition, porosity and high surface area make the MOFs interesting candidates as heterogenous catalysts with active nanoparticles in the framework. The pores in the framework can define the size of the nanoparticles and also function as molecular sieves and thereby introduce catalytic selectivity on the reactant, intermediate and products if the catalytic process is carried out in the pores. The goal of the second subject is to prepare new catalysts with palladium nanoparticles deposited on a series of functionalized UiO-66 structures and to study their effects on reduction of Nitrates/Nitrites in Drinking Water. Different MOF structures (e.g. UiO-66, UiO-66-NH_2 and UiO-66-$(COOH)_2$) are synthesized and characterized. Palladium was deposited onto the UiO-66 frameworks by using a reducing agent and Microwave assisted. The materials were characterized using powder X-ray diffraction (PXRD), scanning electron microscopy (SEM), Brunauer, Emmett and Teller (BET) and thermogravimetric analysis (TGA). The Pd-UiO-66 structures are then used as catalysts for reduction of Nitrates/Nitrites in Drinking Water.

CONTENTS

III. PALLADIUM-MOF COMPOSITES AS CATALYSTS FOR REDUCTION OF NITRATES/NITRITES IN DRINKING WATER……………………………………….69

ILLUSTRATIONS

TABLES

CHAPTER I

INTRODUCTION

A. Porous Materials

1. Introduction to porous materials

Porous solids have attracted considerable attention for many years when used for variety of applications, such as gas storage,[1] separation,[2] catalysis,[3] drug delivery,[4] and many other. The term porous solids refers to any kind of solid material containing pores which are distributed uniformly throughout the solid.[5] The length scale of the material is typically way much larger compared to the pore size. Another definition that is consistent with that proposed by the International Union of Pure and Applied Chemistry (IUPAC), defines a porous solid as one with cavities or channels which are deeper than the width.[6] The total volume in a porous solid consists of the volume of the solid phase and the volume of the pores. The volume fraction of the pore is commonly called porosity. The specific surface area is the extent of available surface per unit mass of material as determined by a given method. The external surface is defined as the area of external surface excluding any porosity, which can thus take into account any surface roughness. The pore size is generally specified as the pore width. The classification of pores according to size has been proposed by the IUPAC into three categories: pores of internal width less than 2 nm, between 2 and 50 nm, and greater than 50 nm that are classified as micropore, mesopore, and macropore, respectively.

The term porous solids encompass a wide range of materials including (but not limited to) zeolites, activated carbon, and porous coordination networks.

2. Coordination Polymer (CP)

The term coordination polymer (CP) is a general terminology that implies coordination compounds that constitutes one-, two-, or three-dimensional (1D, 2D, or 3D) polymeric structures via linking of the metal ions by bridging ligands.[7] CP can be purely inorganic in nature (e.g., palladium(II) chloride and Prussian blue) or extended structures that are comprised of polytopic organic linkers (bipyridyl, polycarboxylates, etc.). A related term to CP is Coordination Network (CN), which is a subset of CP that encompasses all the members excluding the 1D polymers.[7]

A subset of CN where the framework consists entirely of lightweight organic components and held together by strong covalent bonds is categorized as Covalent Organic Frameworks (COFs).[8] Metal-Organic Frameworks (MOFs), can be classed as a subset of CN where the structure consists of metal-based nodes (single ions or clusters) bridged by organic linkers.[7] These will be discussed in more detail in section 2.

More specifically, a sub-category of MOFs that adopt the topology of well-known zeolite structures is classed as zeolitic imidazolate frameworks (ZIFs). The terms porous coordination polymer (PCP) and porous coordination networks (PCN) are relatively new class of porous materials compared to zeolite and activated carbon. Those terminologies are used mostly to describe porous MOFs.[7] The relationship among CP, CN, COFs, MOFs, and ZIFs is schematized in Figure 1.1
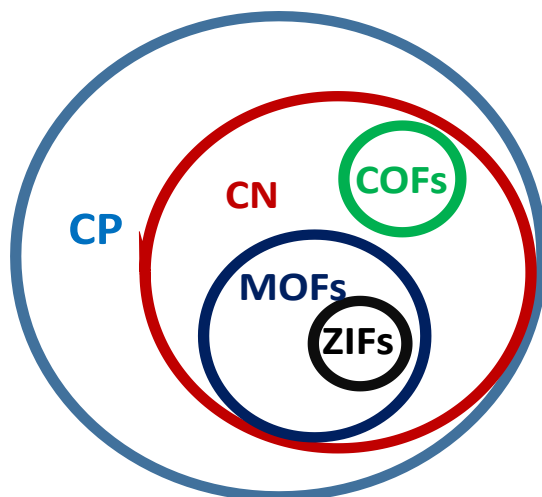
Figure 1.1. diagram representation of the relationship among Coordination Polymer (CP), Coordination Network (CN), Covalent Organic Frameworks (COFs), Metal-Organic Frameworks (MOFs), and Zeolitic Imidazolate Frameworks (ZIFs).[7]

B. Metal-Organic Frameworks (MOFs).

1. Introduction to MOFs

Metal-organic frameworks (MOFs) or porous coordination polymers (PCPs) are essentially crystalline inorganic-organic hybrid materials with coordinative bonding formed by associating metal centers or clusters with organic linker(s) bearing functional groups (Figure 1.2).[9]
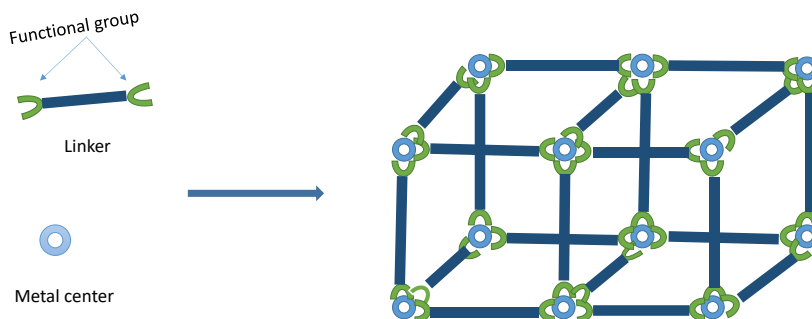
Figure 1.2. General diagram to build MOFs. Organic linkers with at least two functional groups coordinate with metal ions or cluster centers leading to three dimensional framework structures.

3

Discovery of MOFs is a consequence of an increasing interest on understanding and controlling the assembly of coordination polymers at the beginning of 1990s. In this context, Robson was the first to rationalize the formation of the extended networks by taking into account the coordination of metal ions and clusters and the geometry of the bridging ligands.[10] As a natural evolution of these efforts to rationalize and design the network formation in coordination polymers, Yaghi et al. showed the use of a ditopic ligand and introduced the term metal organic framework to the literature for the first time in 1995.[11]

Since the initial definition of metal-organic frameworks by Omar Yaghi in 1995,[12, 13] MOFs have emerged as promising porous materials featuring versatile and adjustable porous topologies, which result from the modular concept of combining metal centers and organic ligands for the construction of extended three-dimensional crystalline structures (Figure 1.2). A large variety of metal centers concerning di-, tri- or tetravalent cations can participate in the building of MOFs architectures. The functional groups of organic linkers connected to the metal centers are most frequently carboxylates, phosphonates, sulfonates and nitrogen derivatives such as triazolate, tetrazolate and imidazolate.[14, 15] Furthermore, the backbone network of the bridging molecules (rigid or flexible) can be functionalized with, for instance, halogeno, amino and sulfonic groups, depending on the desired applications.

Up to date, more than 20,000 MOF structures have been reported and many reviews describing these new porous materials have been reported[16] (Figure 1.3).
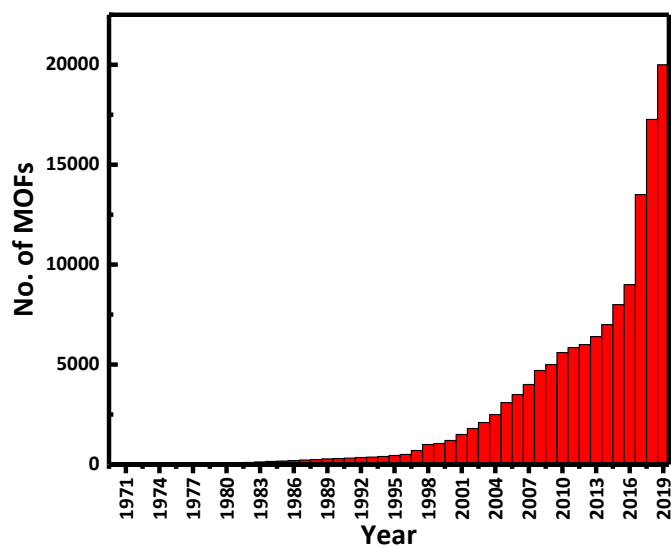
Figure 1.3. : Amount of reported MOF structures between 1970 and 2019.

Although their adsorption properties were noticed since the compounds were first synthesized , they could not be exploited because of their lack of stability regarding air or water.[17] Indeed, these porous materials collapse during the pores evacuation.[18] The first challenge was therefore to access the porosity and to improve the stability of the materials. This was achieved when reference compounds, stable at room temperature and with considerable specific surface area were discovered. For Instance, MOF-5[13, 14] and the MIL-53 family (MIL for Material from the Lavoisier Institute)[19, 20] which have good thermal stability (up to 200 ° C for MOF-5   and 500 ° C for MIL-53 (Al))[13, 21] were the first MOF structures to be activated by dynamic evacuation at low temperature, which paved the way to potential industrial applications.

2. Synthesis

MOFs are commonly named after the institution where they were first discovered, the NOTT family of MOFs is named after researchers in Nottingham,[22] MIL after the Lavoisier Institute in Canada[21] and UiO after the University of Oslo,[23] respectively. Synthesizing MOFs requires conditions that lead to the formation of well-defined inorganic building blocks (often termed as secondary building units, SBUs, as defined by Férey[24] without the decomposition of their organic linkers. G.Férey introduced the concept of SBUs initially used for zeolites, which defines MOFs as the assembly of two building bricks, one referring to inorganic sub-networks and the other to organic ligands. This design makes it possible to identify similar construction patterns with other inorganic porous materials, such as zeolites with which the MOFS share a nomenclature for topological description. G.Férey proposes a classification of MOFs based on the dimensions of their inorganic SBUs. He defines four types of networks (Figure 1.4), which became the basis of a structure prediction model[25] whose effectiveness was validated a few years later with the synthesis of MIL-100.[24]

On the other hand, Yaghi and O'Keeffe et al. defined SBUs as an assembly, discrete or infinite, of metal cations with coordination points linked by organic entities in a successive and periodic manner.[26] To simplify their models, they only considered the topology of the material by representing SBUs (inorganic and organic) with simple geometric shapes,[27, 28] as illustrated in Figure 1.4.

Inorganic units   **Organic units**
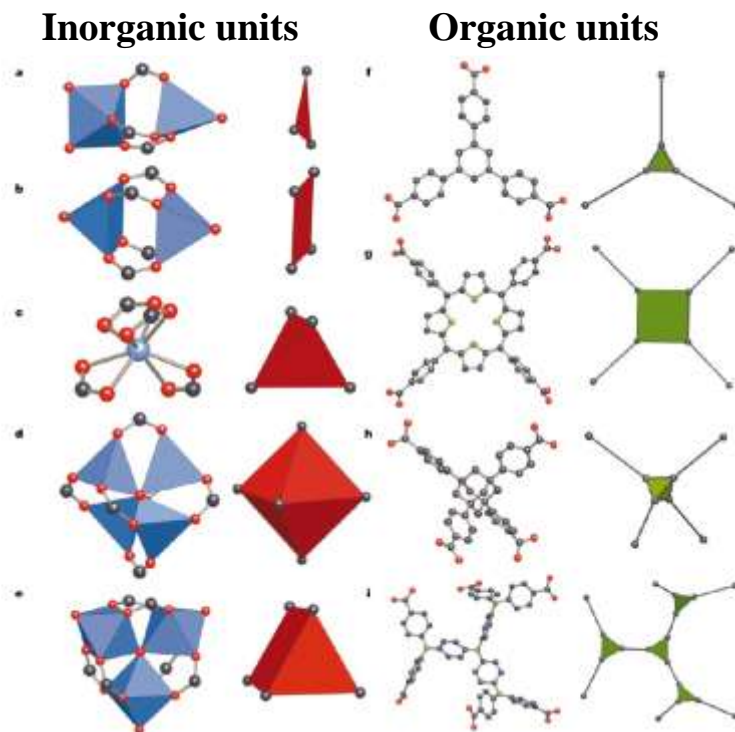
Figure 1.4. Examples of inorganic (left) and organic (right) SBUs with their associated geometric representation according to Yaghi and O'Keeffe.[27]

Furthermore, the thermodynamics and kinetics of crystallization must be satisfied to allow for the nucleation and growth of desired phases. Experimentally, many parameters, either compositional (molar ratios of ligand to metal, initial precursor concentration, metallic salt, pH value, solvent, etc.), or process parameters (temperature, pressure and even reaction time), are found vital to the formation of successful framework structures.[29, 30] Diverse synthesis methods such as conventional hydrothermal/solvothermal, micro-wave assisted, electrochemistry, mechanochemistry and ultrasonic processes are also considered important in terms of crystal morphologies, size, yields of the MOF product and thus their physical and chemical properties.

For example, with conventional heating methods like electric resistance heating, the introduction of micro-wave irradiation into the synthesis of MOFs provides an efficient methodology to synthesize them with short reaction times, narrow particle size distribution, easy morphology control and high crystallinity. To determine with relative efficiency the compositional and process parameters[31] due to the rapid and uniform heating of the reaction solutions.

As mentioned above, the richness of possibilities in terms of linkage between inorganic moieties and linkers renders the delicate estimation of synthesis parameters extremely time-consuming and, ultimately, unachievable. Due to its widespread use in the synthesis of zeolites and zeotypes, which are inorganic compounds, the high-throughput method which enables a systematic investigation of synthesis parameters and a faster and cheaper access to a large variety of synthesis information has proven an ideal tool to better understand the role of parameters involving the formation of MOF materials.[32-37]

a. Conventional Synthesis: Electrical Heating

Since the discovery of MOFs, there have been numerous reports on different methods of synthesizing MOFs.[25, 38] The most common and widely used method is the conventional synthesis which involves heating the reaction mixture by the means of electrical heating. Conventional synthesis can be further classified into two methods which are solvothermal and non solvothermal. According to Rabenau, solvothermal synthesis can be defined as a reaction that is carried out in a closed vessel under autogenous pressure above the solvent's boiling point.[27] Non solvothermal synthesis on

the other hand, involves a reaction that takes place at or below the solvent's boiling point under ambient pressure.

One of the main parameters of growing MOF crystals is the reaction temperature. In most cases, MOF crystals can be grown from a clear solution given that the nucleation energy barrier is exceeded. This can be achieved by increasing the concentration of the reactants by increasing the reaction temperature. The choice of solvent is also crucial in MOF syntheses. A good solvent should have the ability to dissolve a wide range of metal salts and acids. Other favourable characteristics include low reactivity and high boiling point. An example of a solvent which obeys these requirements and widely used in MOF syntheses is *N*,*N*-dimethylformamide (DMF). DMF is a polar aprotic solvent which can accept protons from the acids used in the reactions thus it is able to dissolve a range of acids. Furthermore, a wide reaction temperature range can be employed as DMF has a high boiling point (153 °C). Advantages of conventional synthesis include the ease of carrying out the reactions and in most cases, large crystals suitable for structure determination are obtained *via* this method.[28] On the other hand, long reaction times and high reaction temperatures make this method less energy efficient.

b. Solvent Evaporation and Diffusion

A number of previous work on MOF syntheses focused on solvent evaporation method.[39] Typically, the reagents are fully dissolved in a solvent, which is then allowed to evaporate slowly. As this happens, there is an increase of the solute/reactants concentration above the solubility threshold. This step can induce the precipitation of MOF crystals.

Solvent evaporation can be regarded as an energy efficient process as most reactions take place at room temperature and do not require external energy supply. One of the drawbacks of this method is the long reaction times compared to other synthetic methods. In some cases, a mixture of solvents is used in order to aid the solubility of the reactants and shorten the reaction time by speedier evaporation of the low boiling solvents.

Vapor diffusion is an alternative technique used in producing MOF crystals. In a typical vapor diffusion reaction, a solution of metal salt and ligand is placed in an open container. This container is placed in another larger vessel that contains a volatile base. The larger vessel is sealed and over time the volatile base will diffuse into the reaction mixture thus increasing the acidic ligand:conjugate base ratio by deprotonation. This step can facilitate nucleation of the MOF and subsequently crystallization.

Reaction diffusion process, a recent method, is used to synthesize and control the size and morphology of single crystals of metal-organic framework at room temperature.[40] Diffusion occurs in a gel matrix containing organic ligands. Upon the addition of a liquid solution containing metal ions, a precipitate is formed, which is the MOF (Figure 1.5). Thereby, the formation of the MOF is controlled by the bulk diffusion where the atoms diffuse within the lattice of the crystal.
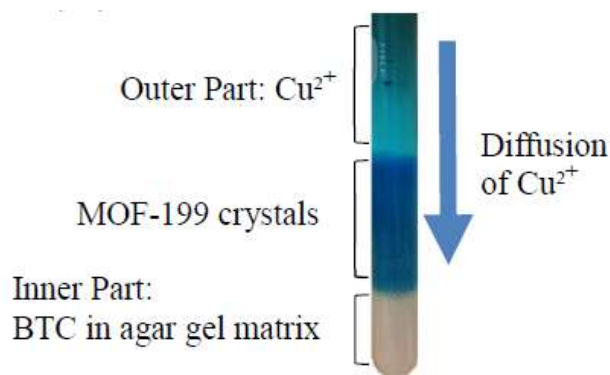
Figure 1.5. Schematic representation of the MOF-199 synthesis via RDF.[40]

c. <u>Microwave-Assisted Synthesis</u>

Microwave-assisted synthesis is an alternative method of producing MOFs using microwave radiation. The energy or heat required to drive the chemical reactions originates from the collisions between molecules as they attempt to align themselves in an electromagnetic field. One of the advantages of microwave-assisted synthesis is the shorter reaction times due to direct heating of the solvent which arises from direct interaction of molecules and radiation. MOFs successfully synthesised using microwave-assisted synthesis include MOF-5 and $[Cu_3(BTC)_2]$ HKUST-1, (BTC = 1,3,5-benzenetricarboxylate). Choi *et al*. reported that MOF-5 microcrystals (2 – 4 μm) could be synthesised in 9 minutes at 95 °C *via* microwave-assisted synthesis[41]. Similar observations were noted for the microwave-assisted synthesis of HKUST-1, in which crystals of HKUST-1 were obtained in a short reaction time (30 minutes) at 180 °C.[33] Schlesinger *et al*. reported that the choice of solvent has an effect on the reaction rate and product yield. Although fast reactions can be anticipated, obtaining single crystals can be challenging due to the high nucleation rates. Thus, microwave-assisted synthesis is normally tailored for the synthesis of nano- or microcrystalline materials.

d. <u>Electrochemical Synthesis</u>

In 2005, researchers at BASF developed a synthetic method for producing MOFs, which was termed electrochemical synthesis.[34] This method eliminates the use of metal salts with the potential of affording products with high purity due to the absence of anions such as nitrate and chloride used in other synthetic methods. In a typical electrochemical reaction, metal ions are continuously fed into the reaction medium which

contains a ligand and a conducting salt *via* anodic dissolution. This method is very

desirable in large scale processes, as the reactions can be carried out continuously,

leading to higher yields in comparison to normal batch type reactions. A number of

zinc(II) and copper(II) based MOFs have been successfully synthesized using this

method such as ZIF-8 and HKUST-1.[34, 35]

e. Mechanochemical Synthesis

All of the synthetic methods described thus far require the presence of solvent in

the reactions. Elimination of, in particular, organic solvents in syntheses is advantageous,

as it addresses some environmental issues related to the treatment of liquid waste.

Mechanochemical synthesis is a solvent-free method to produce MOFs which can be

carried out at room temperature. The method is based on the cleavage of intramolecular

bonds due to mechanical force followed by chemical transformations. First reported for

MOFs in 2006, reaction times are typically short (10 - 60 min) and generally afford

micro- or nanocrystalline products.[36] In some cases, metal oxides can be used instead of

metal salts thus leading to non-toxic water as the only side-product. Liquid-assisted

grinding (LAG) is a modified mechanochemical synthesis which requires the addition of

a minute amount of solvent to assist with the mobility of reactants on the molecular level.

This typically accelerates the reactions thus products are obtained at a shorter time in

comparison to conventional mechanochemical synthesis. A series of isostructural MOFs,

[Ln(BTC)(H$_2$O)] (Ln = Y, Sm, Gd, Tb, Dy, Er, Yb) were successfully synthesised using

the LAG method employing a small quantity of DMF.[37]

f. Sonochemical Synthesis

Sonochemical synthesis was first used in the formation of MOFs in 2008, with the primary aim of investigating energy efficient and green methods of producing crystalline MOFs[26]. This method is based on ultrasound wave to produce small bubbles or cavities which produce ultrasonic energy with temperatures reaching 5000 K and pressures of up to 1000 bar. Chemical reactions can take place in the cavity, on the surface, or in the bulk media. Qiu *et al.* discovered that $[Zn_3(BTC)_2]$ could be obtained at room temperature in an ultrasonic bath.[26] They reported that the reaction time had an important role in the size and product morphology. Spherical particles (100 – 200 nm) were obtained in short reaction times (5 and 10 min) whilst needle-shaped crystals up to 900 nm length were produced with longer reaction times (30 and 90 min).

3. Reticular Chemistry and Functionalization

SBUs have made it possible to rationalize and facilitate the comparison between porous materials. This has led to the concept of isoreticular (Yagi) or scale chemistry (Férey).[26, 27] Its main principle is to replace the organic ligands of an existing structure with ligands of different sizes or functions, while retaining the inorganic brick and the topology of the initial structure. Wider structures are obtained with new properties introduced by new functional groups Figure 1.6.
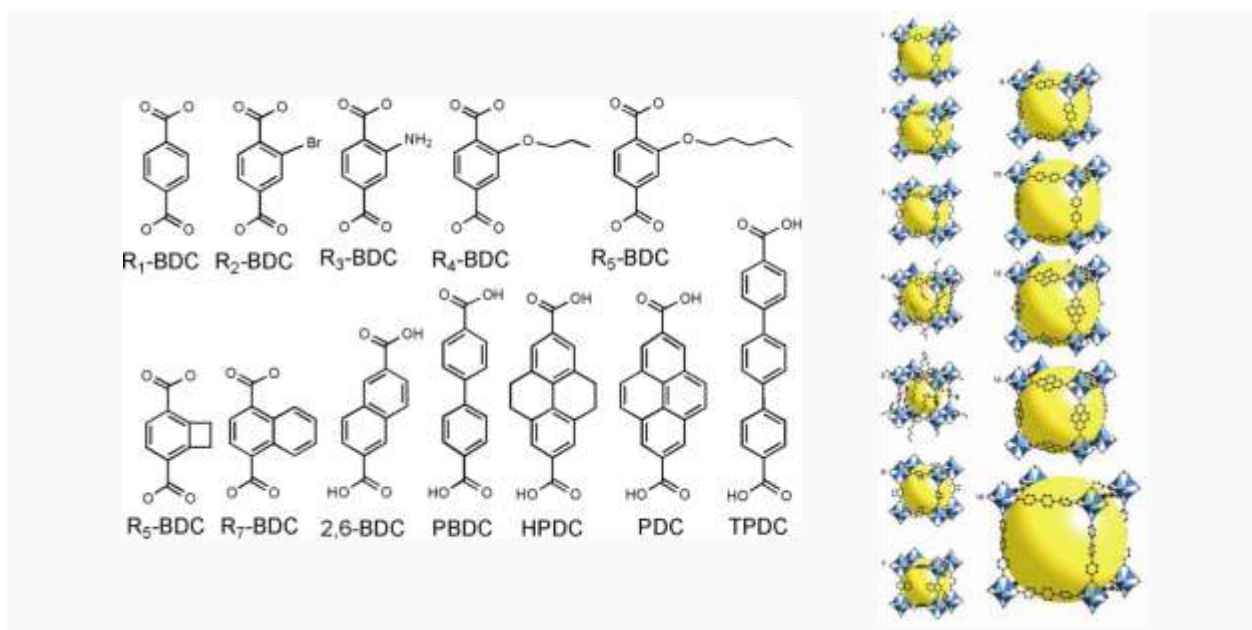
Figure 1.6. Illustration of the principle of isoreticularity with IRMOF (or MOF-5). Extract from Yaghi et al.[27]

In MOF-5, along with the majority of MOFs, it was synthesized by bridging organic ligands contain carboxylate functional groups that act as points of attachment to inorganic metal clusters. The structural features of MOFs allow them to be predesigned, this is also known as reticular chemistry. By judiciously selecting the inorganic and organic components, desired topologies, structures and properties can be obtained.[27] Reticular chemistry is ultimately responsible for the large number of MOFs known to date, an isoreticular series based on MOF-5 (the IRMOF series) was one of the first to be discovered.[42, 43] Isoreticular series of MOFs contain the same underlying connectivity and as a result, share the same overall framework structure. The IRMOF series contains ligands of varying lengths and/or pendant functionality, allowing functionalized materials for specific applications to be created.

The ability to design and predict MOF structures is advantageous when specific materials are required. However, the expected structures are not always obtained, and this is

especially true when the length of the bridging ligand is variable. As the length of the

bridging ligand increases, and provided the MOFs are part of an isoreticular series, so

does their porosity. This is true to a certain extent, although there is a critical

point. Furthermore, when the length of the bridging ligand increases beyond a certain

framework length interpenetration occurs.[44] Framework interpenetration describes the

phenomenon whereby the pore space of an MOF is sufficient for one or more

frameworks, depending on the level of interpenetration, to be able to grow within the

void space of another independent framework[45] (Figure 1.7).
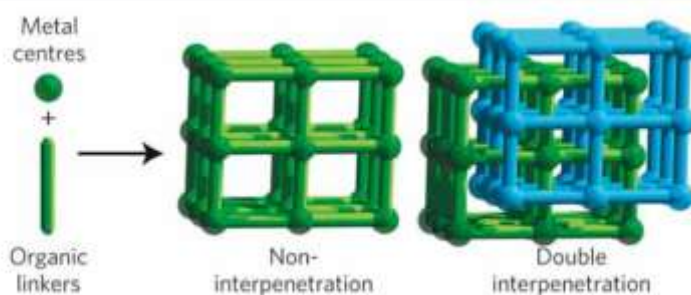
Figure 1.7. Schematic representation of non-interpenetrated and doubly interpenetrated
MOFs. Interpenetration reduces MOF porosity, as the second framework occupies the
pore space of the first framework. The two independent frameworks are colored green,
and the MOF-modified network in blue.[45]

There are a number of reported strategies to control the degree of MOF

interpenetration, these include refining the reaction parameters[14] and template directed

synthesis.[46] In some cases, both interpenetrated and non-interpenetrated structures are

known as the same MOF.[47] Framework interpenetration not only relies on the length of

the bridging ligand, but is also determined by the steric bulk of the ligand.[48, 49]

Interpenetration was initially considered to be a drawback as it reduces porosity.

However, it has since been discovered that reducing the pore diameters can be particularly useful for some applications, such as CO_2 capture.[45, 50, 51]

4. Multivariate MOFs

The combination of multiple ligands of the same length within the same framework results in mixed-ligands or multivariate MOFs (MTV-MOFs) and by combining a number of different functional units highly specialized materials can be obtained. This concept was applied to MOF-5 type materials and up to eight different terephthalate based ligands could be incorporated into a single framework via direct synthetic methods[52] (Figure 1.8).

Functionalised terephthalate ligands → **MTV-MOF**
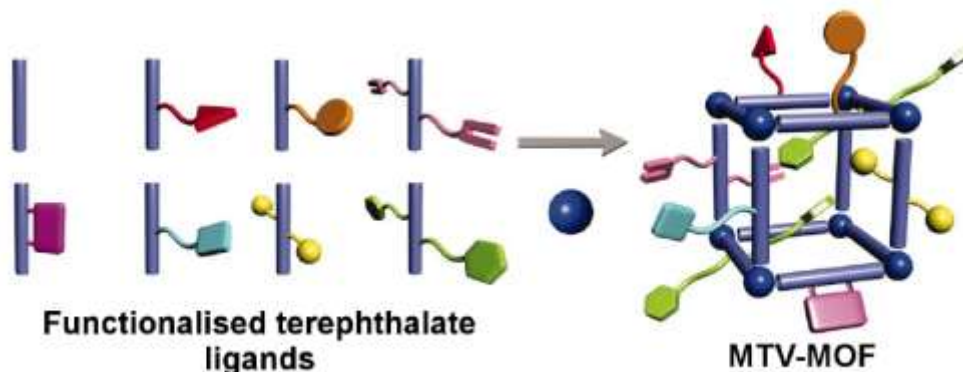
Figure 1.8.   Schematic representation of eight different terephthalate based ligands that can be used to construct a MTV-MOF with the same underlying topology as the parent MOF-5.[52]

5. Properties of MOFs

a. porosity

The richness of the synthesized MOF structures has produced multiple

adsorption behaviors and new properties. Three generations[53, 54] of MOFs have been

described based on their behavior towards adsorption and desorption processes.

-1st generation: non-permanent porosity where the structure collapses

  irreversibly when the adsorbed molecules leave;

-2nd generation: rigid microporous solids with good chemical and thermal properties

which retains their structure after adsorption / desorption processes (e.g. MOF-5,

HKUST-1, MIL-100, MIL-101, UiO-66);

-3rd generation: porous materials referred to as "flexible" which undergo reversible

structural changes following an external stimulus (e.g. MIL-53, MIL-88).

b. <u>Flexibility</u>

Flexibility results in a change in volume or structure of the material generally

due to interactions between the host molecules, the MOF, and the adsorbed molecules.

However, this can also occur under the action of external stimuli such as the adsorption /

desorption of a gas or liquid[55], or temperature[56] or mechanical pressure.[57] Flexibility

results from a cooperative effect of the inorganic component and its organic ligands. In

fact, unlike zeolites which are formed by strong Si-O covalent bonds and which exhibit

only limited flexibility, MOFs are formed with both strong iono-covalent bonds and

weaker bonds (π-stacking, hydrogen bonds) , which are more or less directional and

responsible for their intrinsic structural flexibility.[58] Flexibility is therefore made possible

due to degrees of freedom such as twisting or bending movements within the organic

ligands. This phenomenon is particularly spectacular with the MIL-53s systems.[19, 20]

Atomic displacements and changes in lattice volume previously unseen (of the order of 40%) have been observed after removing the adsorbed molecules (residual synthetic ligands, water, etc.). The authors refer to the phenomenon as " breathing" (or the breathing effect). This is characterized by reversible transitions between metastable states of the same material.

This latest generation of porous materials, also called soft porous crystals (SPCs) form a class of materials in their own right. Kitagawa establishes a first inventory of flexibility phenomena based on the dimensions of the material.[59, 60] While other authors, such as F.X Coudert et al. in 2011[58] and Fischer et al. in 2014[61] were more particularly interested in three-dimensional structures.

Several modes of flexibility have been defined. These include breathing and swelling, which involve volume variations, ligand rotation, sub-network displacement and the gate opening phenomenon which characterizes a transition from an initially non-porous structure towards a porous one[62].

c. Open metal sites

Open metal sites (OMSs) are a widely researched form of active sites that can recognize specific molecules, resulting in highly selective gas trapping.[63] During the gas uptake these unsaturated or open metal sites serve as the first loading sites due to high affinity. The MOFs having metal coordinated solvent or guest molecules can generate the open metal sites. Solvent or guest molecules can be removed from the metal centers of MOFs without causing any structural collapse.[64] The solvent exchange with low boiling

solvents followed by thermal activation at high vacuum can create open metal sites without collapsing the basic MOF framework integrity. The maintained crystallinity in these MOFs, with unsaturated metal coordination creates centers with high affinity for adsorption. In addition, researchers have recognized that MOFs could be used in asymmetric catalysts after incorporation of open metal sites.[65] POST-1 is the first example of MOFs which exhibited catalytic features for an asymmetric chemical reaction as reported by Kim et al..[66]

The well-known MOF is $[Cu_3(btc)_2(H_2O)_3]n$ (btc = 1,3,5-benzenetricarboxylate) or more commonly HKUST-1 (Figure 1.9a). The framework contains Cu^{2+} paddlewheel units, with each Cu atom connected by 4 oxygen atoms of the bridging organic ligands and a water molecule fills the coordination sphere (Figure 1.9b). The framework contains 1 nm pores, with terminal water molecules projecting into the pores and upon dehydration they can be replaced with other molecules, such as pyridine causing a colour change and ultimately altering the pore texture.[67]

Furthermore, it is not only possible to use the paddlewheel motif to incorporate multiple ligands into a single framework; it is also possible to directly assemble materials containing more than one type of carboxylate based ligand.

A series of MOFs (MOF-74) having open metal sites derived from Metal (Mg, Ni, Zn, Co) and 2,5-dihydroxyterephthalic acid where these active sites are important for adsorption.[68]
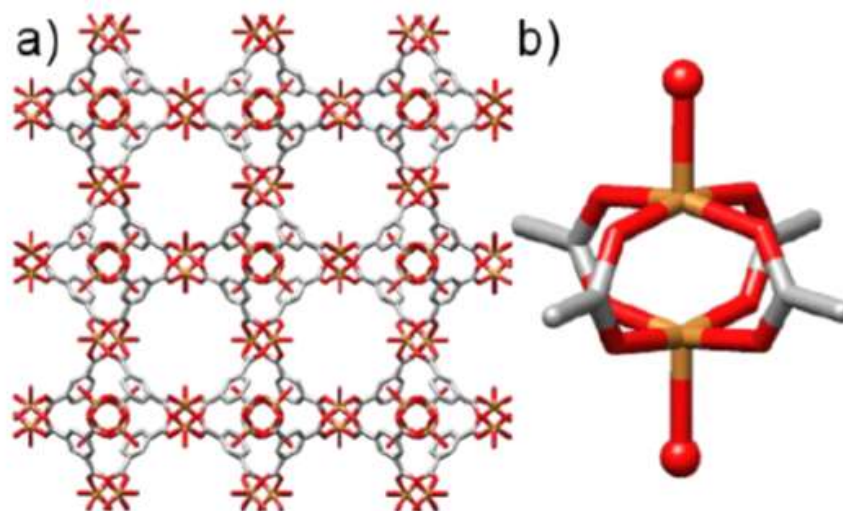
Figure 1.9. a) Portion of the solid-state structure of HKUST-1. b) Cu paddlewheel found in HKUST-1, with the oxygen atoms of the terminal water molecules highlighted as spheres.[69]

6. *Applications of MOFs*

MOFs have received increasing interest over the past 15 years and have been examined for potential use in a number of applications, including gas capture and storage,[1, 70] catalysis,[71, 72] drug delivery[73, 74] and in the biomedical field. A small overview of pertinent examples of each of these applications will be discussed in the following sections.
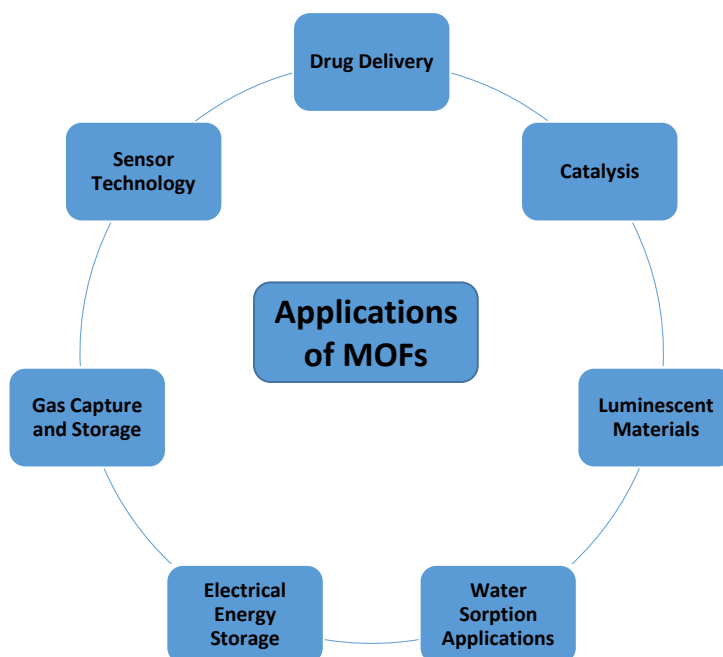
Figure 1.10. Various applications of MOFs.

a. Gas Capture and Storage

The porosity of MOFs is normally evaluated by collecting N_2 adsorption and desorption isotherms at 77 K, then Brunauer–Emmett–Teller (BET) theory is used to calculate a surface area (SA).[75] The SAs of MOFs are usually very high, typically thousands of square meters per gram. Routine SA analysis of MOFs is useful, even if the structure is known as the SA can be used to ensure the framework is completely activated. Considering their porosity and ability to take up large volumes of N_2, it is not surprising that much of the application driven research of MOFs has focused on their potential use as gas capture materials. There are large numbers of reports that investigate the potential of MOFs for the capture and sequestration of gases such as CO_2,[76] H_2[77, 78] and CH_4.[79] Researchers have developed methods to maximize the uptake of the desired gas molecules, with interpenetrated MOFs[45, 50] and those containing open-metal sites[80, 81]

holding great promise as both phenomena have been shown to result in greater interactions between the framework and the adsorbate.

b. Catalysis

The highly ordered arrangement and porosity of MOFs has resulted in their consideration as heterogeneous catalysts for a wide variety of transformations.[82] The catalytic activity of framework materials was investigated as early as 1994,[82] while the ability to tune the chemical functionality and structure of MOFs allows them to be tailored to suit specific catalytic transformations.[71] The porosity of MOFs enables the transport of reagents and products to and from the catalytic sites. There are four main considerations that must be addressed when designing/synthesizing a catalytic MOF: (i) the MOF must be sufficiently stable that upon activation its channels remain open, (ii) the MOF must contain a catalytic center relevant to the transformation in mind, (iii) the MOF must be stable under the catalytic conditions, and (iv) the MOF should be recyclable to allow numerous catalytic cycles to occur. Points (i), (iii) and (iv) are all related and are determined in the main by the stability of the MOF and this has seen an increase in research towards MOFs with improved stabilities, such as Zr MOFs[83] (See Section 2.7), although catalyst deactivation and leaching are not related to MOF stability but can also result in a loss of activity.

There are a number of strategies that can be used to synthesize MOFs with catalytic centers, including open metal sites, functional sites on the ligand scaffold, encapsulation of catalytic species within the pores (such as noble-metal nanoparticles), semiconductor photocatalysis[84] (if the metal clusters have the correct electronic

configuration), postsynthetic modification of pendant functionality and finally grafting of catalytic species to the metal clusters[72] (Figure 1.11).
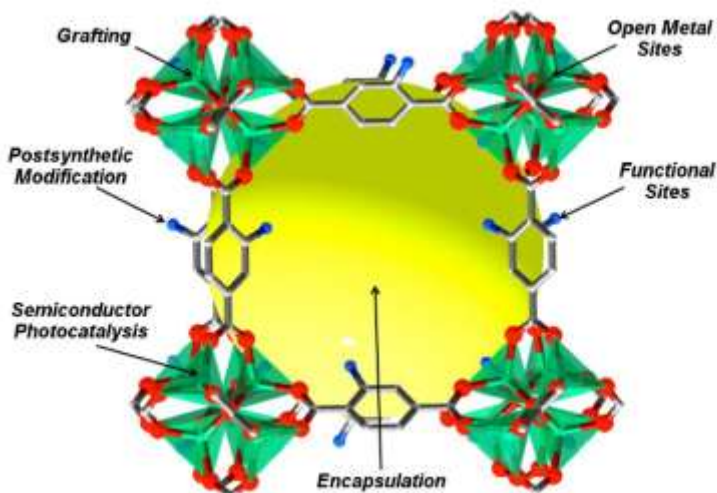
Figure 1.11. Representation of an exemplary MOF, highlighting different routes available for the introduction of catalytic sites.[72]

c. Drug Delivery

MOFs have been realized as potential candidates for biomedical applications, for instance as drug delivery systems[73, 74] and also as MRI contrast agents.[85] The chemical and structural tunability of MOFs allows them to be designed to meet the requirements of the desired application,[27] while more importantly this also enables fine control of their cytotoxicity.[86] It is well-known that MOFs demonstrate low chemical stabilities,[87] but this can be advantageous for drug delivery systems. The MOF has to remain intact for long enough to reach the target area of the body then in-situ degradation of the MOF releases the cargo from the pores to deliver the desired therapeutic effect.

The M^{III} carboxylate based MOFs, typically known as MIL materials, have received widespread interest as drug delivery systems, especially the Fe^{III} analogues due to their low cytotoxicity.[88]

d. <u>Removal of Environmental Contaminants</u>

In recent years, the removal of heavy metal ions and organic contaminants from wastewater has become an emerging application of MOFs.[89] This is due to the possibility to tailor MOF surfaces towards specific targets. Contamination of wastewater from domestic activities and industrial processes continues to be a pressing issue as it can cause detrimental impacts on the environment and human health. A number of MOFs have been shown to effectively remove hazardous organic molecules. These include $[Fe_3O(BDC)_3(DMF)_3]\cdot FeCl_4$, MOF-235 for the removal of organic dyes (methylene blue and methyl orange) and UiO-67 for the removal of organophosphates.[90, 91] Unlike many organic contaminants, inorganic heavy metal pollutants are non-degradable, thus necessitates the use of materials that can directly capture these toxic molecules. The breakthrough in arsenic decontamination was reported in 2015, when Wang *et. al.* observed a significant arsenic uptake capacity in UiO-66 (303 mg/g).[92] Recently, nanosized MOF-74 was employed for arsenic removal from water and a removal capacity of 100 mg/g was obtained. The high uptake was attributed to the strong interaction of arsenate with the exposed metal sites.[68]

In 2013, Yee *et. al.* reported a high mercury loading in a thiol-functionalised MOF $[Zr_6O_4(OH)_4(DMDB)_6]$ UiO-66-(SH)$_2$, (DMDB = 2,5- dimercapto-1,4-

benzenedicarboxylate).[93] The significant mercury uptake from a $Hg(NO_3)_2$ solution

(99.9%) was attributed to the high percentage of thiol groups protruding into the pores.

UiO-66-$(SH)_2$ was also shown to effectively adsorb mercury from the vapor phase. It was

shown that the UiO-66-$(SH)_2$ host framework featured a nearly white photoluminescence

which was distinctly quenched after mercury uptake.

e. The Biomedical Field

Properties of biologically compatible MOFs, called BioMOFs including

BioMILs (Bioactive Materials of the Lavoisier Institute)[88, 94] have been explored for the

controlled release of active principles. Stored in the pores or forming an integral part of

the framework of the MOF, these can be released following an external stimulus,[95] or

gradually dissolved in the biological medium, over periods which can extend over several

days.

f. Commercial Developments of MOFs

Since the first patent filed in 1995 and assigned to the Nalco Chemical

Company, commercialization of MOFs progressed gradually until the first MOF-based

products released in 2016 by MOF Technologies and Numat Technologies.[96, 97]

MOF Apps, founded in 2013, are the exclusive licensee for UiO-66 and the Zirconium-

based family of MOFs. With a focus on MOF applications services, the company aims to

bring research and industry together to identify and develop commercially viable

application opportunities in the areas of gas storage, industrial cooling, toxic gas protection and healthcare. MOF Apps develops and offers integrated solutions using MOFs, which are cost competitive and which outperform state-of-the art systems. MOF Apps have sold the most amount of MOF to a leading vehicle manufacturer in August 2015 to test as adsorbed natural gas fuel platform.[97] ProfMOF founded in 2015 by a group of scientists at the university of Oslo, Inven and Kongsberg, focused on the commercialization of the MOF-material. The ProfMOF catalogue include: CAU-10, UiO-66-BDC, UiO-66-NH$_2$, UiO-66-COOH and UiO-67.[96]

Sigma-Aldrich is a distributor of MOFs supplied by BASF under the product names Basolites and Basosivt. Companies such as BASF and Sigma-Aldrich have marketed MOFs on a small scale, including two versions of MIL-53 (Al) (Basolite ™ A100 with BDC ligands and Basolite ™ A520 with Fumarate ligands) , MOF-5 (Basolite ™ Z100H), IRMOF-8 (Basolite ™ Z200H), HKUST-1 (Basolite ™ C300).[30, 98-100] Some have found industrial applications such as the Basolite © A520 used for methane storage.[100]

To summarize, MOFs have been examined and they have shown great promise for a number of applications, even though only a few examples mentioned are in keeping with the theme of this thesis. However, the take-home message from this section is that the flexibility of MOFs means their structures and properties can be fine tuned, allowing specialized materials suited to very specific applications . The main drawback of MOFs is their low stability; yet the example discussed by Lin *et al.* shows that coating MOF particles with silica, results in hybrid materials offering greatly improved stability.[101] Another approach to increase the stability of MOFs is to design more robust frameworks,

and Zr MOFs[23] are among the most stable MOFs known and hence have received growing interest in recent years.

7. *Zirconium MOFs*

Zirconium MOFs were first reported in the literature in 2008 by Lillerud *et al*. and they have received increasing interest.[23, 102] The MOFs were named UiO-66, UiO-67 and UiO-68 and were part of an isoreticular series containing terephthalate, biphenyl dicarboxylate and terphenyl dicarboxylate bridging ligands respectively. UiO-66 type MOFs (Figure 1.12) contain $Zr_6O_4(OH)_4$ clusters that are 12-connected by bridging organic ligands, resulting in 3-dimensional porous architectures containing both tetrahedral (smaller) and octahedral (larger) pores . Initially, the structures of UiO-66 MOFs had to be solved from powder X-ray diffraction (PXRD) data as single crystals could not be obtained. However, coordination modulation (see Section 2.8) has greatly improved the synthetic capabilities of Zr MOFs, allowing single crystals to be isolated and their solid state structures have since been confirmed by single crystal X-ray diffraction.
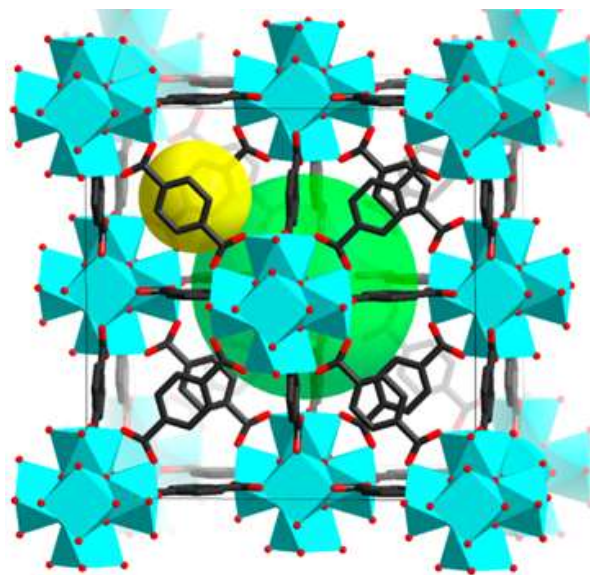
Figure 1.12. Crystal structure of UiO-66. C: black, O: red.

As the length of the bridging ligand increases the MOFs' pore volume increases, however the overall framework structure is unaltered and all UiO-66 type MOFs crystallize in the highly symmetric *Fm-3m* space group (they form part of an isoreticular series). There have been many reports on derivatives of UiO-66 type MOFs containing functionalized bridging organic ligands.[102, 103] UiO-66 type MOFs are typically obtained when linear dicarboxylate ligands are used, however Serre *et al*. showed that using higher synthesis temperatures alternative structures can be obtained. The so called MIL-140 series of MOFs contain 1-dimensional Zr oxide chains and 1-dimensional porous channels while demonstrating high thermal and mechanical stabilities.[104]

Alternative structural topologies have been obtained with ligands presenting different binding geometries. Trigonal tricarboxylate based ligands have been shown to form either 2-dimensional[105] or 3-dimensional[106, 107] Zr MOFs, although in these cases lower connected Zr_6 clusters result (Figure 1.13). The altered geometry of the ligand

results in 6-connected Zr_6 clusters rather than the 12-connected clusters observed in UiO-66 type MOFs and the free coordination sites are capped by either solvent molecules and/or monocarboxylate modulators (coordination modulation – see Section 2.8). Interestingly, changing the terminal modulators attached to the Zr_6 clusters changes the inter-layer separation[105] which allows the porosity to be regulated.[107]

Planar tetracarboxylate based ligands have been used for the construction of Zr MOFs and in the specific case of tetrakis(4-carboxyphenyl)porphyrin (TCPP) Zr MOFs containing typical Zr_6 clusters have been obtained[108, 109] (Figure 1.13), while alternatively it has been shown to result in a MOF containing Zr_8 clusters that were previously unknown in both cluster and MOF chemistry. The presence of porphyrin units presents opportunities for the incorporation of secondary metals and it was shown that the Fe metallated MOF is an effective peroxidase mimic during the oxidation of a number of substrates.[108]
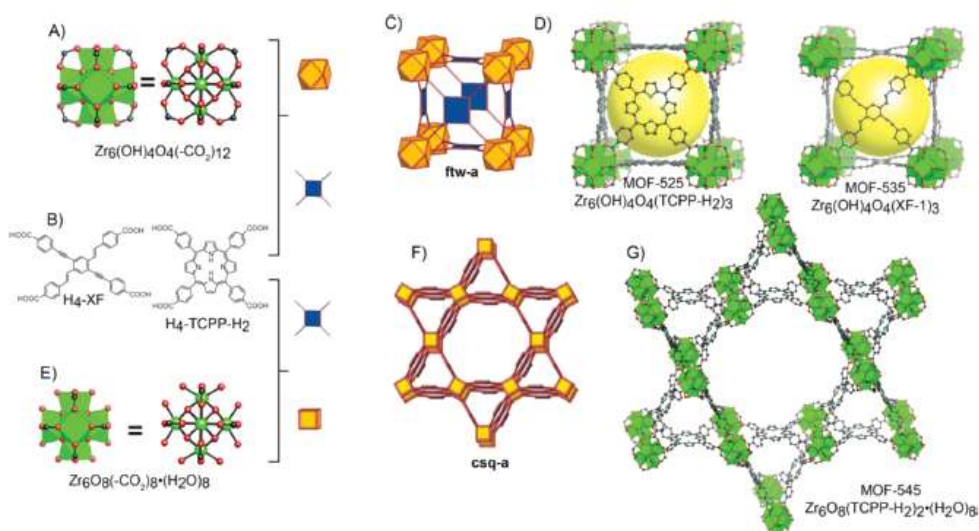
Figure 1.13. Crystal structures of MOF-525, -535, and -545: (A) cube octahedral unit, $Zr_6(OH)_4O_4(CO_2)_{12}$; (B) links used in MOF-525 and -545 (H_4-TCPP-H_2 = $C_{48}H_{30}N_4O_8$) and MOF-535 [2]; (C) ftw topology; (D) MOF-525 and -535; (E) cube unit, $Zr_6O_8(CO_2)_8(H_2O)_8$; (F) csq topology; (G) MOF-545.[109]

Alternatively, a tetracarboxylate pyrene based ligand was used to construct an 8-connected Zr MOF commonly known as NU-1000.[110] NU-1000 has been extensively investigated for a range of cluster modifications as a result of the lower connectivity of the Zr_6 clusters and the presence of terminal OH and H_2O ligands. Postsynthetic exchange of the terminal ligands has been carried out using a process the authors call solvent assisted ligand incorporation.[111] Incorporating perfluorinated alkanes using this procedure increased both the water stability and CO_2 uptake capacities of the NU-1000 materials.[112, 113] Similar to the incorporation of organic compounds, metallation of the Zr_6 clusters of NU-1000 has been investigated and it was found that the nickel metallated material is an efficient catalyst for the oligomerisation of ethylene.[114] Tetrahedral carboxylate based ligands have been used to construct Zr MOFs,[115] and when 4,4′,4″,4‴-methanetetrayltetrabenzoic acid is used Zr MOFs containing either 8-connected or 12-connected Zr_6 clusters have been obtained.[116]

The reason for the high interest in Zr MOFs is their improved thermal[117] and mechanical[118, 119] stabilities compared with traditional late transition metal containing MOFs, resulting in their potential use in a number of applications.[102] The improved stabilities of Zr MOFs is attributable to the resilient coordination bonds between the hard metal ions and the carboxylate oxygen atoms. However, the hard-hard interactions between the metal and the ligand make their syntheses troublesome, as the fast crystallisation kinetics often result in the isolation of amorphous solids without long-range order. In order to access crystalline, phase-pure Zr MOFs it was clear that new

synthetic procedures had to be developed and in 2011 Behrens *et al*. applied coordination modulation to Zr MOFs for the first time.[120]

8. Defected MOFs

Coordination modulation describes the deliberate addition of foreign compounds to MOF syntheses and typically they influence the crystallinity, size and morphology of the resulting products.[121, 122] Modulators are typically monodentate organic compounds, such as acetic, benzoic or formic acid, and their competitive coordination towards the metal clusters influences the coordination equilibrium, allowing the directed syntheses of MOF particles with alternative morphologies. Accessing MOF crystals with different morphologies results in different concentrations of exposed facets and this can ultimately control the materials' physical properties. The ability to control the surface chemistry of MOF particles is still in its infancy however, it is becoming a topic of interest.[123]

One of the first examples of coordination modulation was reported by Kitagawa *et al.* where they described the modulation of an anisotropic Cu framework using acetic acid.[122] Unlike early examples of coordination modulation where the selective attachment of modulators in certain directions is believed to result in directional growth of MOF particles, different behaviours are found upon addition of modulators to the syntheses of Zr MOFs. During the first modulation study of Zr MOFs, benzoic acid, acetic acid and water were investigated as modulators for the syntheses of a variety of UiO-66 type materials.[124] It was found that the addition of modulators altered the size and morphology of the crystals while also improving crystallinity, presumably by controlling the

31

nucleation rate through competitive coordination between the monocarboxylate and the bridging ligand for attachment to the Zr clusters.[125] The scope of modulators used during the synthesis of Zr MOFs has been expanded to include hydrochloric acid,[126] formic acid,[127] hydrofluoric acid,[128] trifluoroacetic acid (TFA)[129] and recently amino acids[130] amongst others.

During the syntheses of Zr MOFs it is difficult to predict how the modulator will affect the materials structural properties and this is determined by the level of modulator incorporation. Synthetic modulators are known to promote defects,[117, 131, 132] which are predominantly caused by missing linkers/clusters.

The first attempt to gain control over defect formation in MOFs was achieved with the modulation approach. It is established that small amounts of monocarboxylic acids, or modulator, slow down the speed of crystallization by impacting the equilibrium reaction (the formation of the framework). In contrast, large modulator concentrations facilitate framework incorporation and in turn the formation of defects. The first report using this approach was given by U. Ravon et al. in 2010, using 2-toluic acid as modulator in the synthesis of MOF-5.[133] Since then, many research groups focused on the synthesis and characterization of defective MOFs.[129, 134] R. A. Fischer,[135] K. P. Lillerud[136] and A.L. Goodwin[137] were one of the first to strongly believe that defects can be exploited to enhance MOFs properties.

Defects alter the physical and structural properties of MOFs, and although they may have initially been considered to be problematic it has now been realised that they can result in improved properties for specific applications.[132] For instance, using hydrochloric acid as a modulator during the synthesis of a range of UiO-66 type MOFs,

higher than expected N_2 uptakes were recorded as a result of defects and subsequently the creation of mesopores. In extreme cases it was found that the experimental surface areas of the MOFs were in agreement with predicted surface areas where four of the twelve ligands were missing.[126] Similarly, when acetic acid was used as a modulator during the synthesis of UiO-66, definitive evidence of missing linkers and the creation of mesopores was obtained from high-resolution neutron powder diffraction[138] (Figure 1.14).The defect concentration was altered by varying the amount of acetic acid, causing visible changes to the colour of the material while the pore volume increased by ~150% and the surface area by ~60% .
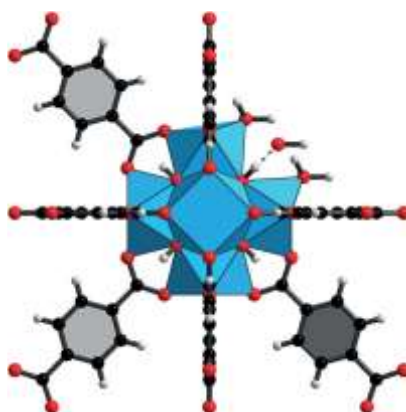
Figure 1.14. Schematic representation of a missing linker defect in UiO-66.[138]

Considering the potential to improve the uptake capacities of Zr MOFs through the creation of defects, which appear to be promoted by the use of synthetic modulators, this area has received large amounts of interest and recently defects have been characterised on the molecular level using single crystal X-ray diffraction.[127] Recently, a comprehensive study performed by Lillerud *et al.* attempted to rationalise the use of

routinely employed modulators and their effect on the porosity and composition of the resulting materials.[136] The authors found that the concentration of defects in UiO-66 could be systematically tuned, increasing with respect to modulator concentration and/or acidity. The defectivity was determined from the measured increase in BET surface area of the materials relative to UiO-66 synthesised in the absence of a modulator.

Under the conditions examined the prominent defect type was found to be missing clusters, with capping formate (from the reaction N,N-dimethylformamide) and modulator molecules found to complete the coordination sphere of the Zr_6 clusters (from dissolution NMR experiments). It was hypothesised that as the acidity of the modulator increases then it is more competitive with the bridging organic ligand and a higher concentration of defects are obtained. Similar results were also found and reported by Bennett *et al.* where higher equivalents of less acidic modulators had to be added to the synthesis of UiO-66 to achieve similar levels of modulator incorporation.[139] The most acidic modulator investigated during the study was TFA, resulting in the inclusion of trifluoroacetate molecules within the framework by attachment to the Zr_6 clusters at defect sites. While it is frequently reported that modulators and/or defects result in altered gas uptake capacities, the trifluoroacetate containing UiO-66 material was found to be more mechanically robust compared with conventionally prepared UiO-66 samples, and this was thought to be due to stronger Zr-carboxylate bonds caused by an electron withdrawing effect of the bound TFA molecules.

The increased mechanical stability of the trifluoroacetate containing material was revealed through its ability to resist collapse under ball milling for at least 10 times longer duration.

34

An interesting study was conducted by Vos *et al*. whereby UiO-66 was synthesised using a combination of hydrochloric acid (HCl) and TFA, resulting in highly crystalline materials.[129] The resulting materials were subsequently investigated as catalysts for the "ene"-type cyclisation of citronellal to isopulegol.

UiO-66-10HCl, that is UiO-66 synthesised in the presence of 10 equivalents of TFA and 1 equivalent of HCl, was observed to contain both physisorbed and cluster bound TFA from thermal analysis and 19F solid-state NMR spectroscopy. Synthesis results a highly defective material containing Zr_6 clusters surrounded by 8 carboxylates rather than the usual 12 – which has a high number of Lewis acid (Zr^{IV}) sites and increased pore dimensions.

During a study by Gutov *et al.* UiO-67 was synthesised in the presence of either formic, benzoic, trifluoroacetic, acetic or hydrochloric acid.[131] The defected materials have an effect on the reactivity of Zr-MOFs. Interestingly, the modulators could be exchanged for L-proline hydrochloride, which may result in chiral materials useful for enantioselective applications.

Recent study showed that the increase in the number of defects significantly increased the conversion of the esterification reaction of butyric acid and butanol to butyl butyrate.[140]

C. Objectives

The research described in this thesis is built upon two projects concerning MOFs. The objective of the first project was to control the defects using different modulators in

UiO-66 structure and to study their effects on Arsenic adsorption. The chemical and physical properties of the defected MOFs such as BET surface area and arsenic uptake capacity were studied. This research was described in Chapter 2.

The aim of the second project is to synthesize functionnalized Zr-MOF structures (UiO-66-NH_2 and UiO-66-$(COOH)_2$). These MOFs were selected for Pd NPs deposition. The formed MOF-Pd heterostructures were studied for nitrate reduction. Moreover, the effect of the Pd-loading on the catalytic performance was investigated. In this regard, we synthesized Pd-UiO-66 catalysts with various Pd loadings and then were used as catalysts for reduction of Nitrates in drinking water. Our research methods and objectives are summarized in the scheme below.
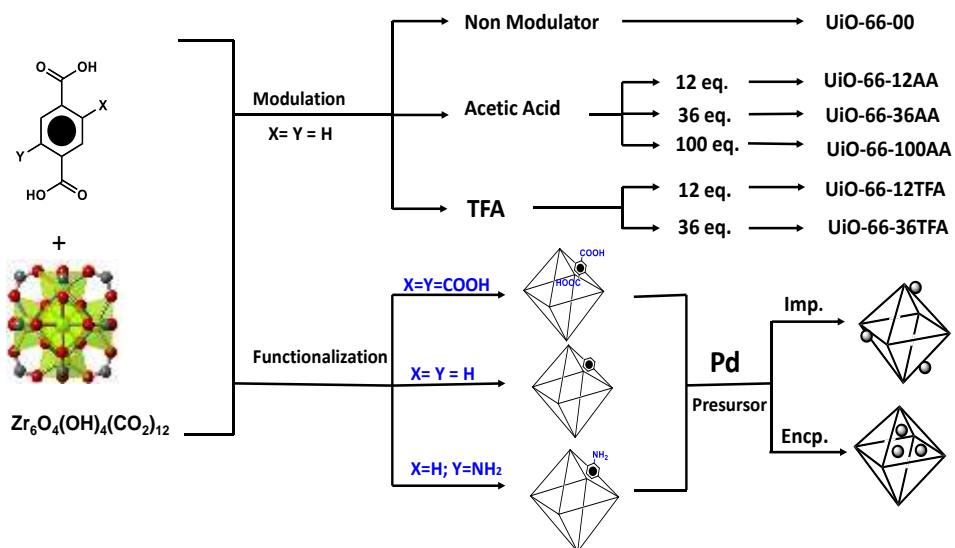
CHAPTER II

DEFECTS ENGINEERING IN UIO-66 STRUCTURE FOR ENHANCED ARSENIC REMOVAL FROM WATER.

A. Introduction

Water represents one of the most valuable resources to the current and future

societies of mankind.[141] Technologic and economic developments are filling the various

water bodies with toxic pollutants that are a major threat to human health. Nowadays,

more than 1.2 billion people in this world lack access to clean and safe drinking water.[142]

Therefore, water issues in regards to the increasing water scarcity as well as water

pollution are regarded as one of the most vital topics of environmental concern to human

beings.

Increasing level of water pollution augments the water scarcity issue. Water

pollutants can be categorized as organic or inorganic.[142] They majorly come from the

agricultural, industrial, and domestic activities that leave behind numerous synthetic

compounds in varying concentrations. Although most of these compounds are present at

low concentrations, many of them raise considerable toxicological concerns. This is

especially the case for inorganic pollutants, which are normally referred to as heavy metal

pollutants.[143] Most heavy metal elements existing as metal cations could be precipitated in

alkaline conditions, whilst some of them forming anionic metal complexes (e.g. chromate,

arsenate/arsenite, and selenate/selenite) are difficult to remove from water streams.[144]

Arsenic is ubiquitous in our environment. It is a component of more than 245 minerals,

including elemental arsenic, arsenides, arsenates, arsenites,[145] etc. Its toxicity has been

well analyzed and clinically studied.[146] In general, the seriousness of arsenic toxicity is dependent upon the mobility and chemistry of particular arsenic species. Inorganic arsenic compounds are considered significantly more toxic than organic forms; arsenite is considered as the more soluble and mobile species, and therefore more toxic in comparison to arsenate.

As a dangerous carcinogen, the International Agency for Research on Cancer (IARC) and the World Health Organization (WHO) have established a series of standards for controlling arsenic residuals in drinkable water. Nowadays, 10 μg/L is the most widely accepted standard concentration allowed for arsenic in drinking water. The regulation standards to remove Arsenic and provide quality water require effective technologies for water decontamination. A cost-effective method involves the use of a permanently porous material to adsorb the contaminants. MOFs are preferred over other porous materials, owing to their customizable chemical functionalities, versatile architectures and milder synthesis conditions.

In this chapter, the water stable Zr-MOFs (UiO-66) of various defect concentrations were successfully prepared and examined as adsorbent for arsenate removal from water. The defects were effectively tuned and controlled by changing the type and the amount of the modulator used in the synthesis procedure. Two types of modulators (acetic acid, AA and trifluoroacetic acid, TFA) were employed, their concentration were varied systematically and their effects on the structural properties of the obtained MOF crystals were investigated and compared with the ideal non modulated UiO-66 MOF. Six samples were synthesized by solvothermal procedure and fully characterized by scanning electron microscope (SEM), powder X-ray diffraction (PXRD),

Brunauer–Emmett–Teller surface area analyzer (BET), Fourier-transform infrared spectroscopy (FT-IR), and thermogravimetric analysis (TGA). Their performance as adsorbents for arsenate removal from water was studied and the thermodynamic and kinetic parameters of the adsorption process were determined and the obtained results were compared with the non-modulated UiO-66 structure. The relationship between the concentration of the sample's defect from one side and arsenate removal efficiency from the other side was also discussed and great insights about the properties and the nature of the defect in the samples and the adsorption extent of each modulated MOF were obtained.

B. Materials and Methods

1. Materials

All chemicals needed for the study were purchased and used directly as received. The zirconium chloride ($ZrCl_4$, 98%), and terephthalic acid ($C_6H_4(CO_2H)_2$, 99%), were obtained from Acros Organics. Acetic acid glacial ($C_2H_4O_2$, 99%), and trifluoroacetic acid were obtained from Fisher Scientific. Sodium arsenate dibasic heptahydrate, *N,N*-dimethylformamide (DMF, Analytical reagent grade), dichloromethane (DCM, Analytical reagent grade), sodium nitrate, sodium carbonate, sodium sulfate, sodium bicarbonate, sodium chloride, sodium formate, and sodium acetate were obtained from Sigma Aldrich.

2. Synthesis of the adsorbents

UiO-66 samples were synthesized under similar conditions to that reported in the literature with slight modifications by changing the ratio of acetic acid and trifluoroacetic

39

acid. Briefly, $ZrCl_4$(1.724g, 7.398 mmol), and terephthalic acid (1.230 g, 7.402 mmol) were dissolved in *N,N*-dimethylformamide (200 mL, 2582 mmol) by sonication for 10 min at room temperature. Following so, deionized water (0.4 mL, 22.2 mmol) and different ratios of modulators (details in Table1) were added to the mixture that was in a 500 mL autoclavable reagent bottle and put in a pre-heated oven at 120 °C for 3 days. The obtained microcrystalline powders were collected from the solutions by centrifugation and washed with 55 mL DMF three times separated by 3 hours' time interval, soaked overnight in the solution, and then washed three times with DCM for three days. After the washing procedure, the collected precipitate was dried in a vacuum oven at 100 °C overnight.

3. *Characterization of the adsorbents*

The 6 samples were fully characterized by scanning electron microscope (SEM/EDX), powder X-ray diffraction (PXRD), Brunauer–Emmett–Teller surface area analyzer (BET), Fourier-transform infrared spectroscopy (FT-IR), and thermogravimetric analysis (TGA). N_2 adsorption-desorption isotherms were measured using a Quantachrome-NOVA 2200e-Surface Area and Pore Size Analyzer that provided significant information concerning the effect of defect on the MOF. Scanning electron microscopy (SEM) imaging was done using a MIRA3 Tescan electron microscope after coating the samples with a thin layer (20 nm) of Platinum. Thermogravimetric analysis (TGA) was performed with a Netzsch TG 209 F1 Libra apparatus under a N_2/air flow from 30 to 1095 °C at a heating rate of 3 K·min⁻¹. Powder x-ray diffraction (PXRD) patterns of the MOF samples were recorded with a Bruker D8 advance x-ray

diffractometer (Bruker AXS GmbH, Karlsruhe, Germany, working at 40 kV and current 40 mA, 2θ range: 6-50°, increment: 0.02°) using Cu Kα radiation (k=1.5418 Å). The infrared (IR) spectra were collected on a FT-IR spectrometer Thermo-Nicolet in the transmittance mode, in the 450–3950 cm^{-1} range. Arsenic concentration was calculated using Atomic Absorption Spectroscopy (AAS) conducted with a Thermo Elemental Analyzer.

4. Arsenate adsorption experiments

Several parameters were changed for the sake of studying the effect of different experimental conditions on the Arsenate removal efficiency. The varying parameters ranged among pH, concentrations, contact time, and temperature. The arsenic solutions used were prepared by dissolving the appropriate mass of sodium arsenate dibasic heptahydrate in a certain volume of deionized water. All arsenic adsorption experiments were done at room temperature except for that involving temperature effect. For the pH, temperature and time effect experiments, 10 mL volume of the arsenate solution with an initial concentration of 100 mg·L^{-1} and 10 mg of activated UiO-66 MOF (6 different samples) adsorbents were placed in Falcon tubes shaken at the rate of 200 rpm for 3 hours.

First of all, kinetic study was done to determine the time of maximum adsorption where each tube was removed from the shaker at the allocated time from 2 minutes to 72 hours. The concentration of As (V) in the solution drops down till it reaches equilibrium after 3 hour.

For the pH effect experiment, each tube had a specified pH which ranged between 2 and 10. The exact pH values were controlled via 1M hydrochloric acid and 2M sodium hydroxide solutions. Whereas, for the temperature effect, every Falcon tube was placed at different temperature between 25 and 55 °C with 10 °C increment. To examine the effect of arsenic concentration on the adsorption capacities, 10 mL arsenate solutions of different concentrations ranging from 10 to 300 mg·L^{-1} (pH = 7.6) and 10 mg of activated UiO-66 MOF (6 different samples) were mixed in each tube. At the end of each experiment, the supernatant was filtered through a 0.20 µm filter and the remaining Arsenic concentrations of the filtrates were measured using atomic absorption spectroscopy.

The equilibrium adsorption capacity q_e (mg·g^{-1}) was calculated using the equation 1

$$q_e = \frac{C_0 - C_e}{m} \ V \ (1)$$

Where C_0 is the initial concentration of arsenate (in mg·L^{-1}), Ce represents the concentration of arsenate at equilibrium (in mg·L^{-1}), m is the mass of the MOF (in g), and V is the volume of the solution (in L).

5. *Arsenic adsorption in the presence of anions*

In studying the effect of anions on Arsenic adsorption, UiO-66-36TFA MOF that showed the highest adsorption capacity was chosen to be worked on. In brief, 7 falcon tubes (15 mL capacity) were used each containing 10 mg of the activated MOF, 10 mL of 60 ppm Arsenic solution and 10 mM of one of the following anions: NaCl, NaNO$_3$, Na$_2$CO$_3$, Na$_2$SO$_4$, NaHCO$_3$, CH$_3$COONa, and HCOONa. After 12 hours shaking at 25 °C,

the solution was filtered and the remaining Arsenic concentration was determined using atomic absorption spectroscopy.

6. Arsenic recycling

10 mL of methanol were added to 30 mg of the As-loaded MOF, and were constantly shaken for 12 hours. Then the recycled samples were dried out and 30 mg were tested with 10 mL arsenic solution of 150 ppm initial concentration. This process was repeated 3 times for the same sample.

C. Results and Discussion

1. Characterization

The experimental PXRD patterns of the six MOFs shown in Figure 2.1(A) are identical revealing sharp narrow peaks and matching perfectly with the reported one in the literature[53] without any additional peaks, confirming the high phase purity and crystallinity of the MOF samples. It is noteworthy to mention that the PXRD pattern of UiO-66-36TFA represented in Figure S1 showed the presence of an extra broad peak at $3.8°$ which is believed to correspond to the ordered missing cluster defects in the UiO-66 structure. The proposed defect is related to the reflected Bragg peak from (100) plane of the missing cluster defect due to the 3-periodic 8-connected reo net. To evaluate the surface area and the porosity of the synthesized MOFs, textural properties were examined by N_2 adsorption/ desorption technique at 77 K. The obtained isotherms are exposed in Figure 2.1(B) whereas the resulted Brunauer–Emmett–Teller (BET) surface areas, and

pore volumes are summarized in Table 2.1. All the MOF samples had similar type-I

behaviors that are in good agreement with the reported observations in the literature.

Depending on the type of modulator and its ratio, the resulting surface area and

porosity vary between the different samples. As expected, the surface area and porosity

were the lowest for the sample synthesized without any modulator and they increased as

the amount of modulator increased from one side, and as the acidity of the modulator

raised (pKa decreased) from another side in a way that they were higher for the samples

modulated with trifluoroacetic acid than that with acetic acid. These two factors showed

the important extent to which the characteristics of UiO-66 can be tuned by the addition of

acidic modulator. Quantitatively, the BET surface areas of the MOF samples differed

considerably, ranging from 1041 $m^2 \cdot g^{-1}$ (without any modulator) to 1690 $m^2 \cdot g^{-1}$ (with

TFA) and increasing in the trend mentioned above.

Table 2.1. Reaction conditions and Textural properties of the synthesized MOFs.

Samples	UiO-66-00	UiO-66-12AA	UiO-66-36AA	UiO-66-100AA	UiO-66-12TFA	UiO-66-36TFA
Number of moles of modulator (mmol)	-	88.8	266.4	740.2	88.8	266.4
Surface Area $(m^2 \cdot g^{-1})$	1041	1172	1295	1500	1546	1690

Pore volume $(cc \cdot g^{-1})$	0.32	0.37	0.41	0.43	0.46	0.52
Particle size (Average $\pm$ SD, nm)	99 $\pm$ 22	112 $\pm$ 18	171 $\pm$ 42	287 $\pm$ 39	120 $\pm$ 13	168 $\pm$ 26
Missing linkers number per Zr_6 formula	0.80	1.08	1.76	1.86	2.65	2.75
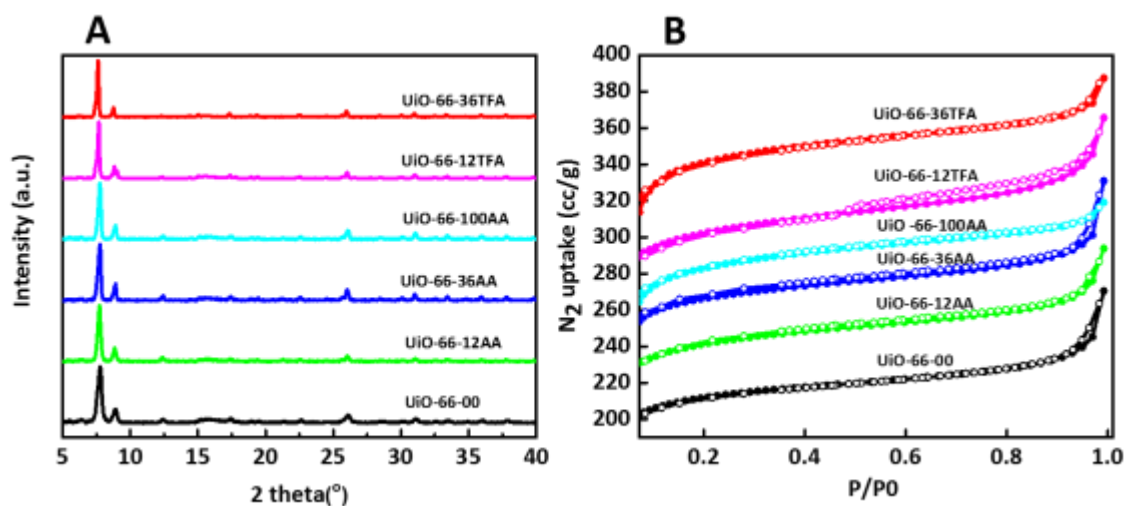
Figure 2.1. (A) X-ray diffraction analysis of the UiO-66 samples. (B) N_2 adsorption-desorption isotherms of the UiO-66 samples, Adsorption (filled circles); Desorption (empty circles).

The morphology of the crystals were investigated by HRSEM and representative images are depicted in Figure 2.2. The obtained micrographs show uniform octahedral shaped crystals of the samples of high modulator concentrations

(above 12 equivalents) indicating their homogeneity and high purity. The average

particle size of each sample was calculated through SEM images and the values are

represented in Table 1. Typically, adding 88.8 mmol of acetic acid (UiO-66-12AA)

resulted in irregular, aggregated, and smaller crystals with the size of 112 nm and it

increased with the increase in the amount of added acetic acid. However, adding the same

number of moles of trifluoroacetic acid gave relatively larger crystals of size 120 nm and

this size also elevated with the increase in the TFA amount to give well-defined

octahedral shape for UiO-66-35TFA.
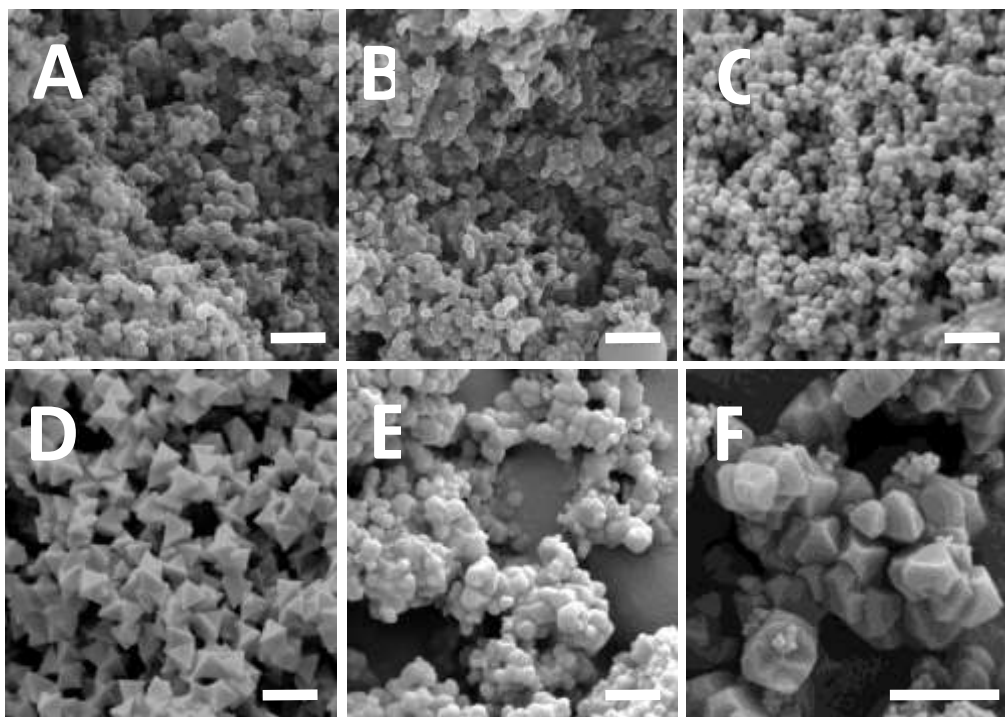
Figure 2.2. SEM images of the studied MOFs A(UiO-66), B (UiO-66-12AA), C (UiO-66-36AA), D (UiO-66-100AA), E (UiO-66-12TFA), F (UiO-66-36TFA) with a 1 μm scale bar.

Thermogravimetric analysis (TGA) was used to reveal the structural "imperfections" of the studied MOFs by calculating the number of missing linkers in each sample according to the method reported previously in the literature. The TGA curves for the six MOFs presented in Figure 2.3 are normalized and W_{end}, the end weight of the TGA run, is taken to be 100%. W_{theo} represents the theoretical weight loss plateau, W_{exp} is the experimental weight loss plateau, and Temp pl. is the temperature at which the plateau (W_{exp}) is reached.
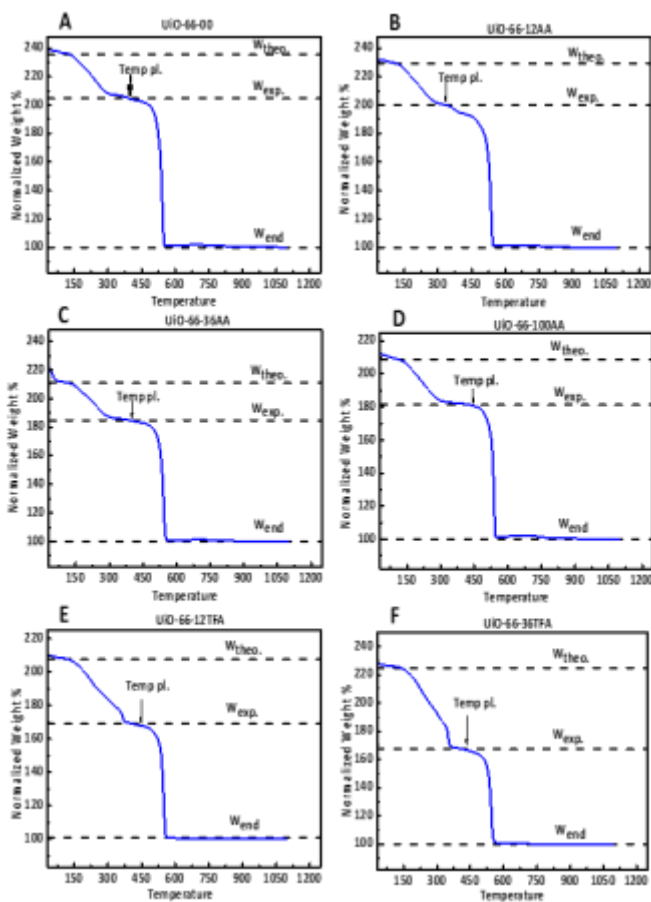
Figure 2.3. TGA curves of the studied MOFs A(UiO-66), B (UiO-66-12AA), C (UiO-66-36AA), D (UiO-66-100AA), E (UiO-66-12TFA), F (UiO-66-36TFA).Lower horizontal line (- -) represents the lower end of the theoretical TGA weight loss plateau (W_{end}), upper horizontal line (- -) represents the upper end of the theoretical TGA weight-loss Plateau (W_{theo}), middle horizontal line (- -) represents the upper end of the experimental TGA weight-loss plateau (Wexp).

By examining the six TGA curves, three weight losses could be observed in each one; the first weight loss is due to the removal of the adsorbed H_2O, and it occurs in the range of 35-100 °C which is a common temperature range for all the MOFs. The second step is the dehydroxylation of the Zirconium cluster and elimination of the monocarboxylate linkers and it extends from 100 °C till Temp pl. that is specific for each MOF. Temp pl. is the temperature of the combustion of the linker and it marks the beginning of the third step which is the framework destruction phase. Since Temp pl. is unique for each MOF, then the temperature range for the third step is different for each one. By analyzing Figure 2.3, the third weight decrease step of UiO-66-00 and UiO-66-36AA starts from 390 °C, whereas it was found to be 350 °C for UiO-66-12AA and 450 °C for the remaining three samples (UiO-66-100AA, UiO-66-12TFA, and UiO-66-36TFA). TGA is considered an effective tool in investigating quantitatively the defects present in the MOFs. The theory behind this is the fact that the number of missing linkers found in a structure is inversely proportional to the weight loss plateau related to linker combustion. That is, the higher the number of missing linkers, the lower the percentage of the linker mass relative to the total mass of the structure and thus the smaller the related weight loss plateau observed. The gap between the line representing W_{theo} and the one representing W_{end} and that between W_{exp} and W_{end} indicates respectively the theoretical and experimental weight losses attributed to the linker combustion. It could be noticed that the theoretical weight loss is greater than the experimental one assuring the fact that the samples are linker deficient. The number of missing linkers was than calculated for all samples and the obtained values are included in Table 2.1.

D. As Adsorption Study

1. pH Effect

After the synthesis and full characterization of the six UiO-66 MOF samples, their ability to be employed as adsorbents for arsenate removal from water was investigated. Taking into consideration the enormous effect of solution pH in the process of adsorption, as it not only influences the structure and surface charge of the adsorbent but also the various species of arsenate ions involved, several experimental batches were conducted to study the pH effect and thus to identify the optimal pH of arsenate adsorption.

Arsenate is pH dependent, for example, at pH below 2.1, the predominating form is H_3AsO_4, and as pH increases from 2.1 to 6.7, $H_2AsO_4^-$ becomes predominant. Finally, when the pH becomes greater than 6.7, the $HAsO_4^{2-}$ species invade.[92]

Getting into the details of the experiment, the MOFs were dispersed in arsenate solutions of pH values between 2 and 10 and the results are shown in Figure 2.4. As shown in the figure, all the MOFs except UiO-66-36TFA followed the same trend, the highest removal efficiency was at acidic conditions (pH = 2), then it dropped down to the minimum as pH increased to 4, to finally increase as pH increased to 10. On the other hand, UiO-66-36TFA showed approximately the same behavior among all pHs (decrease of 15%) indicating its stability and its independency on solution pH in the adsorption process.
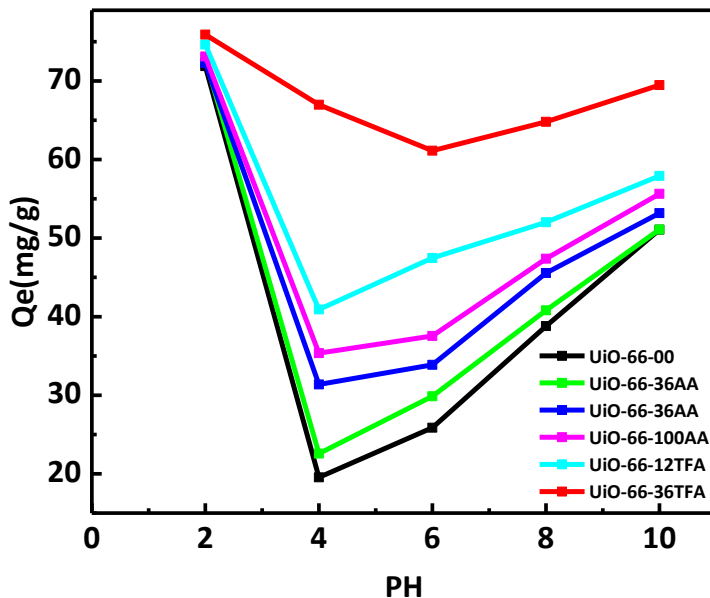
Figure 2.4. Adsorption of As at different pH values $C_\circ = 100$ mg $\cdot L^{-1}$, V = 10 mL, m = 10 mg, and t = 3 hours.

In order to study the surface charges of the different samples, Zeta potential was performed for UiO-66 and UiO-66-36TFA and the data are shown in Figure 2.5. Both MOFs showed the same zero point charge at pH= 4.3, which implies the positive charge of the adsorbents' surfaces below this pH and their negative charge above it. By comparing these data and that of arsenic predominant species at each pH, it could be concluded that electrostatic attraction played a certain role in this mechanism; for example, starting from 2.2 to 4.3 pH range, the uptake was high since the negatively charged arsenate were strongly attached to the positively charged surfaces of the MOF samples and decreased to the minimum at the zero point charge (pH= 4.5) because of the neutrality of the adsorbent surface. At pH = 2, the arsenate is in its neutral form (H_3AsO_4), so the adsorption was expected to be very low due to the absence of charge; however, it was noticed that the highest uptake was at this pH indicating that electrostatic

interaction wasn't the only controlling factor in the process. Arsenate ions attach to the

MOF via two coordination processes that are semi acid-base interaction in a way that

very acidic conditions favors the release of H^+ from H_3AsO_4 and thus increase its binding

to the hydroxyl sites in the sample. From the obtained graph, it can be seen that the

removal efficiency increased as the defect increased (ratio of modulator was greater or

the acidity of it was higher (lower pKa)); in other words the removal capacity was the

lowest for UiO-66 having no added modulator, it increased as acetic acid concentration

increased (UiO-66-12AA < UiO-66-36AA < UiO-66-100AA). Furthermore, all acetic

acid modulated MOFs showed lower adsorption ability than those modulated with TFA

and the highest efficiency was recorded for UiO-66-36TFA of highest defect. Despite all

of this and for practical reasons, all the thermodynamic and kinetic studies will be

performed at neutral pH.
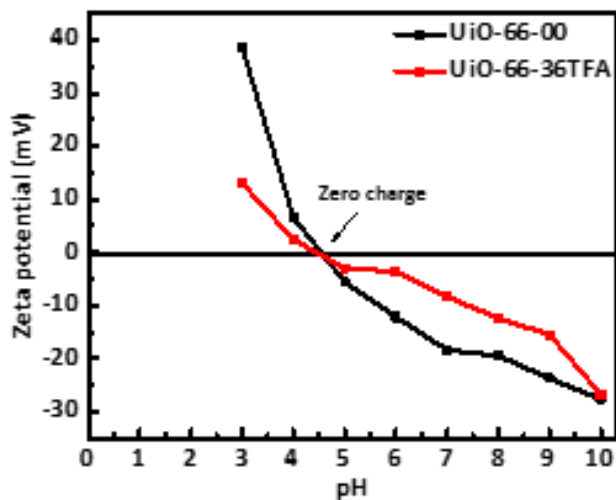
Figure 2.5. Zeta potential measurement at different pHs where the two MOFs showed the
same zero point charge at pH= 4.3.

2. Concentration Effect

The arsenate adsorption isotherms on the six MOF samples were performed over various concentrations of arsenic solution ranging from 10 to 300 ppm. In the six samples, the adsorption capacity increased as the concentration increased until it reached the saturation at 280 ppm. This attitude is justified by the fact that higher concentration gradient means larger mass transfer (more driving force). In addition, it provides more available arsenic ions in the vicinity of the active sites on the surface of the MOF, thus increasing the probability of surface adsorption. Concerning the variation in the adsorption capacities, it was noticed that also here the capacity increased as the defect increased. The collected data was investigated by Langmuir (equation 2) and Freundlich (equation 3) models, and plotted in Figure 2.6B and C for UiO-66-36TFA and in Figure A2-A4, for the remaining samples; whereas the parameters of the best fits are shown in Table S1.

$$\frac{C_e}{q_e} = \frac{C_e}{q_{max}} + \frac{1}{K_L q_{max}} \quad (2)$$

$$\ln q_e = \ln K_F + \frac{1}{n} \log C_e \quad (3)$$
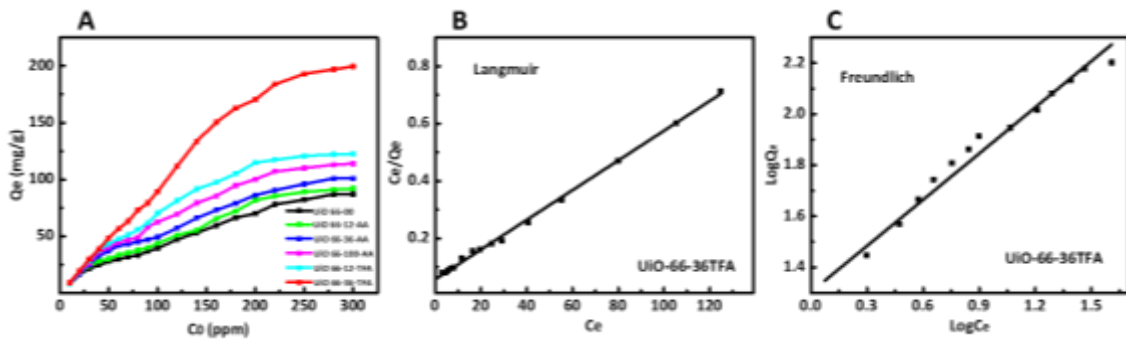
Figure 2.6. (A) Arsenate removal by modulated MOFs at different concentrations (10 mg·L^{-1} ≤ [As] ≤ 300 mg·L^{-1}) from water, (B) Data fitting using Langmuir and (C) Freundlich models for UiO-66-36TFA.

Where q_e (mg·g^{-1}) is the adsorbed quantity at equilibrium, C_e (mg·g^{-1}) is the concentration at equilibrium, q_{max} represents the maximum adsorption capacity, K_L (L·mg^{-1}) is an equilibrium constant linked to the binding strength, n and K_F (L·mg^{-1}) are Freundlich constants that express the adsorption capacity and adsorption intensity, respectively. The highest correlation coefficient (R^2) determines the type of isotherm, in the six samples, Langmuir model had the greater R^2 indicating a monolayer process (Figures A2-A4). Surprisingly, UiO-66-36TFA had the highest uptake not only among the 6 tested samples (200 mg·g^{-1}), but also among all reported MOFs and most of the commercial and synthetic adsorbents as summarized in Table 2.2.

This proved the importance of defect control in the adsorption process making defected UiO-66 samples a great prospective for water treatment.

Table 2.2. Comparison of arsenate adsorption among prevailing adsorbents

Adsorbent	Max. adsorption capacity (mg·g^{-1})	Ref.
Aluminium-loaded Shirasu-zeolite	5.63 at pH 7	[147]
Calcined mesoporous silica	11 at pH 7	[148]
Fe-BTC	12.3 at pH 4	[149]
Commercial TiO$_2$	14.2 at	[150]
Activated alumina grains	15.9 at pH 5	[151]
MIL-53(Fe)	21.3 at pH 5	[152]
Zirconium oxide	45 at pH 7	[153]

HT-Zn-MOF-74	48.7 at pH 7	[68]
ZIF-8	60 at pH 7	[154]
Amorphous zirconium oxide Nanoparticles	95 at pH 2	[155]
RT-Zn-MOF-74	99 at pH 7	[68]
AUBM-1	103.1 at pH 7	[68]
MIL-53(Al)	105.6 at pH 8	[156]
Zirconium immobilized nano-scale carbon	110 at pH 2	[153]
UiO-66-NH$_2$ treated with HCl	161.3 at pH 7	[157]
β-FeOOH NRs/CF	172.9 at pH 6	[158]
Zirconium based nanoparticle	256.4 at pH 3	[159]
UiO-66	303.3 at pH 2 147.7 at pH 7	[92]
UiO-66-00	89.3 at pH 7	This study
UiO-66-12AA	93.3 at pH 7	This study
UiO-66-36AA	103.0 at pH 7	This study
UiO-66-100AA	129.0 at pH 7	This study
UiO-66-12TFA	138.4 at pH 7	This study
UiO-66-36TFA	200.0 at pH 7	This study

3. Temperature Effect

Temperature is a crucial factor to be studied in the process of waste water treatment, keeping in mind the fact that polluted water is released by industry over different temperatures. Figure 2.7 represents the effect of temperature on arsenic adsorption experiments.
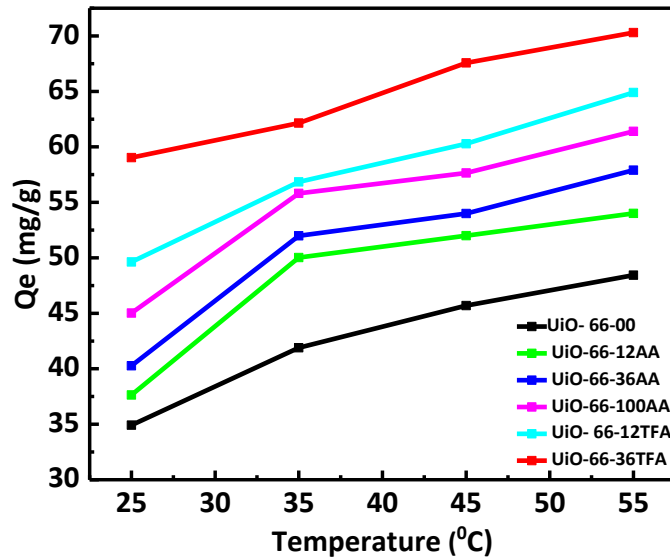
Figure 2.7. Adsorption of As at different temperatures. C_o = 100 mg·L^{-1}, V = 10 mL, m = 10 mg, and t = 3 hours.

Two trends were observed, the first one is represented by the increase in the adsorption capacity as the temperature increased, where the highest capacity was for UiO-66-36TFA and increased from 58 mg·g^{-1} to 70 mg·g^{-1} as temperature increased from 25 °C till 55 °C. While the second trend showed high capacities with increasing the MOF defect (increasing modulator acidity or modulator ratio).

In studying the thermodynamics of the reaction, Van't Hoff equation (equation 4) was used to calculate the adsorption enthalpy ($\Delta H°$) and entropy ($\Delta S°$):

$$\ln K_L = \frac{\Delta S^\circ}{R} - \frac{\Delta H^\circ}{RT} \quad (4)$$

Where K_L is the equilibrium constant calculated using the formula $K_L = qe/Ce$ (L·g^{-1}). By

plotting lnK vs. 1/T as shown in Figure S5, the enthalpy and the entropy of the various

MOF samples are illustrated in Table 2.3.

After calculating the values of entropy and enthalpy, Gibbs free energy was calculated

from equation 5 and the results were represented in Table 2.3.

$$\Delta G^\circ = \Delta H^\circ - T\Delta S^\circ \quad (5)$$

Table 2.3. Thermodynamic parameters of arsenate adsorption over the synthesized
samples at different temperatures.

	ΔH° (kJ·mol^{-1})	ΔS° (J·mol^{-1}·k^{-1})	ΔG° (kJ·mol^{-1})			
			298 K	308K	318 K	328 K
UiO-66-00	15.12	45.87	1.45	0.99	0.53	0.074
UiO-66-12AA	16.11	51.07	0.89	0.38	- 0.13	- 0.64
UiO-66-36AA	19.56	62.59	0.91	0.29	- 0.34	- 0.97
UiO-66-1000AA	18.04	59.07	0.43	- 0.16	- 0.75	- 1.34
UiO-66-12TFA	16.66	55.94	- 0.011	- 0.57	-1.13	- 1.69
UiO-66-36TFA	14.06	50.06	- 0.86	-1.36	-1.86	-2.36

For all samples studied, the change in enthalpy (ΔH_{ads}) are calculated to be

positive and within the same range (14.06 and 19.56). Because of their positive values of

all the samples, it can be deduced that the process of arsenate removal is an endothermic process, taking place on the surface of the samples (mostly Physisorption on the surface), and due to strong interaction forces between the arsenate anions and the Lewis acid sites or the Brønsted acid sites created by the defects on the frameworks as fully developed in the introduction. Concerning ΔS°, its positive value (ranging from 45.87 and 62.59) shed the light on the randomness of solid/solution interface and on the raise in the degree of freedom of the arsenate being adsorbed.

Finally, concerning the values of ΔG, the results were interesting. All ΔG° for the non-defected UiO-66 sample were positive and started to decrease as the defect increased till they became negative at all temperatures for both TFA modulated samples with the lowest ΔG° (highest in magnitude) for the most defected UiO-66-36TFA MOF. These negative values demonstrate a great implication on the spontaneity of the adsorption process and the increasing trend assured the importance of defect in making the adsorption reaction spontaneous for enhanced arsenic adsorption. This is explained by the fact that more defected samples have more exposed open metal sites for the arsenate ions to be attached on.

4. Kinetics study

In order to investigate the mechanistic aspects of the arsenate adsorption, practical understanding of the arsenate adsorption kinetics on the various defected UiO-66 samples must be acquired and the equilibrium of the adsorption process must be determined. To study the adsorption rate of the adsorbents with increasing defect toward arsenate, the arsenate uptake as function of contact time was studied and the obtained results are shown in Figure 2.8A. With time, the remaining arsenate concentration

declined until it reached equilibrium. By analyzing the kinetic curves, it could be noticed that the adsorption was fast at the beginning when the concentration gradient was high and slowed down as time passed by. It can be also clearly seen, that higher and faster adsorption was observed for the highly defected sample which can be explained by the fact that more adsorption sites are available in UiO-66-36TFA structure. To explore deeply the mechanism of adsorption, pseudo-first-order (equation 6) and pseudo-second-order (equation 7) kinetic models are used to extract the kinetic parameters of the adsorption process.   Briefly, the pseudo-first-order model proposes that the rate of variation in the solute concentration with time and the variation in the adsorbent concentration in addition to the quantity of adsorbate over time are logarithmically proportional. However, the pseudo-second-order model suggests that the adsorption capacity of the adsorbent is directly proportional to the number of active sites occupied on it.

$$\ln(q_e - q_t) = \ln q_e - k_1 t \quad (6)$$

$$\frac{t}{q_t} = \frac{1}{k_2 q_e^2} + \frac{t}{q_e} \quad (7)$$

Where q_e (mg·g^{-1}) is the equilibrium adsorption capacity found experimentally, q_t (mg·g^{-1}) is the adsorption quantity at time t, and k_1 (min^{-1}) and k_2 (g·mg^{-1}·min^{-1}) are the pseudo-first-order and pseudo-second-order rate constants respectively.

The fitted data for UiO-66-36TFA is given in Figure 2.8 B and C whereas for the remaining MOFs data fits are shown in Figures A8- A10. The resulted parameters are summarized in Table A2.
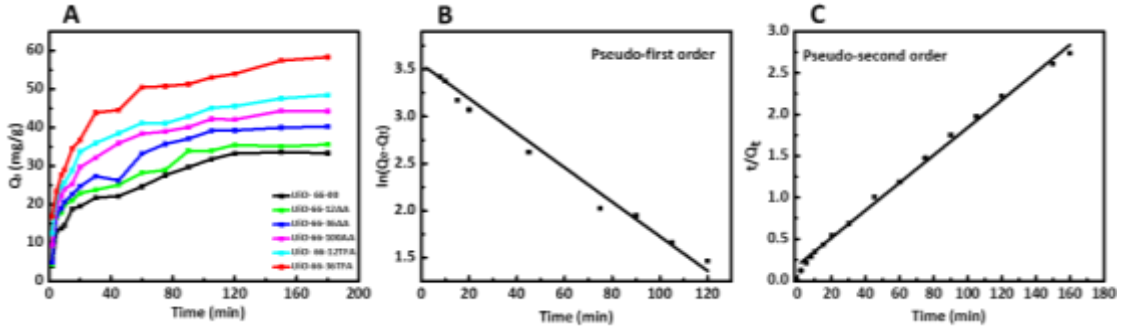
Figure 2.8. (A) Arsenate uptake as a function of contact time, (B) Pseudo-first-order fit for UiO-66-36TFA, (C) pseudo-second-order fit for UiO-66-36TFA. $C_\circ = 100$ mg·L^{-1}, V = 10 mL, m = 10 mg and T = 25 °C.

For all the MOF samples, the correlation coefficients (R^2) of the pseudo-second-order model had greater value than pseudo-first-order, and the calculated equilibrium capacity q_e was found to in good agreement with the experimental one. The obtained results indicate that the kinetics of adsorption followed the pseudo-second order model. This implies that the chemisorption process is forceful and the arsenates are greatly adsorbed on the surface.

For better analysis of the overall rate of the adsorption process, an intra-particle diffusion model[160] was developed through equation 8

$$q_t = k_{id}.t^{1/2} + \theta \quad (8)$$

Where k_{id} represents intra-particle diffusion rate constant (mg (g·min$^{1/2}$)$^{-1}$), and θ is a constant linked to the thickness of the boundary layer (mg·g^{-1}) which increases with θ. The plots of q_t against $t^{1/2}$ for all samples are displayed in Figure A9 and show that the rates of adsorption are obviously three step-controlled process (multistage controlled). The adsorption process starts with the diffusion of arsenate to the surface of the MOF (external surface adsorption) followed by the progressive adsorption of arsenic ions in the

59

samples (intra-particle diffusion) and the third step is due to diffusion of arsenate on the binding sites of the MOFs till equilibrium is reached (intra-particle diffusion starts to slow down). The rate constants of the three linear steps for each sample were calculated from the slope of the intra-particle diffusion and represented in table S1. Interestingly, UiO-66-36TFA showed the highest values for the three rates assuring the high arsenate uptake by comparison to other MOFs. Add to that, the first step is the fastest one of the highest rate, whereas the last step is the slowest one. Therefore, the external diffusion is the fastest step and the intraparticle diffusion is the rate determining one.

5. *Mechanism of the arsenate uptake*

As mentioned in all above experiments, the arsenate uptake always followed a certain trend and this was due to the missing linker defects that dominate the UiO-66 MOFs modulated with monocarboxylic acids. First of all, the origin of defects must be understood where they are compensated by a group of modulators. Theoretically, during the synthesis procedure, the linker and the modulator compete for carboxylate (CO_2^-) sites on the MOF cluster ($Zr_6(OH)_4O_4(CO_2)_{12}$); however, to generate missing linker defect, the modulator must deprotonate before coordinating with the MOF and must bind to at least 1 of the 12 sites on 12 different clusters that are close to each other. As the ratio of the competing modulator increases, the probability of modulator remaining linked to the cluster raises, and thus more missing linker defect can be obtained. Moreover, more acidic modulator (lower pKa value) has higher deprotonation ability and thus more defected framework.

It has been demonstrated that the first adsorption pathway for arsenate by a non-defected UiO-66 is the μ3-O through anion exchange with the bridging hydroxyl groups on the Zr-cluster, which results in the formation of four Zr-OH groups in a unit Zr_6 cluster (Figure 2.9).

However, in a highly defected UiO-66 structure, the preferred pathway for arsenate uptake by UiO-66 structure is most likely via adsorption on the missing linker sites on the Zr_6 nodes via a singly or doubly coordination mode (Figure 2.9). After filling these sites, secondary binding pathways are possible, by exchanging certain BDC linkers with arsenate leading to the formation of arsenic complexes in the MOF framework and thus by increasing the defects number, more free sites become available for arsenate to bind to Zr cluster which explain the fast and high uptake capacity of UiO-66-36TFA.
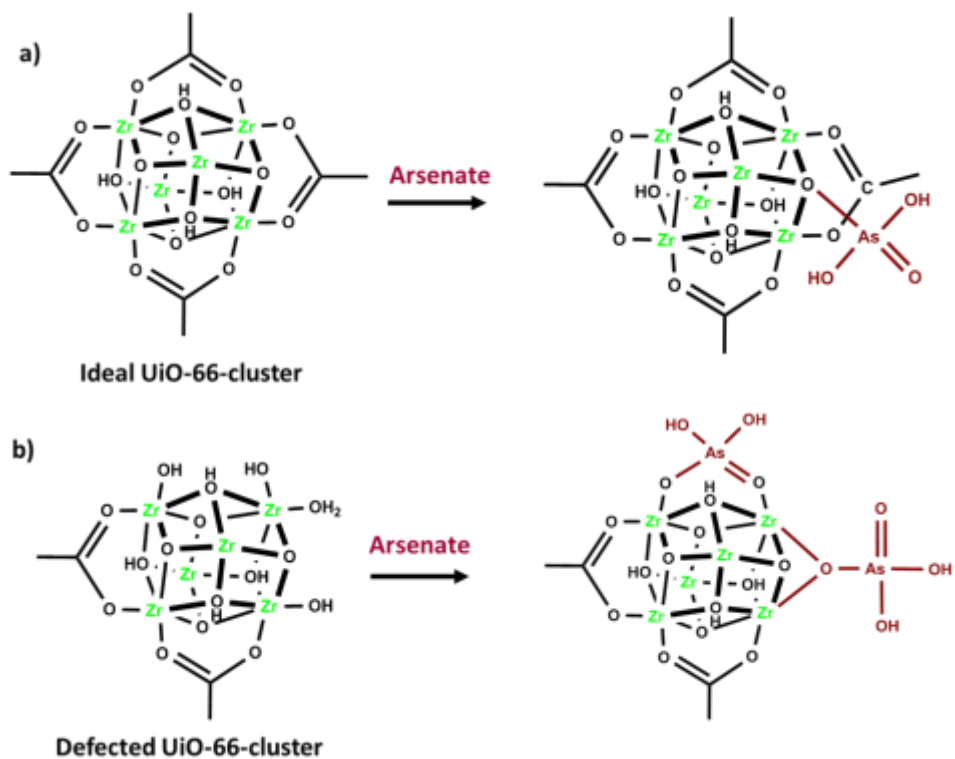
Figure 2.9. Possible mode of Adsorption of Arsenate on the ideal Zirconium cluster (a) and the defected one (b).

With this in mind, it is clear now why the arsenate removal increased as the defect increased whether by increasing the acid amount or the acidity of the modulator since less linker molecules were found and thus more available free sites for As (V) to attach. This is assured in Figure 2.10A where the arsenate uptake increases proportionally to the number of missing linkers. Figure 2.10B shows the change in the maximal arsenate uptake as function of the particle size. The size follows a certain trend within the samples made with the same modulator, however it is not the case by comparing all of the samples with each other. In other words, it is probably that there is no strong relationship between the particle size and the adsorption capacity indicating that the adsorption on the surface of the MOFs isn't the main driving force for the process.

However, other factors could have contributed to this increase in the uptake capacity.

Figure 2.10C and D represent the variation in the adsorption capacity compared to that of

the BET surface area and pore volume respectively for the studied samples. Having large

pore volume and high surface area are two of the most interesting characteristics in

MOFs. In theory, this means that more free acid sites exposed to the arsenate molecules,

thus higher adsorption. It is clear from the obtained trends that As uptake increases with

surface area and pore volume of the studied samples. From these data, It could be

suggested that high surface area, large pore volume and high defect density are important

parameters for the development of efficient As adsorbents.
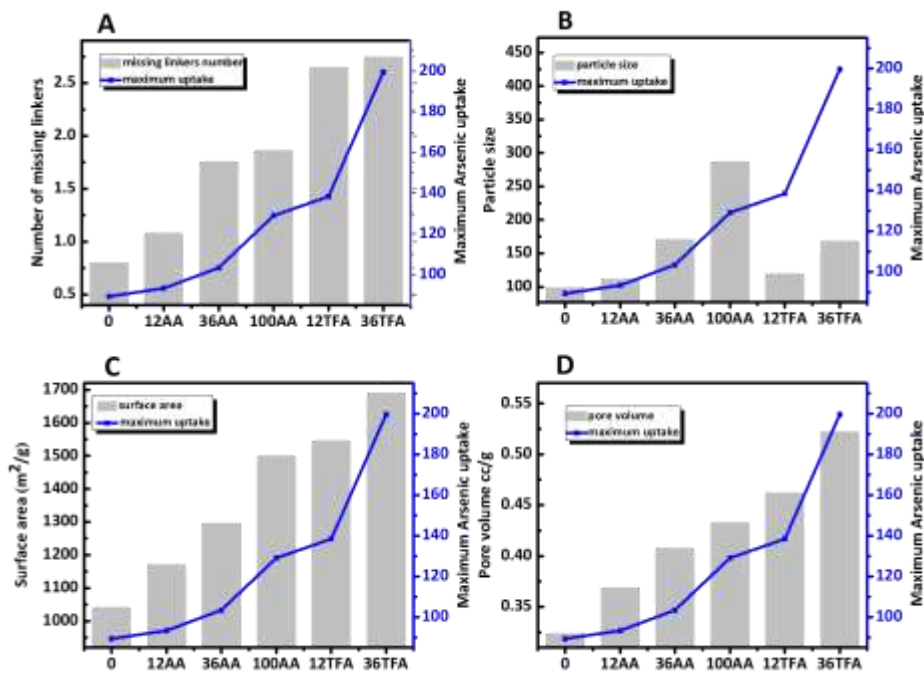
Figure 2.10. Effect of missing linkers (A), particle size (B), surface area (C), and pore
volume (D) on the maximal Arsenic uptake.

6. Removal of Ultratrace (ppb) Arsenate

Since arsenate found in drinking water is found at the ppb (part per billion) level, removal of low concentration As (V) by the defected MOF samples was tested using the most defected MOF sample (UiO-66-36TFA) and compared to the UiO-66 sample. To this end, 3 batches were prepared each of different mass of the six samples (5, 10 and 15 mg) separately added to 5 mL of 50 ppb arsenate solution. Interestingly, all the arsenate ions were removed in all the tested samples regardless of the type and amount of adsorbent used. To further investigate their capacities on lower concentration level, 5 mg of each adsorbent was added to 5 ppb arsenate solution. Surprisingly, this small amount of all the MOFs was able to eliminate all the arsenic species in the solutions. These great results pushed us toward further investigation for the parameters of ultratrace arsenate removal, so an additional experiment using much lower masses of the adsorbents (0.01-2 mg) to remove 5 ppb concentration of arsenate. The obtained results are given in Figure 2.11, and show that as the uptake percentage was directly proportional to the adsorbent mass. The arsenate removal percentage increased from 80 % to 100 % for UiO-66-36TFA as the mass increased from 0.01 mg to 0.5 mg. However, 1 mg of the non-modulated MOF was needed to accomplish 100% As removal.

This result demonstrates that UiO-66-36TFA showed not only higher elimination percentage than the non-modulated UiO-66, but also reached the equilibrium (100% removal) at lower mass (0.5 mg) that is half the mass UiO-66 needed to reach the full adsorption (1 mg).
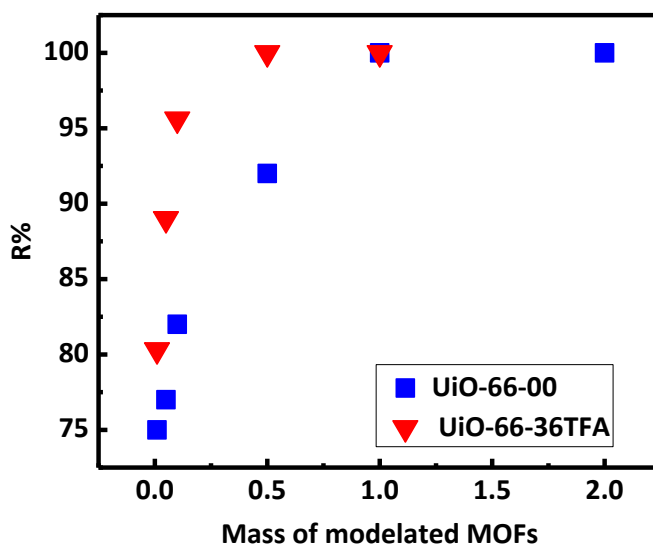
Figure 2.11. Effect of the mass of UiO-66-00 and UiO-66-36TFA on the removal efficiency of As solution at low concentration (5 ppb). M = 0.01, 0.05, 0.1, 0.5, 1.0, and 2.0 mg, V = 5 ml.

7. Post Adsorption Characterizations

The used samples of UiO-66-36TFA after the adsorption were investigated by

FTIR, PXRD, TGA, and SEM-EDX. Adsorption of Arsenic was confirmed by FTIR as

presented in Figure 2.12A where a new peak was observed at 864 cm^{-1} that is related to

the combination of both symmetric and asymmetric stretching vibrations of the As-O

bond. Moreover, the peak at 1020 cm^{-1} which is attributed to the vibrations of O-H

groups on Zr-cluster (Zr–OH) decreased in intensity in the sample after As adsorption,

which means that these OH groups were engaged in the adsorption process. The PXRD

patterns of the MOF after adsorption of Arsenic presented in Figure 2.12B comply

perfectly with the one before adsorption, assuring the well-retained crystallinity and high

stability of UiO-66 MOF structure. Moreover, SEM-EDX image shown in Figure A10

reveals the presence of As on the surface of the crystals in addition It shows the

reservation of the framework morphology after the adsorption of arsenic species within the UiO-66 framework. By comparing the TGA analysis for the sample before and after adsorption found in Figure 2.12C, two decomposition steps that are related to the adsorption of arsenate were observed and a higher mass is left at the final stage of analysis corresponding to the remained non-volatile arsenic oxide.

The above data shows great evidences for the strong interactions between arsenate and the MOF adsorbents which are in good agreement with kinetic and thermodynamic studies.
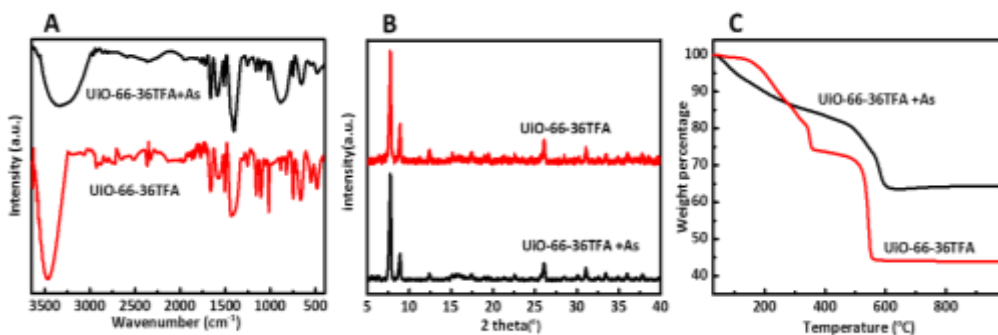
Figure 2.12. (A) IR spectra, (B) PXRD patterns, and (C) TGA curves for UiO-66-36TFA before and after As adsorption.

8. *Anionic coexistence experiments*

To study the practicability of the synthesized samples in real life water treatment application, other anionic interactions that are coexisting in water must be taken into consideration because of the ability of competing with arsenate for the sorbent adsorptive sites. Accordingly, arsenic removal experiments were conducted in the presence of the following anions separately: sodium nitrate, sodium carbonate, sodium sulfate, sodium

bicarbonate, sodium chloride, sodium formate, and sodium acetate. As displayed in Figure A11, the presence of these anions didn't cause any significant change in the arsenate uptake except in the case of sodium carbonate. This non-effective action indicated the preferable affinity for arsenate over these coexisting anionic species. However, sodium carbonate decreased the uptake to less than half that without any added anion and this could be attributed to the competition between arsenate and carbonate ions for the same available adsorption sites that are found on the surface of adsorbents.

9. *Reusability test*

Investigating the reusability of the studied sorbent is of crucial importance; in particular, UiO-66-36TFA of greatest defect was studied. While choosing the regenerant, certain properties must be taken into consideration including the efficiency of their desorbing capacity, keeping the adsorbent surface non-damaged, and cost effectiveness. The best regenerant tested was methanol. After collecting the post adsorbing MOF samples, they were treated with fresh methanol several times to desorb arsenate from the MOF material before being dried out well in the vacuum oven for the following run. The adsorption test was repeated two more times where in each cycle, the same adsorption capacity was attained without any decrease in uptake amount as shown in Figure 2.13 Therefore, UiO-66-36TFA can be used as a potential recyclable adsorbent for Arsenate elimination.
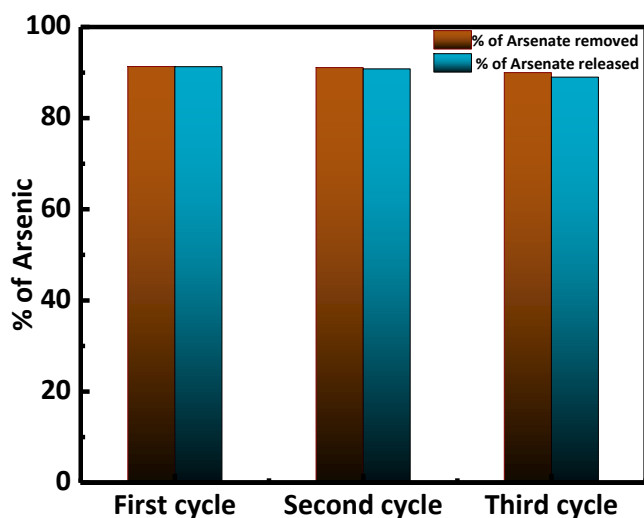
Figure 2.13. Removal of As from water after regeneration of UiO-66-36TFA for three cycles. $C_0 = 150$ mg·L^{-1}, V = 10 mL, m = 30 mg.

E. Conclusion

To summarize, Zirconium based MOFs with adjusted defects have been successfully synthesized and fully characterized. Their ability to remove arsenic from water was evaluated and discussed by according to the structural features of the synthesized MOFs. After studying the sample properties and performing the adsorption experiments, it was concluded that UiO-66-36TFA, which was the most defected sample, showed the highest arsenate adsorption (200 mg·g^{-1}) not only among its competitors but also among all previously reported arsenate adsorbents. In addition, the enormous performance of these adsorbents in real water samples demonstrated their feasibility for practical applications. Examining their phenomenal characteristics, simple fabrication procedure, high crystallinity and chemical stability, impressive arsenate removal, fast

kinetics, and perfect regeneration/recyclability, made them of great potentials toward

being the best compelling candidate for arsenate purification from drinking water.

CHAPTER III

PALLADIUM-MOF COMPOSITES AS CATALYSTS
FOR REDUCTION OF NITRATES/NITRITES
IN DRINKING WATER

A. Introduction

With the discovery of metal-organic frameworks (MOFs), a new generation of hybrid organic-inorganic porous materials attracted lots of attention. Based on the combination of inorganic building blocks with organic molecules, networks with high accessible pore volumes and quasi infinite structural possibilities can be created. Moreover, the porosity enables the infiltration and stabilization of metal nanoparticles (NPs), while the well-defined structure and the tunable functionality of both the metal cluster and the organic linker provides relevant characteristics for molecule specific selectivity. These properties opened up new prospects for investigations in the field of catalysis and other applications, such as chemical sensing or energy conversion and storage. However, the precise control of the NPs inside the host framework with respect to size, shape, spatial distribution and composition is challenging. Diverse efforts towards the synthesis of NP-MOF systems by the utilization of post-synthetic loading of precursors, including solution and vapor based techniques, have been conducted and yielded promising systems with homogeneously distributed and small sized NPs.

Nitrate pollution is one of the most important issues in water quality.[161] Different parts of the world have been facing the problem of nitrate contaminated surface and groundwaters.[162] The World Health Organization (WHO) have developed some

regulations and guidelines regarding NO_3^- accumulation in ground waters. The guideline values for NO_3^- and NO_2^- in drinking water dictated by the WHO are 50 and 3 mg/L, respectively. Several nations have also limited the maximum NH_4^+ levels The removal of NO_3^- from water has been traditionally carried out by biological nitrification-denitrification which is a well-known, effective and cost-effective method. However, this method is not recommended for the treatment of drinking water because of the risk of biological contamination. Some other technologies based on the reduction of NO_3^- such as advanced reduction processes have also been tested recently.[163] The catalytic reduction of NO_3^- is one of the more suitable for drinking water to 0.5 mg/L[164] technologies for the potabilization of ground water polluted with NO_3^-. It uses H_2 as reactant in the presence of a metallic catalyst containing a noble metal from group VIII, usually palladium, for the conversion of NO_3^- to N_2.[165]

In this chapter, we investigate the use of UiO-66 and its functionalized derivatives (UiO-66-NH$_2$ UiO-66-2COOH) as highly porous and/or functionalized substrates for Pd Nps loading to produce composite catalysts for the the catalytic reduction of NO_2^- and NO_3^- in the presence of H_2. To this end, a series of functionalized Pd-MOFs composites are synthesized using different loading methods including impregnation and encapsulation. The full characterization of the composites are provided and the initial testing results are presented. The prepared Pd-UiO-66 composites show promising catalytic activities for nitrite reduction. Furthurmore, the removal capacities of Nitrites/Nitrates from water can be controlled by adjusting the Pd NPs content in the composites and by varying the functional group of MOFs.

B. MOFs as hosts for nanoparticles

Since the development of nanoparticle-MOF composites several examples in this field have been reported, most of them are summarized in diverse review articles.[166-168] Generally, the formation of inorganic NPs inside the porous structure of MOFs can be achieved by two different approaches. The first one known as "ship in a bottle" concept comprises the post-infiltration of the existing framework with the guest molecules and subsequent reduction or decomposition of those, while the second one can be described as "ship around a bottle" method (or template synthesis) with an assembly of the MOF around active species in situ.[169]

Metal-on-MOF materials can be divided into different classes with respect to the nanoparticle location and size.[168] Depending on the synthetic methods used, it is possible to control the resulting class of hybrid material to a certain degree. Until now a common designation for the classification of metal-MOFs was only provided by Meilikhov et al.[168]

C. Preparation Techniques of NP-MOF composites

There are two main synthesis techniques used to incorporate nanomaterials within MOFs: impregnation and encapsulation. Impregnation indicates that the nanoparticles are formed within the MOF pores, whereas encapsulation describes the crystallization of the MOF around preformed nanomaterials. Additionally, several alternative nanomaterial incorporation methods have been reported.
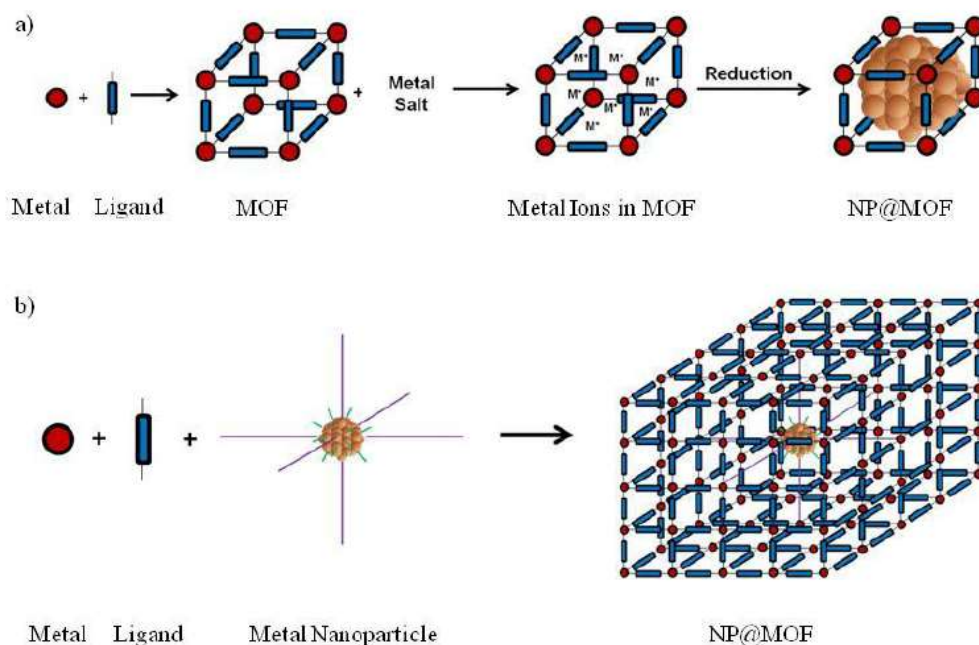
Figure 3.1. Illustration of MOF composite synthesis via (a) impregnation and (b) encapsulation.

1. Impregnation

As illustrated in Figure 3.1, the impregnation technique occurs in three steps: (1) the preparation and activation of the MOF; (2) the infiltration of a metal precursor into the preformed MOF pores; and (3) the reduction, oxidation, or decomposition of the metal precursor. There are several predominant infiltration methods used for preparing NP-MOF via impregnation: solution impregnation,[171] the double solvent approach,[172] incipient wetness impregnation,[173] hemical vapor deposition,[174, 175] and solid grinding.[176] After infiltration, the metal precursor is either oxidized[175] or reduced using UV irradiation,[172] redox-active MOFs,[174, 176] or chemical reducing agents such as NaBH$_4$[171] or H$_2$.[174] Studies have shown that the infiltration method influences NP-MOF properties

73

such as metal loading and nanoparticle location. For instance, solvent-based infiltration methods are limited by the solubility of the metal precursors, competitive incorporation of the metal and solvent in the pore space, and solvent desorption, which causes the precursors to deposit on the surface of the MOF.[177]

Overall, the impregnation technique offers both advantages and limitations. The most notable advantage is the utilization of the uniform pore size distribution to quench nanoparticle growth, which stabilizes the particles in the MOF pores and yields nanoparticles with the size and shape of the MOF pores. Theoretically, impregnation offers a method for controlling nanoparticle size and shape by exploiting the extensive collection of MOF structures, specifically the various pore structures, to tune the nanoparticle properties. However, there are several limitations. First, strong interactions between the nanoparticles and the MOF are often necessary to control the particle location and limit growth. There are only a limited number of MOFs known to sufficiently interact with the particles in order to limit particle mobility and growth. Often, functional groups are necessary to sufficiently immobilize the metal nanoparticles within the pores to limit particle aggregation on the surface.[178] Second, many MOFs are microporous, which is advantageous for gas separation; however, the metal precursors are often too large to diffuse within the micropores limiting the framework selection. Third, the high temperatures and reduction procedures can destroy the MOF structure and porosity.[174, 176] Finaly, the particles block the pores, reducing the available surface area and pore volume.[176]

2. Encapsulation

As depicted in Figure 3.1, encapsulation describes the growth of the MOF on and around preformed nanomaterials. The preformed nanomaterials, either functionalized with a surface-assembled monolayer (SAM)[179] or "naked,[180]" are incorporated with the MOF precursors and crystallization proceeds around the nanomaterials. There have been several MOF synthesis procedures used to encapsulate nanomaterials, mainly: solvothermal, microwave, sonochemical or ultrasonic, mechanochemical, and room temperature crystallization.[181]

Encapsulation has the potential to overcome many of the limitations presented by impregnation. Specifically, growing the MOF around the nanomaterial adds the nanomaterial to the framework, rather than trapping it within the pores. The specific surface area of the composite will still be reduced relative to the parent MOF because of the increased density. Also, by starting with preformed, stabilized nanomaterials, the complete collection of MOF structures can, theoretically, be utilized since specific MOF chemistry is not required to quench and immobilize the NPs. Finally, the greatest advantage of encapsulation is the capability to incorporate nanomaterials that exceed the MOF pore size,[179] which means that nanomaterials designed for specific applications can be coupled with the MOF support.

There are extensive studies of nanomaterials that demonstrate the ability to tune the optic, electric, magnetic, and catalytic properties by controlling the size, shape, composition, and structure of the materials.[182] Furthermore, the catalytic activity is strongly dependent on the nanoparticle diameter.[183] The nanomaterial shape is also influential. For instance, palladium can be shaped into nanocubes,[184] nanorods,[185] and nanoplates.[186] Therefore, the

synthetic control and understanding of nanomaterials is available, and by using the

encapsulation technique, well designed nanomaterials can be coupled with MOFs to

engineer chemically unique nanoporous materials.
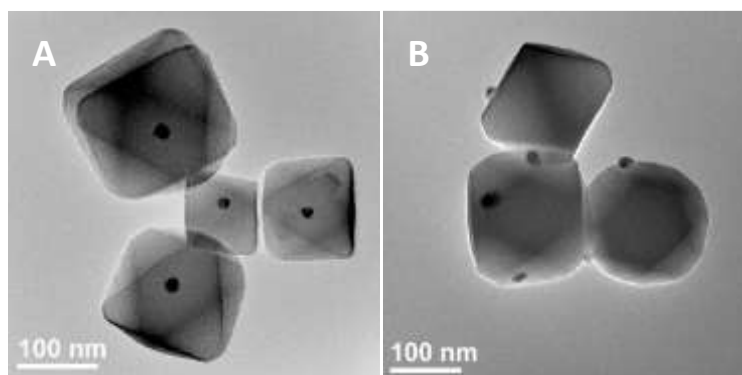
Figure 3.2. TEM images of (A) Cu Nanocrystales NC inside UiO-66, (B) Cu on UiO-66.[187]

D. Materials and Methods

1. Materials

The organic linkers used are terephthalic Acid (99 %, Acros Organics), 2-

Aminoterephthalic Acid (99 %, Sigma Aldrich) and 1,2,4,5-benzenetetracarboxylic acid

(96 %, Sigma Aldrich). All these chemicals were used directly without further

purification. The zirconium chloride (98 %, Acros Organics) and zirconium oxychloride

(98 %, Acros Organics), served as the metal salts in the MOF synthesis. Dimethyl

formamide (DMF, Analytical reagent grade, Fisher Scientific) was used as a solvent in

the MOF production and for their washing later on. Dichloromethane (DCM, Analytical

reagent grade, Fisher Scientific) was used for the second stage of MOFs washing. Acetic

Acid (99 %, Acros Organics) and Formic Acid (98-100%, Fisher Scientific) served as

modulators in the synthesis of MOFs. For the palladium loading, Etanol (99 %, pure, Acros Organics) were used as a solvent. Palladium chloride (37 %, Acros Organics) were used as precursor.

2. Synthesis of UiO-66

The MOF was synthesised in 500 mL autoclavable reagent bottle where terephthalic acid (510 mg, 5,1 mmol) was dissolved in 285 mL of DMF and the mixture was sonicated for 10 minutes. Then $ZrCl_4$ (795 mg, 5,1 mmol) was added to the solution and the mixture was sonicated for further 10 minutes. 15 mL of Acetic Acid was then added to the solution and the reaction mixture was placed in a preheated oven at 120°C for 52 hours. The precipitated white powder was washed using DMF (3 times for three days) and then DCM (3 times for three days). The product was then collected by centrifugation and dried under dynamic vacuum overnight at 85°C.

3. Synthesis of UiO-66-NH$_2$

In 500 mL autoclavable reagent bottle, 412 mg of 2-aminoterphtalic acid was dissolved in 190 mL of DMF and the mixture was sonicated for 10 minutes. 530 mg of $ZrCl_4$ were then added to the solution that was sonicated for another 10 minutes before the addition of 10 mL of acetic acid. The mixture was sonicated for a few minutes and was afterwards put in oven at 120°C for 52 hours.

4. Synthesis of UiO-66-2COOH

The MOF was synthesised in a 20 mL vial where 1, 2, 4, 5-benzenetetracarboxylic acid (47 mg, 0.184 mmol) was dissolved in 4 mL DMF by sonicating the mixture for 10 minutes. After sonication, $ZrOCl_2.8H_2O$ (59.5 mg, 0.184 mmol) was added to the solution. The mixture was sonicated for another 10 minutes and then 4 mL of formic acid were added to the solution. The reaction mixture was sonicated for a few minutes and was then placed in a preheated oven at 130°C for 5 hours. The obtained white powder was purified by washing with DMF and then with DCM several times, then it was collected by centrifugation and dried in a vacuum oven at 85°C.

5. Synthetic of Pd/MOF Composites

By impregnation

a. First method (Xwt%Pd-UiO-66-Y)

This method was used for UiO-66, UiO-66-NH_2 and UiO-66-2COOH. In a 250 mL scintillation vial, palladium acetate (appropriate amount of Pd($CH_3COO)_2$) was dissolved in DMF (100 mL) by sonication for 10 min. UiO-66-Y (UiO-66, UiO-66-NH_2 or UiO-66-2COOH) (500 mg) was then added to the Palladium solution. The reaction mixture was then stirred on a hot plate at 110 °C for 20 hour. The resulting grayish microcrystalline powder (Figure 3.3) was centrifuged, and the supernatant was discarded. The solids were washed with MeOH for 2 days and the solution was exchanged with fresh MeOH two times per day. The solids were collected by centrifugation and dried under dynamic vacuum at 80 °C. The resulting samples were 0.6%Pd-UiO-66-Y, and 1.44%Pd/UiO-66-Y.

Figure 3.3. Photograph showing the color change of the UiO-66 before and after the loading of palladium.

b. Second method (Pd/MOF-1)

This method was used for UiO-66. UiO-66 (100 mg) was dispersed in water and then the Pdcl$_2$ (1 mg/mL) was added to it. Then the mixture was stirred for 24 h at room temperature and the solid was separated by centrifugation to get rid of the unnecessary metal ions from the solution. The obtained solid was redispersed in water and NaBH$_4$ was added in it. Then, the mixture was placed into the microwave oven and irradiated at 30° C for 20 min. The obtained Pd/MOF-1 were washed with deionized water and dried in a vaccum oven at 80 °C for 7h.

c. Third method (Pd/MOF-2)

This method was used for UiO-66. 50 mg of UiO-66 were suspended in anhydrous ethanol (15 mL). A stock solution (1 mg/mL) of PdCl$_2$ was prepared in anhydrous ethanol. An adequate volume of palladium solution was added to the

dispersion of 50 mg MOFs in ethanol under sonication. After 30 min of sonication, the vessel was capped and transferred to the microwave reactor (150°C, 30 min). The Pd/MOF-2 were washed with deionized water and dried in a vaccum oven at 70 °C overnight.

By encapsulation

d. Fourth method (Pd/MOF-3)

This method was used for UiO-66. 100 mg H_2BDC (terephthalic acid), 133.6 mg $ZrCl_4$, 9.5 mg $pdcl_2$, and the required amount of acetic acid(90 equiv. to Zr) were dissolved in 40 mL of DMF under H_2/N_2.The tube was sealed and the mixture was subjected to ultrasonication for 0.5 h, and then stirred at 120 ℃ for 24 h. The obtained Pd/MOF-3 were washed with ethanol for 2d and dried in a vaccum oven at 80 °C overnight.

e. Sample preparation for atomic absorption measurement

Sample preparation is an important step in chemical analysis. Exactly 10 mg of sample was weighed and dissolved in 1 ml Hydrofluoric acid (HF) and aqua-regia, then the content was sonicated for 10 minutes. Finally, deionized water was added and the volume made up to 10mL.

E. RESULTS AND DISCUSSION

1. Characterization

UiO-66-Y MOFs and Pd/MOF Composites obtained are collected and characterized via several techniques including PXRD, SEM, TGA, BET, AAS and HRTEM.

a. Powder X-ray Diffraction

The PXRD patterns for the synthesised UiO-66-Y MOFs and Pd/MOF Composites were recorded. Figure 3.4 shows that all PXRD patterns of the synthesised MOFs have sharp narrow peaks that are in complete accordance with the theoretical one. This reflects the high crystallinity and purity of all prepared catalysts. Additionnally, no peak that could be attributed to PdNps could be observed in the pxrd of the composites. This is due to the low loading % of Pd NPs.
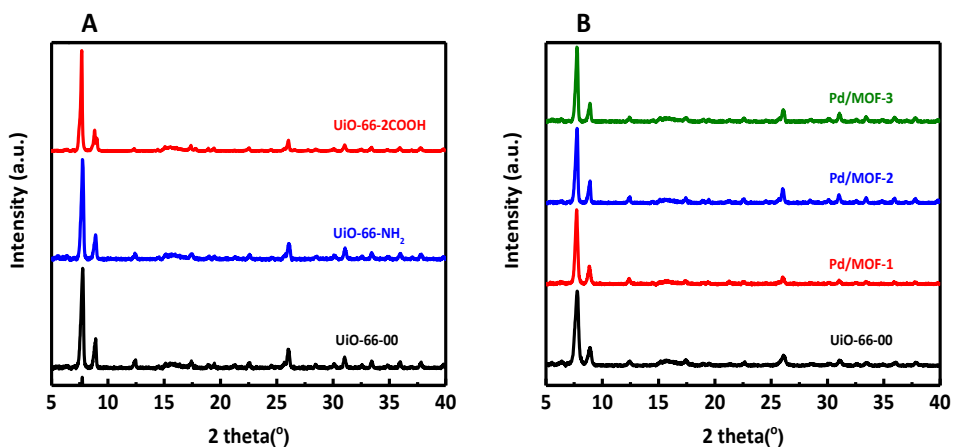
Figure 3.4. PXRD pattern of UiO-66-Y MOFs (A) and Pd/MOF Composites (B).

b. Thermogravimetric Analysis (TGA)

Thermogravimetric analysis (TGA) measures the mass change in a sample as a function of temperature, under a controlled atmosphere. It provides a quantitative measurement of the mass changes in a material associated with both material transitions and thermal degradation and thus can be used in the determination of the thermal stability and decomposition products of a material.The thermal stability of the synthesised UiO-66-Y MOFs and Pd/MOF Composites was evaluated by TGA. Fig 3.5 shows two main weight losses for UiO-66 stuctures. The first one occurs at a temperature between 50 and 200°C and is of about 5% of the total sample weight. This weight loss is attributed to the evaporation of the physiosorbed water/solvent. A significant weight loss of around 40% is observed between 400 °C and 500°C. The residual weight remaining after the decomposition could coincide to the formation of zirconium oxide. This plateau is an indication of the disintegration of these MOFs at those temperature.
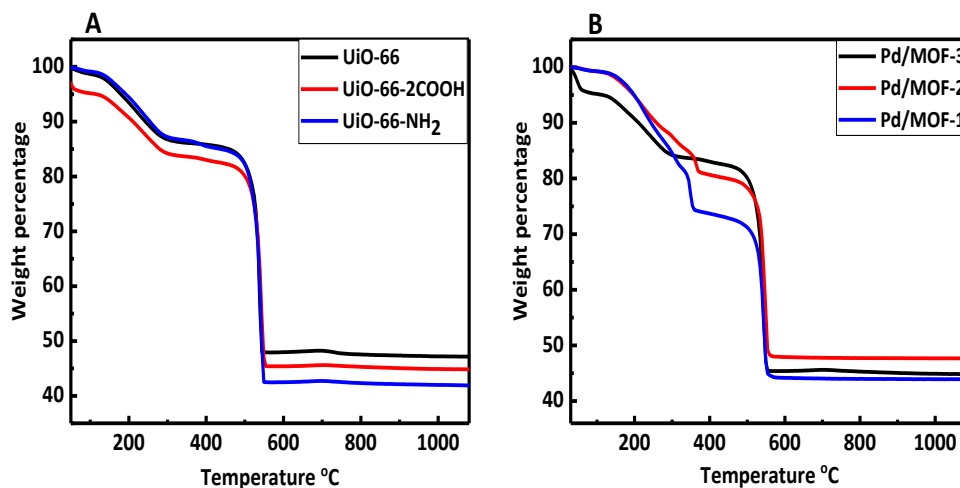
Figure 3.5. TGA Curves for : A (UiO-66, UiO-66-NH$_2$ and UiO-66-2COOH), B (Pd-MOF-1, Pd-MOF-2 and Pd-MOF-3).

c. N$_2$ Adsorption and BET (Brunauer-Emmett-Teller) Calculation

The Brunauer-Emmett-Teller (BET) was used to determine the surface area with respect to P/P$_0$. The samples were degassed at 150 °C under vacuum for 7 h prior to the sorption analysis measurements. The calculated surface areas of UiO-66, UiO-66-NH$_2$ and UiO-66-2COOH are 1092, 970 and 310 respectively. For UiO-66-2COOH, the obtained small value in the surface area is expected since these groups are blocking the pores aperture and therefore leading to a decrease of the accessible surface area.
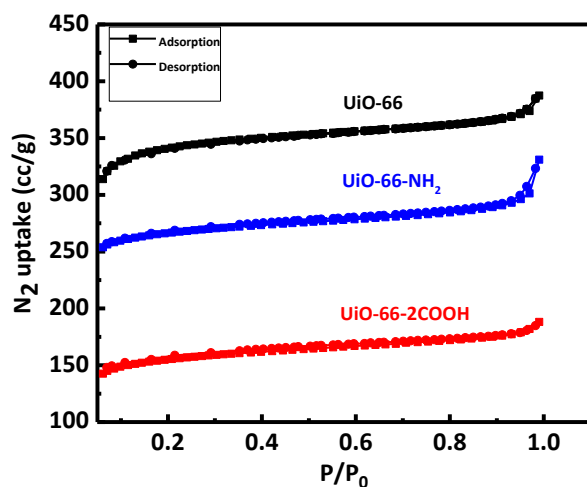
Figure 3.6. Nitrogen isotherms of UiO-66, UiO-66-2COOH and UiO-66-NH$_2$

d. Scanning Electron Microscopy (SEM)

SEM images of different synthesised MOFs and MOF composites are shown in figure 3.7. The images show that UiO-66 samples and the Pd MOF composites display identical octahedral crystal shapes. However, the size of these crystals varies based on the functional groups and the average particle size obtained were 296 nm, 108 nm and 47 nm for UiO-66, UiO-66-NH$_2$ and UiO-66-2COOH respectively. As for the composites,

the low SEM resolution did not allow us to observe the small Pd-NPs within the

composite. Nevertheless, the shape of the MOF crystals was not affected upon loading

the Pd crystals through impregnation and encapsulation. This demonstrate the high

stability of UiO-66 crystals.
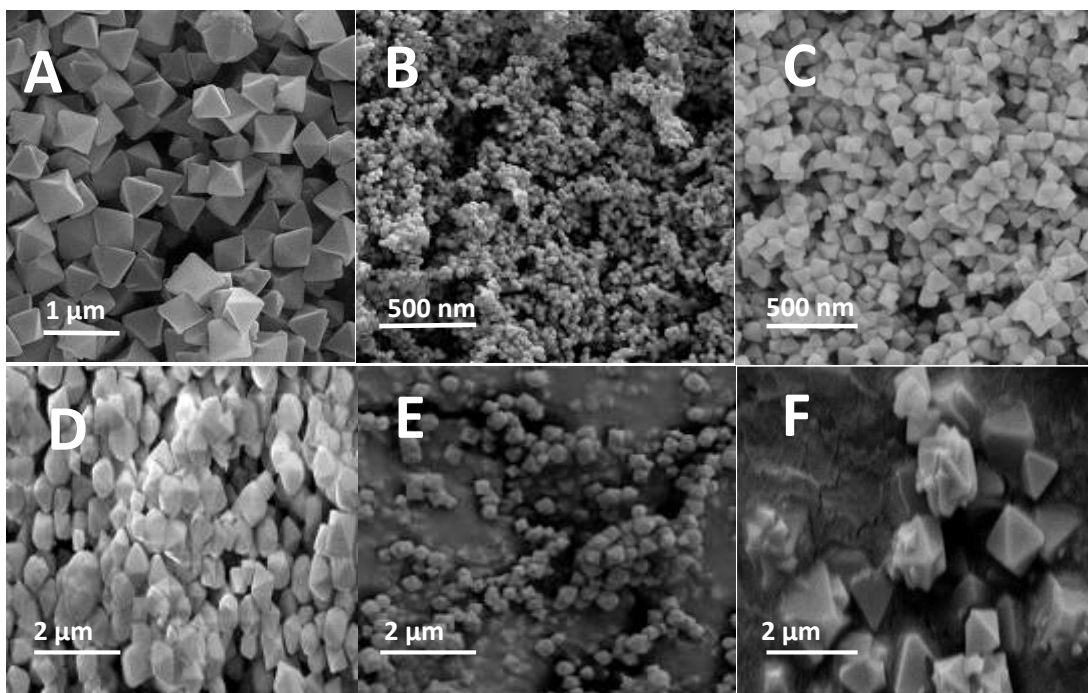
Figure 3.7. SEM images of A (UiO-66), B (UiO-66-2COOH), C (UiO-66-NH$_2$), D (Pd/MOF-1), E (Pd/MOF-2) and F (Pd/MOF-3)

e. Atomic Absorption Spectroscopy (AAS)

In order to determine the exact amount of Pd within the Pd-MOF composites,

Atomic absorption was performed on digested samples of the different synthesized

composites. The obtained results are summarized in table 3.1.

84

Table 3.1. Concentration of palladium and catalytic performance of Pd-UiO-66-y catalysts for removal Nitrites from water. Conditions: room temperature, nitrite concentration: 3mmol, 50mg catalyst.

Sample	Palladium concentration (ppm)	Palladium Wt%	Nitrite Conversion
Pd/MOF-1	14.13	2.94	74.25
Pd/MOF-2	6.34	1.32	47.62
Pd/MOF-3	26.87	5.59	Not tested
UiO-66	zero	zero	6.25
0.6Wt% Pd-UiO-66	2.94	0.60	20.64
1.44Wt% Pd-UiO-66	7.15	1.44	44.05
UiO-66-NH$_2$	zero	zero	15.90
0.6Wt% Pd-UiO-66-NH$_2$	2.59	0.60	25.84
1.44Wt% Pd-UiO-66-NH$_2$	6.92	1.44	46.38
UiO-66-2COOH	zero	zero	15.37
0.6Wt% Pd-UiO-66-2COOH	2.62	0.60	11.43
1.44Wt% Pd-UiO-66-2COOH	7.05	1.44	34.89

| Pd/Al$_2$O$_3$ | Not reported | 1.10 | 60.00 |

f. Transmission Electron Microscopy (TEM)

To further investigate the successful loading of Pd Nps on and /or at the MOF crystals. TEM images were recorded for Pd-MOF-1, PdMOF-2 and Pd-MOF-3. Typical images are presented in Figure 3.8. It can be seen from Figure 3.8 that the Pd NPs were deposited on the surface of UiO-66 (Figure 3.8 A,B,C and D) for PdMOF-1 and PdMOF-2. As for Pd-MOF-3 the pd-NPs seem to be encapsulated within the pores (Figure 3.8 E and F) of the MOF. In addition, it can be seen that the Pd nanoparticles are well dispersed on the surface of UiO-66 (Figure A,B,C and D). From the obtained images, we can conclude that Pd-MOF-2 sample which was prepared via microwave assisted technique, shows better and homogeneous Np dispersion.
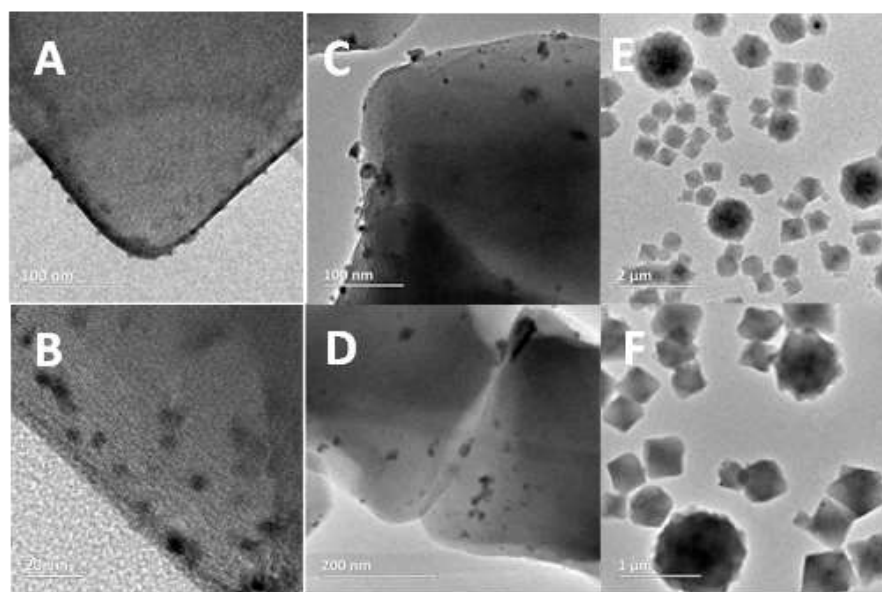
Figure 3.8. TEM images for Pd/MOF-1(A and B), Pd/MOF-2 (C and D) and Pd/MOF-3(E and F).

The palladium nanoparticles were examined by HRTEM, showing fringes separated by 0.23 nm and representing the lattice periodicities for interlayer distances of 0.23 nm. This is in good agreement (within experimental error) with the calculated value from single crystal data of palladium (0.2244 nm for (111) lattice plane) (Figure 3.9). This further demonstrate the formation of Pd (0) within the MOF–Pd composites.
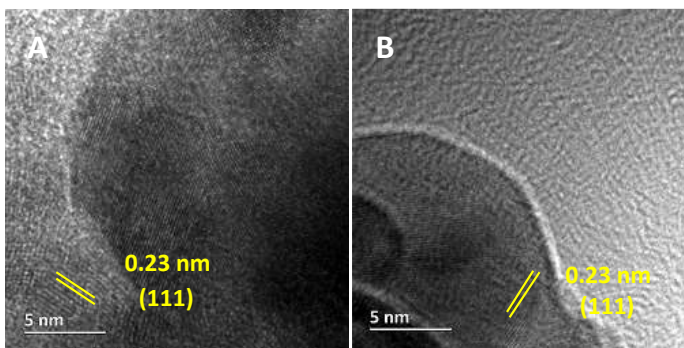
Figure 3.9. HRTEM images of the Pd Nps deposited on the MOFs crystals showing the d-spacing values of 0.23 nm which corresponds to (111) planes.

2. Catalytic activity test

Nitrate and Nitrite denitration mechanism was proposed for the first time by Vorlop et al. and it is based on the catalytic hydrogenation using Pd-Cu catalysts. Nitrates are selectively reduced with hydrogen to nitrogen via intermediate nitrites and nitric oxide.[188] Ammonia is formed as an undesired side product (Scheme 3.1). The limit for ammonia is 0.5 mg/l. The reaction mechanism is illustrated below :

$$2NO_3^- + 2H_2 \rightarrow 2NO_2^- + 2H_2O$$

$$2NO_2^- + 3H_2 + 2H^+ \rightarrow N_2 + 4H_2O$$

$$NO_2^- + 3H_2 + 2H^+ \rightarrow NH_4^+ + 2H_2O$$
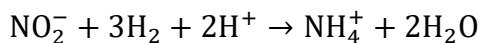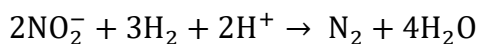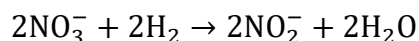
Scheme 3.1. Reactions in the catalytic removal of nitrates.

The Pd-UiO66 composites that are prepared by impregnation (Pd-MOF-1 and Pd-MOF-2) and by encapsulation (Pd-MOF-3) in addition to the Functionnalized composites (xWtPd-UiO-66-y) were employed as catalysts for the hydrogenation of Nitrites in water. The initial results were summarized in table 3.1. The catalyst performance was related to three factors: (1) the presence of functional group in MOFs, (2) the percentage of palladium loaded in MOFs, (3) the method used in the synthesis of Pd-MOF composites.

It is clear that UiO-66 sample shows some activity, and the efficiency increases by adding of carboxylic or amino functional groups. Which means that these functional groups play a key role in the reduction reaction. As for the composites, the highest conversion was obtained for Pd-MOF-1 which was synthesized by impregnation using sodium borohydride ($NaBH_4$) as reducing agent. The Pd content in this composite sample was 2.93Wt%. And it was clear that the increase in the Pd loading (from 1.32Wt% in Pd-MOF-2 to 2.93Wt% in Pd-MOF-1) is accompanied by an improvement in the catalytic activity(from 47.62% to 74.25% respectivily). This demonstrates that the Pd Nps do not aggregate on the surface of the UiO-66 structures under our experimental conditions. However,the conversion that was achieved in Pd-MOF-2 (1.32Wt% -47.62%) remains lower than that in Pd/Al_2O_3 (1.10Wt%-60.00%).

F. Conclusion

In this work, the activity of a new class of heterogeneous catalysts was investigated. Zr-based Metal-Organic Frameworks (UiO-66, UiO-66-2COOH and UiO-66-NH$_2$) and a series of functionalized Pd-MOFs composites were successfully synthesized and used as catalysts for nitrite reduction. Where the prepared catalysts showed promising catalytic activities for nitrite reduction.

CHAPTER IV

CONCLUSION AND FUTURE WORK

In this study, water stable defected Zr-MOF (UiO-66) was synthesized and applied as an adsorbent to uptake arsenate species. The UiO-66 adsorbents functioned excellently across a broad pH range, from very acidic 2 to basic 9, with the best adsorption performance at pH 7 among other adsorbents. The presence of some common anions had little influence on the arsenic adsorption process. After studying the sample properties and performing the adsorption experiments, it was concluded that UiO-66-36TFA, which was the most defected sample, showed the highest arsenate adsorption (200 mg·g^{-1}) not only among its competitors but also among all previously reported arsenate adsorbents. In addition, the enormous performance of these adsorbents in real water samples demonstrated their feasibility for practical applications. Examining their phenomenal characteristics, simple fabrication procedure, high crystallinity and chemical stability, impressive arsenate removal, fast kinetics, and perfect regeneration/recyclability, made them of great potential toward being the best competing candidate for arsenate purification from drinking water.

To conclude, this study provides significant new insights to the application of MOFs in water treatment. The enhanced adsorption capacity of defected UiO-66 adsorbent compared to most conventional nanoparticle adsorbents was due to the highly porous structure containing zirconium oxide clusters, which provides a larger contact area and more active sites in unit space. With the superior adsorption performance towards

aquatic arsenic species, defected UiO-66 could work as a promising advanced adsorbent in the arsenic decontamination industry.

For the future work, one can try different methods and synthesize different structures. This thesis has been mainly focused on the use of defected UiO-66 for Arsenic adsorption and on the synthesis of the functionalized Pd/MOF composites for removal Nitrate/Nitrite from water. The following ideas could be tested:

- It could be interesting to synthesize the functionalized UiO-66 (UiO-66-NH$_2$ and UiO-66-2COOH) with different modulator ratios for the test of Arsenic removal from water.
- It would be interesting to investigate the effect of the Expansion of the organic linkers used in the UiO-66 topology on their performance for pollutants removal and on the loading efficiency of Nps.
- We should be able to identify the best synthesis methods for the encapsulation and / or decoration of UiO-66 by palladium nanoparticles.

- The synthesized materials would be further investigated for the removal of other pollutants for water; such as pesticides and antibiotics.

REFERENCES

1.   Morris, R. E.; Wheatley, P. S., Gas storage in nanoporous materials. *Angewandte Chemie International Edition* **2008,** *47* (27), 4966-4981.

2.   Chang, F.; Zhou, J.; Chen, P.; Chen, Y.; Jia, H.; Saad, S. M.; Gao, Y.; Cao, X.; Zheng, T., Microporous and mesoporous materials for gas storage and separation: a review. *Asia-Pacific Journal of Chemical Engineering* **2013,** *8* (4), 618-626.

3.   Hammond, C.; Padovan, D.; Tarantino, G., Porous metallosilicates for heterogeneous, liquid-phase catalysis: perspectives and pertaining challenges. *Royal Society open science* **2018,** *5* (2), 171315.

4.   Vilaça, N. l.; Morais-Santos, F.; Machado, A. F.; Sirkecioğlu, A.; Pereira, M. F.; Sardo, M.; Rocha, J. o.; Parpot, P.; Fonseca, A. n. M.; Baltazar, F. t., Micro-and mesoporous structures as drug delivery carriers for salicylic acid. *The Journal of Physical Chemistry C* **2015,** *119* (7), 3589-3595.

5.   Lucatorto, T.; De Graef, M.; Wong, P.-Z., *Methods of the Physics of Porous Media*. Academic Press: 1999; Vol. 35.

6.   Rouquerol, J.; Rouquerol, F.; Llewellyn, P.; Maurin, G.; Sing, K. S., *Adsorption by powders and porous solids: principles, methodology and applications*. Academic press: 2013.

7.   Seth, S.; Matzger, A. J., Metal–organic frameworks: examples, counterexamples, and an actionable definition. *Crystal Growth & Design* **2017,** *17* (8), 4043-4048.

8.   Diercks, C. S.; Yaghi, O. M., The atom, the molecule, and the covalent organic framework. *Science* **2017,** *355* (6328), eaal1585.

9.   Zhou, H.-C.; Long, J. R.; Yaghi, O. M., Introduction to metal–organic frameworks. ACS Publications: 2012.

10.   Hoskins, B.; Robson, R., Design and construction of a new class of scaffolding-like materials comprising infinite polymeric frameworks of 3D-linked molecular rods. A reappraisal of the zinc cyanide and cadmium cyanide structures and the synthesis and structure of the diamond-related frameworks [N (CH3) 4][CuIZnII (CN) 4] and CuI [4, 4', 4'', 4'''-tetracyanotetraphenylmethane] BF4. xC6H5NO2. *Journal of the American Chemical Society* **1990,** *112* (4), 1546-1554.

11.   Yaghi, O.; Li, G., Mutually interpenetrating sheets and channels in the extended structure of [Cu (4, 4′-bpy) Cl]. *Angewandte Chemie International Edition in English* **1995,** *34* (2), 207-209.

12.   Tomic, E., Thermal stability of coordination polymers. *Journal of Applied Polymer Science* **1965,** *9* (11), 3745-3752.

13.   Li, H.; Eddaoudi, M.; O'Keeffe, M.; Yaghi, O. M., Design and synthesis of an exceptionally stable and highly porous metal-organic framework. *nature* **1999,** *402* (6759), 276.

14.   Yaghi, O. M.; Li, G.; Li, H., Selective binding and removal of guests in a microporous metal–organic framework. *Nature* **1995,** *378* (6558), 703.

15.   Chen, J.; Natarajan, S.; Thomas, J. M.; Jones, R. H.; Hursthouse, M. B., A Novel Open-Framework Cobalt Phosphate Containing a Tetrahedrally Coordinated Cobalt (ii) Center: CoPO4· 0.5 C2H10N2. *Angewandte Chemie International Edition in English* **1994,** *33* (6), 639-640.

16.   Slater, A. G.; Cooper, A. I., Function-led design of new porous materials. *Science* **2015,** *348* (6238), aaa8075.

17.   Buser, H.; Schwarzenbach, D.; Petter, W.; Ludi, A., The crystal structure of Prussian blue: Fe4 [Fe (CN) 6] 3. xH2O. *Inorganic Chemistry* **1977,** *16* (11), 2704-2710.

18.   Robl, C., Water clustering in the zeolite-like channel structure of Na2Zn [C6H2 (COO) 4]· 9H2O. *Materials research bulletin* **1992,** *27* (1), 99-107.

19.   Millange, F.; Serre, C.; Férey, G., Synthesis, structure determination and properties of MIL-53as and MIL-53ht: the first Cr iii hybrid inorganic–organic microporous solids: Cr iii (OH)·{O 2 C–C 6 H 4–CO 2}·{HO 2 C–C 6 H 4–CO 2 H} x. *Chemical Communications* **2002,** (8), 822-823.

20.   Serre, C.; Millange, F.; Thouvenot, C.; Nogues, M.; Marsolier, G.; Louër, D.; Férey, G., Very Large Breathing Effect in the First Nanoporous Chromium (III)-Based Solids: MIL-53 or CrIII (OH)⊙{O2C– C6H4– CO2}⊙{HO2C– C6H4– CO2H} x⊙ H2O y. *Journal of the American chemical society* **2002,** *124* (45), 13519-13526.

21.   Loiseau, T.; Serre, C.; Huguenard, C.; Fink, G.; Taulelle, F.; Henry, M.; Bataille, T.; Férey, G., A rationale for the large breathing of the porous aluminum terephthalate (MIL-53) upon hydration. *Chemistry–A European Journal* **2004,** *10* (6), 1373-1382.

22.   Lin, X.; Telepeni, I.; Blake, A. J.; Dailly, A.; Brown, C. M.; Simmons, J. M.; Zoppi, M.; Walker, G. S.; Thomas, K. M.; Mays, T. J., High capacity hydrogen adsorption in Cu (II) tetracarboxylate framework materials: the role of pore size, ligand functionalization, and exposed metal sites. *Journal of the American Chemical Society* **2009,** *131* (6), 2159-2171.

23.   Cavka, J. H.; Jakobsen, S.; Olsbye, U.; Guillou, N.; Lamberti, C.; Bordiga, S.; Lillerud, K. P., A new zirconium inorganic building brick forming metal organic frameworks with exceptional stability. *Journal of the American Chemical Society* **2008,** *130* (42), 13850-13851.

24.   Férey, G., Building units design and scale chemistry. *Journal of Solid State Chemistry* **2000,** *152* (1), 37-48.

25.   Férey, G.; Mellot-Draznieks, C.; Loiseau, T., Real, virtual and not yet discovered porous structures using scale chemistry and/or simulation. A tribute to Sten Andersson. *Solid state sciences* **2003,** *5*, 79-94.

26.   Rowsell, J. L.; Yaghi, O. M., Metal–organic frameworks: a new class of porous materials. *Microporous and mesoporous materials* **2004,** *73* (1-2), 3-14.

27.   Yaghi, O. M.; O'Keeffe, M.; Ockwig, N. W.; Chae, H. K.; Eddaoudi, M.; Kim, J., Reticular synthesis and the design of new materials. *Nature* **2003,** *423* (6941), 705.

28.   Rosi, N. L.; Kim, J.; Eddaoudi, M.; Chen, B.; O'Keeffe, M.; Yaghi, O. M., Rod packings and metal− organic frameworks constructed from rod-shaped secondary building units. *Journal of the American Chemical Society* **2005,** *127* (5), 1504-1518.

29.   Stock, N.; Biswas, S., Synthesis of metal-organic frameworks (MOFs): routes to various MOF topologies, morphologies, and composites. *Chemical reviews* **2011,** *112* (2), 933-969.

30.   Mueller, U.; Schubert, M.; Teich, F.; Puetter, H.; Schierle-Arndt, K.; Pastre, J., Metal–organic frameworks—prospective industrial applications. *Journal of Materials Chemistry* **2006,** *16* (7), 626-636.

31.   Hwang, Y. K.; Chang, J. S.; Park, S. E.; Kim, D. S.; Kwon, Y. U.; Jhung, S. H.; Hwang, J. S.; Park, M. S., Microwave fabrication of MFI zeolite crystals with a fibrous morphology and their applications. *Angewandte Chemie International Edition* **2005,** *44* (4), 556-560.

32.   Bauer, S.; Bein, T.; Stock, N., High-throughput investigation and characterization of cobalt carboxy phosphonates. *Inorganic chemistry* **2005,** *44* (16), 5882-5889.

33.   Forster, P. M.; Stock, N.; Cheetham, A. K., A High-Throughput Investigation of the Role of pH, Temperature, Concentration, and Time on the Synthesis of Hybrid Inorganic–Organic Materials. *Angewandte Chemie International Edition* **2005,** *44* (46), 7608-7611.

34.   Bauer, S.; Stock, N., Implementation of a Temperature-Gradient Reactor System for High-Throughput Investigation of Phosphonate-Based Inorganic–Organic Hybrid Compounds. *Angewandte Chemie International Edition* **2007,** *46* (36), 6857-6860.

35.   Banerjee, R.; Phan, A.; Wang, B.; Knobler, C.; Furukawa, H.; O'Keeffe, M.; Yaghi, O. M., High-throughput synthesis of zeolitic imidazolate frameworks and application to CO2 capture. *Science* **2008,** *319* (5865), 939-943.

36.   Ahnfeldt, T.; Guillou, N.; Gunzelmann, D.; Margiolaki, I.; Loiseau, T.; Férey, G.; Senker, J.; Stock, N., [Al4 (OH) 2 (OCH3) 4 (H2N-bdc) 3]· x H2O: A 12-Connected Porous Metal–Organic Framework with an Unprecedented Aluminum-Containing Brick. *Angewandte Chemie International Edition* **2009,** *48* (28), 5163-5166.

37.   Han, S.; Huang, Y.; Watanabe, T.; Dai, Y.; Walton, K. S.; Nair, S.; Sholl, D. S.; Meredith, J. C., High-throughput screening of metal–organic frameworks for CO2 separation. *ACS combinatorial science* **2012,** *14* (4), 263-267.

38.   Férey, G.; Serre, C.; Mellot-Draznieks, C.; Millange, F.; Surblé, S.; Dutour, J.; Margiolaki, I., A hybrid solid with giant pores prepared by a combination of targeted chemistry, simulation, and powder diffraction. *Angewandte Chemie International Edition* **2004,** *43* (46), 6296-6301.

39.   Kitagawa, S.; Kitaura, R.; Noro, S. i., Functional porous coordination polymers. *Angewandte Chemie International Edition* **2004,** *43* (18), 2334-2375.

40.   Issa, R.; Hmadeh, M.; Al-Ghoul, M. In *Control of Particle Size and Morphology of MOF-199 Crystals via a Reaction-Diffusion Framework*, Defect and Diffusion Forum, Trans Tech Publ: 2017; pp 39-47.

41.   Demessence, A.; Horcajada, P.; Serre, C.; Boissière, C.; Grosso, D.; Sanchez, C.; Férey, G., Elaboration and properties of hierarchically structured optical thin films of MIL-101 (Cr). *Chemical Communications* **2009,** (46), 7149-7151.

42.   Thomas, K. M., Adsorption and desorption of hydrogen on metal–organic framework materials for storage applications: comparison with other nanoporous materials. *Dalton transactions* **2009,** (9), 1487-1505.

43.   Rowsell, J. L.; Yaghi, O. M., Effects of functionalization, catenation, and variation of the metal oxide and organic linking units on the low-pressure hydrogen adsorption properties of metal– organic frameworks. *Journal of the American Chemical Society* **2006,** *128* (4), 1304-1315.

44.   Jiang, H.-L.; Makal, T. A.; Zhou, H.-C., Interpenetration control in metal–organic frameworks for functional applications. *Coordination Chemistry Reviews* **2013,** *257* (15-16), 2232-2249.

45.   Yang, S.; Lin, X.; Lewis, W.; Suyetin, M.; Bichoutskaia, E.; Parker, J. E.; Tang, C. C.; Allan, D. R.; Rizkallah, P. J.; Hubberstey, P., A partially interpenetrated metal–organic framework for selective hysteretic sorption of carbon dioxide. *Nature materials* **2012,** *11* (8), 710.

46.   Ma, S.; Sun, D.; Ambrogio, M.; Fillinger, J. A.; Parkin, S.; Zhou, H.-C., Framework-catenation isomerism in metal– organic frameworks and its impact on hydrogen uptake. *Journal of the American Chemical Society* **2007,** *129* (7), 1858-1859.

47.   Ferguson, A.; Liu, L.; Tapperwijn, S. J.; Perl, D.; Coudert, F.-X.; Van Cleuvenbergen, S.; Verbiest, T.; Van Der Veen, M. A.; Telfer, S. G., Controlled partial interpenetration in metal–organic frameworks. *Nature chemistry* **2016,** *8* (3), 250.

48.   Go, Y. B.; Wang, X.; Jacobson, A. J., (6, 3)-honeycomb structures of Uranium (VI) benzenedicarboxylate derivatives: The use of noncovalent interactions to prevent interpenetration. *Inorganic chemistry* **2007,** *46* (16), 6594-6600.

49.   Farha, O. K.; Malliakas, C. D.; Kanatzidis, M. G.; Hupp, J. T., Control over catenation in metal– organic frameworks via rational design of the organic building block. *Journal of the American Chemical Society* **2009,** *132* (3), 950-952.

50.   Yao, Q.; Su, J.; Cheung, O.; Liu, Q.; Hedin, N.; Zou, X., Interpenetrated metal–organic frameworks and their uptake of CO 2 at relatively low pressures. *Journal of Materials Chemistry* **2012,** *22* (20), 10345-10351.

51.   Liu, J.; Thallapally, P. K.; McGrail, B. P.; Brown, D. R.; Liu, J., Progress in adsorption-based CO 2 capture by metal–organic frameworks. *Chemical Society Reviews* **2012,** *41* (6), 2308-2322.

52.   Deng, H.; Doonan, C. J.; Furukawa, H.; Ferreira, R. B.; Towne, J.; Knobler, C. B.; Wang, B.; Yaghi, O. M., Multiple functional groups of varying ratios in metal-organic frameworks. *Science* **2010,** *327* (5967), 846-850.

53.   Horike, S.; Shimomura, S.; Kitagawa, S., Soft porous crystals. *Nature chemistry* **2009,** *1* (9), 695.

54.   Kitagawa, S.; Kondo, M., Functional micropore chemistry of crystalline metal complex-assembled compounds. *Bulletin of the Chemical Society of Japan* **1998,** *71* (8), 1739-1753.

55.   Férey, G.; Serre, C., Large breathing effects in three-dimensional porous hybrid matter: facts, analyses, rules and consequences. *Chemical Society Reviews* **2009,** *38* (5), 1380-1399.

56.   Liu, Y.; Her, J.-H.; Dailly, A.; Ramirez-Cuesta, A. J.; Neumann, D. A.; Brown, C. M., Reversible structural transition in MIL-53 with large temperature hysteresis. *Journal of the American Chemical Society* **2008,** *130* (35), 11813-11818.

57.   Beurroies, I.; Boulhout, M.; Llewellyn, P. L.; Kuchta, B.; Férey, G.; Serre, C.; Denoyel, R., Using pressure to provoke the structural transition of metal–organic frameworks. *Angewandte Chemie International Edition* **2010,** *49* (41), 7526-7529.

58.   Coudert, F. X.; Boutin, A.; Jeffroy, M.; Mellot-Draznieks, C.; Fuchs, A. H., Thermodynamic methods and models to study flexible metal–organic frameworks. *ChemPhysChem* **2011,** *12* (2), 247-258.

59.   Kitagawa, S.; Uemura, K., Dynamic porous properties of coordination polymers inspired by hydrogen bonds. *Chemical Society Reviews* **2005,** *34* (2), 109-119.

60.   Uemura, K.; Matsuda, R.; Kitagawa, S., Flexible microporous coordination polymers. *Journal of solid state chemistry* **2005,** *178* (8), 2420-2429.

61.   Schneemann, A.; Bon, V.; Schwedler, I.; Senkovska, I.; Kaskel, S.; Fischer, R. A., Flexible metal–organic frameworks. *Chemical Society Reviews* **2014,** *43* (16), 6062-6096.

62.   Kitaura, R.; Seki, K.; Akiyama, G.; Kitagawa, S., Porous coordination-polymer crystals with gated channels specific for supercritical gases. *Angewandte Chemie International Edition* **2003,** *42* (4), 428-431.

63.   Chen, B.; Eddaoudi, M.; Hyde, S.; O'Keeffe, M.; Yaghi, O., Interwoven metal-organic framework on a periodic minimal surface with extra-large pores. *Science* **2001,** *291* (5506), 1021-1023.

64.   Hwang, Y. K.; Hong, D.-Y.; Chang, J.-S.; Seo, H.; Yoon, M.; Kim, J.; Jhung, S. H.; Serre, C.; Férey, G., Selective sulfoxidation of aryl sulfides by coordinatively unsaturated metal centers in chromium carboxylate MIL-101. *Applied Catalysis A: General* **2009,** *358* (2), 249-253.

65.   Yoon, M.; Srirambalaji, R.; Kim, K., Homochiral metal–organic frameworks for asymmetric heterogeneous catalysis. *Chemical reviews* **2011,** *112* (2), 1196-1231.

66.   Seo, J. S.; Whang, D.; Lee, H.; Im Jun, S.; Oh, J.; Jeon, Y. J.; Kim, K., A homochiral metal–organic porous material for enantioselective separation and catalysis. *Nature* **2000,** *404* (6781), 982.

67.   Chui, S. S.-Y.; Lo, S. M.-F.; Charmant, J. P.; Orpen, A. G.; Williams, I. D., A chemically functionalizable nanoporous material [Cu3 (TMA) 2 (H2O) 3] n. *Science* **1999,** *283* (5405), 1148-1150.

68.   Abu Tarboush, B. J.; Chouman, A.; Jonderian, A.; Ahmad, M.; Hmadeh, M.; Al-Ghoul, M., Metal–Organic Framework-74 for Ultratrace Arsenic Removal from Water: Experimental and Density Functional Theory Studies. *ACS Applied Nano Materials* **2018,** *1* (7), 3283-3292.

69.   Yakovenko, A. A.; Reibenspies, J. H.; Bhuvanesh, N.; Zhou, H.-C., Generation and applications of structure envelopes for porous metal–organic frameworks. *Journal of Applied Crystallography* **2013,** *46* (2), 346-353.

70.   Li, J.-R.; Kuppler, R. J.; Zhou, H.-C., Selective gas adsorption and separation in metal–organic frameworks. *Chemical Society Reviews* **2009,** *38* (5), 1477-1504.

71.   Lee, J.; Farha, O. K.; Roberts, J.; Scheidt, K. A.; Nguyen, S. T.; Hupp, J. T., Metal–organic framework materials as catalysts. *Chemical Society Reviews* **2009,** *38* (5), 1450-1459.

72.   Gascon, J.; Corma, A.; Kapteijn, F.; Llabres i Xamena, F. X., Metal organic framework catalysis: Quo vadis? *Acs Catalysis* **2013,** *4* (2), 361-378.

73.   Horcajada, P.; Chalati, T.; Serre, C.; Gillet, B.; Sebrie, C.; Baati, T.; Eubank, J. F.; Heurtaux, D.; Clayette, P.; Kreuz, C., Porous metal–organic-framework nanoscale carriers as a potential platform for drug delivery and imaging. *Nature materials* **2010,** *9* (2), 172.

74.   Huxford, R. C.; Della Rocca, J.; Lin, W., Metal–organic frameworks as potential drug carriers. *Current opinion in chemical biology* **2010,** *14* (2), 262-268.

75.   Walton, K. S.; Snurr, R. Q., Applicability of the BET method for determining surface areas of microporous metal− organic frameworks. *Journal of the American Chemical Society* **2007,** *129* (27), 8552-8556.

76.   Sumida, K.; Rogow, D. L.; Mason, J. A.; McDonald, T. M.; Bloch, E. D.; Herm, Z. R.; Bae, T.-H.; Long, J. R., Carbon dioxide capture in metal–organic frameworks. *Chemical reviews* **2011,** *112* (2), 724-781.

77.   Murray, L. J.; Dincă, M.; Long, J. R., Hydrogen storage in metal–organic frameworks. *Chemical Society Reviews* **2009,** *38* (5), 1294-1314.

78.   Suh, M. P.; Park, H. J.; Prasad, T. K.; Lim, D.-W., Hydrogen storage in metal–organic frameworks. *Chemical reviews* **2011,** *112* (2), 782-835.

79.   He, Y.; Zhou, W.; Qian, G.; Chen, B., Methane storage in metal–organic frameworks. *Chemical Society Reviews* **2014,** *43* (16), 5657-5678.

80.   Britt, D.; Furukawa, H.; Wang, B.; Glover, T. G.; Yaghi, O. M., Highly efficient separation of carbon dioxide by a metal-organic framework replete with open metal sites. *Proceedings of the National Academy of Sciences* **2009,** *106* (49), 20637-20640.

81.   Kong, X.; Scott, E.; Ding, W.; Mason, J. A.; Long, J. R.; Reimer, J. A., CO2 dynamics in a metal–organic framework with open metal sites. *Journal of the American Chemical Society* **2012,** *134* (35), 14341-14344.

82.   Fujita, M.; Kwon, Y. J.; Washizu, S.; Ogura, K., Preparation, clathration ability, and catalysis of a two-dimensional square network material composed of cadmium (II) and 4, 4'-bipyridine. *Journal of the American Chemical Society* **1994,** *116* (3), 1151-1152.

83.   Jrad, A.; Tarboush, B. J. A.; Hmadeh, M.; Ahmad, M., Tuning acidity in zirconium-based metal organic frameworks catalysts for enhanced production of butyl butyrate. *Applied Catalysis A: General* **2019,** *570*, 31-41.

84.   Elcheikh Mahmoud, M.; Audi, H.; Assoud, A.; Ghaddar, T. H.; Hmadeh, M., Metal–Organic Framework Photocatalyst Incorporating Bis (4′-(4-carboxyphenyl)-terpyridine) ruthenium (II) for Visible-Light-Driven Carbon Dioxide Reduction. *Journal of the American Chemical Society* **2019,** *141* (17), 7115-7121.

85.   McKinlay, A. C.; Morris, R. E.; Horcajada, P.; Férey, G.; Gref, R.; Couvreur, P.; Serre, C., BioMOFs: metal–organic frameworks for biological and medical applications. *Angewandte Chemie International Edition* **2010,** *49* (36), 6260-6266.

86.   Tamames-Tabar, C.; Cunha, D.; Imbuluzqueta, E.; Ragon, F.; Serre, C.; Blanco-Prieto, M. J.; Horcajada, P., Cytotoxicity of nanoscaled metal–organic frameworks. *Journal of Materials Chemistry B* **2014,** *2* (3), 262-271.

87.   Low, J. J.; Benin, A. I.; Jakubczak, P.; Abrahamian, J. F.; Faheem, S. A.; Willis, R. R., Virtual high throughput screening confirmed experimentally: porous coordination polymer hydration. *Journal of the American Chemical Society* **2009,** *131* (43), 15834-15842.

88.   Horcajada, P.; Serre, C.; Vallet-Regí, M.; Sebban, M.; Taulelle, F.; Férey, G., Metal–organic frameworks as efficient materials for drug delivery. *Angewandte Chemie International Edition* **2006,** *45* (36), 5974-5978.

89.   Seo, P. W.; Bhadra, B. N.; Ahmed, I.; Khan, N. A.; Jhung, S. H., Adsorptive removal of pharmaceuticals and personal care products from water with functionalized metal-organic frameworks: remarkable adsorbents with hydrogen-bonding abilities. *Scientific reports* **2016,** *6*, 34462.

90.   Haque, E.; Jun, J. W.; Jhung, S. H., Adsorptive removal of methyl orange and methylene blue from aqueous solution with a metal-organic framework material, iron terephthalate (MOF-235). *Journal of Hazardous materials* **2011,** *185* (1), 507-511.

91.   Zhu, X.; Li, B.; Yang, J.; Li, Y.; Zhao, W.; Shi, J.; Gu, J., Effective adsorption and enhanced removal of organophosphorus pesticides from aqueous solution by Zr-based MOFs of UiO-67. *ACS applied materials & interfaces* **2014,** *7* (1), 223-231.

92.   Wang, C.; Liu, X.; Chen, J. P.; Li, K., Superior removal of arsenic from water with zirconium metal-organic framework UiO-66. *Scientific Reports* **2015,** *5*, 16613.

93.   Yee, K.-K.; Reimer, N.; Liu, J.; Cheng, S.-Y.; Yiu, S.-M.; Weber, J.; Stock, N.; Xu, Z., Effective mercury sorption by thiol-laced metal–organic frameworks: in strong acid and the vapor phase. *Journal of the American Chemical Society* **2013,** *135* (21), 7795-7798.

94.   Horcajada, P.; Serre, C.; Maurin, G.; Ramsahye, N. A.; Balas, F.; Vallet-Regi, M.; Sebban, M.; Taulelle, F.; Férey, G., Flexible porous metal-organic frameworks for a controlled drug delivery. *Journal of the American Chemical Society* **2008,** *130* (21), 6774-6780.

95.   Lohe, M. R.; Gedrich, K.; Freudenberg, T.; Kockrick, E.; Dellmann, T.; Kaskel, S., Heating and separation using nanomagnet-functionalized metal–organic frameworks. *Chemical Communications* **2011,** *47* (11), 3075-3077.

96.   Rubio-Martinez, M.; Avci-Camur, C.; Thornton, A. W.; Imaz, I.; Maspoch, D.; Hill, M. R., New synthetic routes towards MOF production at scale. *Chemical Society Reviews* **2017,** *46* (11), 3453-3480.

97.   Dhainaut, J.; Avci-Camur, C.; Troyano, J.; Legrand, A.; Canivet, J.; Imaz, I.; Maspoch, D.; Reinsch, H.; Farrusseng, D., Systematic study of the impact of MOF densification into tablets on textural and mechanical properties. *CrystEngComm* **2017,** *19* (29), 4211-4218.

98.   Jeremias, F.; Fröhlich, D.; Janiak, C.; Henninger, S. K., Advancement of sorption-based heat transformation by a metal coating of highly-stable, hydrophilic aluminium fumarate MOF. *RSC Advances* **2014,** *4* (46), 24073-24082.

99.   Czaja, A. U.; Trukhan, N.; Müller, U., Industrial applications of metal–organic frameworks. *Chemical Society Reviews* **2009,** *38* (5), 1284-1293.

100.   Gaab, M.; Trukhan, N.; Maurer, S.; Gummaraju, R.; Müller, U., The progression of Al-based metal-organic frameworks–From academic research to industrial production and applications. *Microporous and Mesoporous Materials* **2012,** *157*, 131-136.

101.   Tanaka, K.; Muraoka, T.; Hirayama, D.; Ohnish, A., Highly efficient chromatographic resolution of sulfoxides using a new homochiral MOF–silica composite. *Chemical Communications* **2012,** *48* (68), 8577-8579.

102.   Bai, Y.; Dou, Y.; Xie, L.-H.; Rutledge, W.; Li, J.-R.; Zhou, H.-C., Zr-based metal–organic frameworks: design, synthesis, structure, and applications. *Chemical Society Reviews* **2016,** *45* (8), 2327-2367.

103.   Hu, Z.; Zhao, D., De facto methodologies toward the synthesis and scale-up production of UiO-66-type metal–organic frameworks and membrane materials. *Dalton Transactions* **2015,** *44* (44), 19018-19040.

104.   Guillerm, V.; Ragon, F.; Dan-Hardi, M.; Devic, T.; Vishnuvarthan, M.; Campo, B.; Vimont, A.; Clet, G.; Yang, Q.; Maurin, G., A series of isoreticular, highly stable, porous zirconium oxide based metal–organic frameworks. *Angewandte Chemie International Edition* **2012,** *51* (37), 9267-9271.

105.   Ma, J.; Wong-Foy, A. G.; Matzger, A. J., The role of modulators in controlling layer spacings in a tritopic linker based zirconium 2D microporous coordination polymer. *Inorganic chemistry* **2015,** *54* (10), 4591-4593.

106.   Wang, R.; Wang, Z.; Xu, Y.; Dai, F.; Zhang, L.; Sun, D., Porous zirconium metal–organic framework constructed from 2D→ 3D interpenetration based on a 3, 6-connected kgd net. *Inorganic chemistry* **2014,** *53* (14), 7086-7088.

107.   Liang, W.; Chevreau, H.; Ragon, F.; Southon, P. D.; Peterson, V. K.; D'Alessandro, D. M., Tuning pore size in a zirconium–tricarboxylate metal–organic framework. *CrystEngComm* **2014,** *16* (29), 6530-6533.

108.   Feng, D.; Gu, Z. Y.; Li, J. R.; Jiang, H. L.; Wei, Z.; Zhou, H. C., Zirconium-metalloporphyrin PCN-222: mesoporous metal–organic frameworks with ultrahigh stability as biomimetic catalysts. *Angewandte Chemie International Edition* **2012,** *51* (41), 10307-10310.

109.   Morris, W.; Volosskiy, B.; Demir, S.; Gándara, F.; McGrier, P. L.; Furukawa, H.; Cascio, D.; Stoddart, J. F.; Yaghi, O. M., Synthesis, structure, and metalation of two new highly porous zirconium metal–organic frameworks. *Inorganic chemistry* **2012,** *51* (12), 6443-6445.

110.   Mondloch, J. E.; Bury, W.; Fairen-Jimenez, D.; Kwon, S.; DeMarco, E. J.; Weston, M. H.; Sarjeant, A. A.; Nguyen, S. T.; Stair, P. C.; Snurr, R. Q., Vapor-phase metalation by atomic layer deposition in a metal–organic framework. *Journal of the American Chemical Society* **2013,** *135* (28), 10294-10297.

111.   Karagiaridi, O.; Bury, W.; Mondloch, J. E.; Hupp, J. T.; Farha, O. K., Solvent-assisted linker exchange: an alternative to the de novo synthesis of unattainable metal–organic frameworks. *Angewandte Chemie International Edition* **2014,** *53* (18), 4530-4540.

112.   Deria, P.; Mondloch, J. E.; Tylianakis, E.; Ghosh, P.; Bury, W.; Snurr, R. Q.; Hupp, J. T.; Farha, O. K., Perfluoroalkane functionalization of NU-1000 via solvent-assisted ligand incorporation: synthesis and CO2 adsorption studies. *Journal of the American Chemical Society* **2013,** *135* (45), 16801-16804.

113.   Deria, P.; Chung, Y. G.; Snurr, R. Q.; Hupp, J. T.; Farha, O. K., Water stabilization of Zr 6-based metal–organic frameworks via solvent-assisted ligand incorporation. *Chemical science* **2015,** *6* (9), 5172-5176.

114.   Li, Z.; Schweitzer, N. M.; League, A. B.; Bernales, V.; Peters, A. W.; Getsoian, A. B.; Wang, T. C.; Miller, J. T.; Vjunov, A.; Fulton, J. L., Sintering-resistant single-site nickel catalyst supported by metal–organic framework. *Journal of the American Chemical Society* **2016,** *138* (6), 1977-1982.

115.	Zhang, Q.; Su, J.; Feng, D.; Wei, Z.; Zou, X.; Zhou, H.-C., Piezofluorochromic metal–organic framework: A microscissor lift. *Journal of the American Chemical Society* **2015,** *137* (32), 10064-10067.

116.	Furukawa, H.; Gándara, F.; Zhang, Y.-B.; Jiang, J.; Queen, W. L.; Hudson, M. R.; Yaghi, O. M., Water adsorption in porous metal–organic frameworks and related materials. *Journal of the American Chemical Society* **2014,** *136* (11), 4369-4381.

117.	Shearer, G. C.; Chavan, S.; Ethiraj, J.; Vitillo, J. G.; Svelle, S.; Olsbye, U.; Lamberti, C.; Bordiga, S.; Lillerud, K. P., Tuned to perfection: ironing out the defects in metal–organic framework UiO-66. *Chemistry of Materials* **2014,** *26* (14), 4068-4071.

118.	Wu, H.; Yildirim, T.; Zhou, W., Exceptional mechanical stability of highly porous zirconium metal–organic framework UiO-66 and its important implications. *The journal of physical chemistry letters* **2013,** *4* (6), 925-930.

119.	Rogge, S. M.; Wieme, J.; Vanduyfhuys, L.; Vandenbrande, S.; Maurin, G.; Verstraelen, T.; Waroquier, M.; Van Speybroeck, V., Thermodynamic insight in the high-pressure behavior of UiO-66: effect of linker defects and linker expansion. *Chemistry of Materials* **2016,** *28* (16), 5721-5732.

120.	Wißmann, G.; Schaate, A.; Lilienthal, S.; Bremer, I.; Schneider, A. M.; Behrens, P., Modulated synthesis of Zr-fumarate MOF. *Microporous and Mesoporous Materials* **2012,** *152*, 64-70.

121.	Hermes, S.; Witte, T.; Hikov, T.; Zacher, D.; Bahnmüller, S.; Langstein, G.; Huber, K.; Fischer, R. A., Trapping metal-organic framework nanocrystals: an in-situ time-resolved light scattering study on the crystal growth of MOF-5 in solution. *Journal of the American Chemical Society* **2007,** *129* (17), 5324-5325.

122.	Tsuruoka, T.; Furukawa, S.; Takashima, Y.; Yoshida, K.; Isoda, S.; Kitagawa, S., Nanoporous nanorods fabricated by coordination modulation and oriented attachment growth. *Angewandte Chemie International Edition* **2009,** *48* (26), 4739-4743.

123.	McGuire, C. V.; Forgan, R. S., The surface chemistry of metal–organic frameworks. *Chemical communications* **2015,** *51* (25), 5199-5217.

124.	Schaate, A.; Roy, P.; Godt, A.; Lippke, J.; Waltz, F.; Wiebcke, M.; Behrens, P., Modulated synthesis of Zr-based metal–organic frameworks: from nano to single crystals. *Chemistry–A European Journal* **2011,** *17* (24), 6643-6651.

125.	Zahn, G.; Zerner, P.; Lippke, J.; Kempf, F. L.; Lilienthal, S.; Schröder, C. A.; Schneider, A. M.; Behrens, P., Insight into the mechanism of modulated syntheses: in situ synchrotron diffraction studies on the formation of Zr-fumarate MOF. *CrystEngComm* **2014,** *16* (39), 9198-9207.

126.	Katz, M. J.; Brown, Z. J.; Colón, Y. J.; Siu, P. W.; Scheidt, K. A.; Snurr, R. Q.; Hupp, J. T.; Farha, O. K., A facile synthesis of UiO-66, UiO-67 and their derivatives. *Chemical Communications* **2013,** *49* (82), 9449-9451.

127.	Trickett, C. A.; Gagnon, K. J.; Lee, S.; Gándara, F.; Bürgi, H. B.; Yaghi, O. M., Definitive molecular level characterization of defects in UiO-66 crystals. *Angewandte Chemie International Edition* **2015,** *54* (38), 11162-11167.

128.	Han, Y.; Liu, M.; Li, K.; Zuo, Y.; Wei, Y.; Xu, S.; Zhang, G.; Song, C.; Zhang, Z.; Guo, X., Facile synthesis of morphology and size-controlled zirconium metal–organic framework UiO-66: the role of hydrofluoric acid in crystallization. *CrystEngComm* **2015,** *17* (33), 6434-6440.

129.	Vermoortele, F.; Bueken, B.; Le Bars, G. l.; Van de Voorde, B.; Vandichel, M.; Houthoofd, K.; Vimont, A.; Daturi, M.; Waroquier, M.; Van Speybroeck, V., Synthesis modulation as a tool to increase the catalytic activity of metal–organic frameworks: the unique case of UiO-66 (Zr). *Journal of the American Chemical Society* **2013,** *135* (31), 11465-11468.

130.   Gutov, O. V.; Molina, S.; Escudero-Adán, E. C.; Shafir, A., Modulation by Amino Acids: Toward Superior Control in the Synthesis of Zirconium Metal–Organic Frameworks. *Chemistry–A European Journal* **2016,** *22* (38), 13582-13587.

131.   Gutov, O. V.; Hevia, M. G. l.; Escudero-Adán, E. C.; Shafir, A., Metal–organic framework (MOF) defects under control: insights into the missing linker sites and their implication in the reactivity of zirconium-based frameworks. *Inorganic chemistry* **2015,** *54* (17), 8396-8400.

132.   Fang, Z.; Bueken, B.; De Vos, D. E.; Fischer, R. A., Defect-engineered metal–organic frameworks. *Angewandte Chemie International Edition* **2015,** *54* (25), 7234-7254.

133.   Ravon, U., The development of new materials such MOFs for CO 2 capture and alkylation of aromatic compounds. **2010**.

134.   Karagiaridi, O.; Lalonde, M. B.; Bury, W.; Sarjeant, A. A.; Farha, O. K.; Hupp, J. T., Opening ZIF-8: a catalytically active zeolitic imidazolate framework of sodalite topology with unsubstituted linkers. *Journal of the American Chemical Society* **2012,** *134* (45), 18790-18796.

135.   Kozachuk, O.; Luz, I.; Llabres i Xamena, F. X.; Noei, H.; Kauer, M.; Albada, H. B.; Bloch, E. D.; Marler, B.; Wang, Y.; Muhler, M., Multifunctional, defect-engineered metal–organic frameworks with ruthenium centers: sorption and catalytic properties. *Angewandte Chemie International Edition* **2014,** *53* (27), 7058-7062.

136.   Shearer, G. C.; Chavan, S.; Bordiga, S.; Svelle, S.; Olsbye, U.; Lillerud, K. P., Defect engineering: tuning the porosity and composition of the metal–organic framework UiO-66 via modulated synthesis. *Chemistry of Materials* **2016,** *28* (11), 3749-3761.

137.   Cliffe, M. J.; Wan, W.; Zou, X.; Chater, P. A.; Kleppe, A. K.; Tucker, M. G.; Wilhelm, H.; Funnell, N. P.; Coudert, F.-X.; Goodwin, A. L., Correlated defect nanoregions in a metal–organic framework. *Nature communications* **2014,** *5*, 4176.

138.   Wu, H.; Chua, Y. S.; Krungleviciute, V.; Tyagi, M.; Chen, P.; Yildirim, T.; Zhou, W., Unusual and highly tunable missing-linker defects in zirconium metal–organic framework UiO-66 and their important effects on gas adsorption. *Journal of the American Chemical Society* **2013,** *135* (28), 10525-10532.

139.   Van de Voorde, B.; Stassen, I.; Bueken, B.; Vermoortele, F.; De Vos, D.; Ameloot, R.; Tan, J.-C.; Bennett, T. D., Improving the mechanical stability of zirconium-based metal–organic frameworks by incorporation of acidic modulators. *Journal of Materials Chemistry A* **2015,** *3* (4), 1737-1742.

140.   Jrad, A.; Hmadeh, M.; Tarboush, B. J. A.; Awada, G.; Ahmad, M., Structural engineering of Zr-based metal-organic framework catalysts for optimized biofuel additives production. *Chemical Engineering Journal* **2020,** *382*, 122793.

141.   Fairbairn, N.; Small, W.; Shannon, K.; Wood, E.; Kerr, T., Seeking refuge from violence in street-based drug scenes: women's experiences in North America's first supervised injection facility. *Social Science & Medicine* **2008,** *67* (5), 817-823.

142.   Tesh, S. J.; Scott, T. B., Nano-composites for water remediation: A review. *Advanced Materials* **2014,** *26* (35), 6056-6068.

143.   Shafie, N. A.; Aris, A. Z.; Zakaria, M. P.; Haris, H.; Lim, W. Y.; Isa, N. M., Application of geoaccumulation index and enrichment factors on the assessment of heavy metal pollution in the sediments. *Journal of Environmental Science and Health, Part A* **2013,** *48* (2), 182-190.

144.   Xu, J.; Murphy, S. L.; Kochanek, K. D.; Bastian, B.; Arias, E., Deaths: final data for 2016. **2018**.

145.   Chung, J.-Y.; Yu, S.-D.; Hong, Y.-S., Environmental source of arsenic exposure. *Journal of preventive medicine and public health* **2014,** *47* (5), 253.

146.   Jomova, K.; Jenisova, Z.; Feszterova, M.; Baros, S.; Liska, J.; Hudecova, D.; Rhodes, C.; Valko, M., Arsenic: toxicity, oxidative stress and human disease. *Journal of Applied Toxicology* **2011,** *31* (2), 95-107.

147.   Xu, Y.-h.; Nakajima, T.; Ohki, A., Adsorption and removal of arsenic(V) from drinking water by aluminum-loaded Shirasu-zeolite. *Journal of Hazardous Materials* **2002,** *92* (3), 275-287.

148.   Fryxell, G. E.; Liu, J.; Hauser, T. A.; Nie, Z.; Ferris, K. F.; Mattigod, S.; Gong, M.; Hallen, R. T., Design and Synthesis of Selective Mesoporous Anion Traps. *Chemistry of Materials* **1999,** *11* (8), 2148-2154.

149.   Zhu, B.-J.; Yu, X.-Y.; Jia, Y.; Peng, F.-M.; Sun, B.; Zhang, M.-Y.; Luo, T.; Liu, J.-H.; Huang, X.-J., Iron and 1,3,5-Benzenetricarboxylic Metal–Organic Coordination Polymers Prepared by Solvothermal Method and Their Application in Efficient As(V) Removal from Aqueous Solutions. *The Journal of Physical Chemistry C* **2012,** *116* (15), 8601-8607.

150.   Hu, J.-S.; Zhong, L.-S.; Song, W.-G.; Wan, L.-J., Synthesis of Hierarchically Structured Metal Oxides and their Application in Heavy Metal Ion Removal. *Advanced Materials* **2008,** *20* (15), 2977-2982.

151.   Lin, T.-F.; Wu, J.-K., Adsorption of Arsenite and Arsenate within Activated Alumina Grains: Equilibrium and Kinetics. *Water Research* **2001,** *35* (8), 2049-2057.

152.   Vu, T. A.; Le, G. H.; Dao, C. D.; Dang, L. Q.; Nguyen, K. T.; Nguyen, Q. K.; Dang, P. T.; Tran, H. T.; Duong, Q. T.; Nguyen, T. V., Arsenic removal from aqueous solutions by adsorption using novel MIL-53 (Fe) as a highly efficient adsorbent. *Rsc Advances* **2015,** *5* (7), 5261-5268.

153.   Suzuki, T. M.; Bomani, J. O.; Matsunaga, H.; Yokoyama, T., Preparation of porous resin loaded with crystalline hydrous zirconium oxide and its application to the removal of arsenic. *Reactive and Functional Polymers* **2000,** *43* (1), 165-172.

154.   Jian, M.; Liu, B.; Zhang, G.; Liu, R.; Zhang, X., Adsorptive removal of arsenic from aqueous solution by zeolitic imidazolate framework-8 (ZIF-8) nanoparticles. *Colloids and Surfaces A: Physicochemical and Engineering Aspects* **2015,** *465*, 67-76.

155.   Cui, H.; Li, Q.; Gao, S.; Shang, J. K., Strong adsorption of arsenic species by amorphous zirconium oxide nanoparticles. *Journal of Industrial and Engineering Chemistry* **2012,** *18* (4), 1418-1427.

156.   Li, J.; Wu, Y.-n.; Li, Z.; Zhu, M.; Li, F., Characteristics of arsenate removal from water by metal-organic frameworks (MOFs). *Water Science and Technology* **2014,** *70* (8), 1391-1397.

157.   Chang, Z.-W.; Lee, Y.-J.; Lee, D.-J., Adsorption of hydrogen arsenate and dihydrogen arsenate ions from neutral water by UiO-66-NH2. *Journal of Environmental Management* **2019,** *247*, 263-268.

158.   Ge, X.; Ma, Y.; Song, X.; Wang, G.; Zhang, H.; Zhang, Y.; Zhao, H., β-FeOOH nanorods/carbon foam-based hierarchically porous monolith for highly effective arsenic removal. *ACS applied materials & interfaces* **2017,** *9* (15), 13480-13490.

159.   Ma, Y.; Zheng, Y.-M.; Chen, J. P., A zirconium based nanoparticle for significantly enhanced adsorption of arsenate: Synthesis, characterization and performance. *Journal of Colloid and Interface Science* **2011,** *354* (2), 785-792.

160.   Srihari, V.; Das, A., The kinetic and thermodynamic studies of phenol-sorption onto three agro-based carbons. *Desalination* **2008,** *225* (1-3), 220-234.

161.   Majumdar, D.; Gupta, N., Nitrate pollution of groundwater and associated human health disorders. *Indian journal of environmental health* **2000,** *42* (1), 28-39.

162.   Gambhir, R. S.; Kapoor, V.; Nirola, A.; Sohi, R.; Bansal, V., Water pollution: Impact of pollutants and new promising techniques in purification process. *Journal of Human Ecology* **2012,** *37* (2), 103-109.

163.	Vellanki, B. P.; Batchelor, B.; Abdel-Wahab, A., Advanced reduction processes: a new class of treatment processes. *Environmental engineering science* **2013,** *30* (5), 264-271.

164.	Della Rocca, C.; Belgiorno, V.; Meriç, S., Heterotrophic/autotrophic denitrification (HAD) of drinking water: prospective use for permeable reactive barrier. *Desalination* **2007,** *210* (1-3), 194-204.

165.	Hörold, S.; Tacke, T.; Vorlop, K. D., Catalytical removal of nitrate and nitrite from drinking water: 1. Screening for hydrogenation catalysts and influence of reaction conditions on activity and selectivity. *Environmental Technology* **1993,** *14* (10), 931-939.

166.	Moon, H. R.; Lim, D.-W.; Suh, M. P., Fabrication of metal nanoparticles in metal–organic frameworks. *Chemical Society Reviews* **2013,** *42* (4), 1807-1824.

167.	Kim, C. R.; Uemura, T.; Kitagawa, S., Inorganic nanoparticles in porous coordination polymers. *Chemical Society Reviews* **2016,** *45* (14), 3828-3845.

168.	Isaeva, V.; Tkachenko, O.; Afonina, E.; Kozlova, L.; Kapustin, G.; Grünert, W.; Solov'Eva, S.; Antipin, I.; Kustov, L., 2-Butyne-1, 4-diol hydrogenation over palladium supported on Zn2+-based–MOF and host–guest MOF/calix [4] arene materials. *Microporous and Mesoporous Materials* **2013,** *166*, 167-175.

169.	Juan-Alcañiz, J.; Gascon, J.; Kapteijn, F., Metal–organic frameworks as scaffolds for the encapsulation of active species: state of the art and future perspectives. *Journal of materials chemistry* **2012,** *22* (20), 10102-10118.

170.	Gole, B.; Sanyal, U.; Banerjee, R.; Mukherjee, P. S., High loading of Pd nanoparticles by interior functionalization of MOFs for heterogeneous catalysis. *Inorganic chemistry* **2016,** *55* (5), 2345-2354.

171.	Zhang, D.; Guan, Y.; Hensen, E. J.; Chen, L.; Wang, Y., Porous MOFs supported palladium catalysts for phenol hydrogenation: A comparative study on MIL-101 and MIL-53. *Catalysis Communications* **2013,** *41*, 47-51.

172.	Hou, C.; Xu, Q.; Wang, Y.; Hu, X., Synthesis of Pt@ NH 2-MIL-125 (Ti) as a photocathode material for photoelectrochemical hydrogen production. *RSC Advances* **2013,** *3* (43), 19820-19823.

173.	Sabo, M.; Henschel, A.; Fröde, H.; Klemm, E.; Kaskel, S., Solution infiltration of palladium into MOF-5: synthesis, physisorption and catalytic properties. *Journal of Materials Chemistry* **2007,** *17* (36), 3827-3832.

174.	Hermes, S.; Schröter, M. K.; Schmid, R.; Khodeir, L.; Muhler, M.; Tissler, A.; Fischer, R. W.; Fischer, R. A., Metal@ MOF: Loading of highly porous coordination polymers host lattices by metal organic chemical vapor deposition. *Angewandte Chemie International Edition* **2005,** *44* (38), 6237-6241.

175.	Müller, M.; Zhang, X.; Wang, Y.; Fischer, R. A., Nanometer-sized titania hosted inside MOF-5. *Chemical Communications* **2009,** (1), 119-121.

176.	Ishida, T.; Nagaoka, M.; Akita, T.; Haruta, M., Deposition of gold clusters on porous coordination polymers by solid grinding and their catalytic activity in aerobic oxidation of alcohols. *Chemistry–A European Journal* **2008,** *14* (28), 8456-8460.

177.	Esken, D.; Zhang, X.; Lebedev, O. I.; Schröder, F.; Fischer, R. A., Pd@ MOF-5: limitations of gas-phase infiltration and solution impregnation of [Zn4O (bdc) 3](MOF-5) with metal–organic palladium precursors for loading with Pd nanoparticles. *Journal of Materials Chemistry* **2009,** *19* (9), 1314-1319.

178.	Gole, B.; Sanyal, U.; Mukherjee, P. S., A smart approach to achieve an exceptionally high loading of metal nanoparticles supported by functionalized extended frameworks for efficient catalysis. *Chemical Communications* **2015,** *51* (23), 4872-4875.

179.   Lu, G.; Li, S.; Guo, Z.; Farha, O. K.; Hauser, B. G.; Qi, X.; Wang, Y.; Wang, X.; Han, S.; Liu, X., Imparting functionality to a metal–organic framework material by controlled nanoparticle encapsulation. *Nature chemistry* **2012,** *4* (4), 310.

180.   Liu, H.; Chang, L.; Chen, L.; Li, Y., In situ one-step synthesis of metal–organic framework encapsulated naked Pt nanoparticles without additional reductants. *Journal of Materials Chemistry A* **2015,** *3* (15), 8028-8033.

181.   Zhang, N.; Zhu, B.; Peng, F.; Yu, X.; Jia, Y.; Wang, J.; Kong, L.; Jin, Z.; Luo, T.; Liu, J., Synthesis of metal–organic-framework related core–shell heterostructures and their application to ion enrichment in aqueous conditions. *Chemical Communications* **2014,** *50* (57), 7686-7689.

182.   Xia, Y.; Xiong, Y.; Lim, B.; Skrabalak, S. E., Shape-controlled synthesis of metal nanocrystals: simple chemistry meets complex physics? *Angewandte Chemie International Edition* **2009,** *48* (1), 60-103.

183.   Haruta, M., Size-and support-dependency in the catalysis of gold. *Catalysis today* **1997,** *36* (1), 153-166.

184.   Xiong, Y.; Chen, J.; Wiley, B.; Xia, Y.; Yin, Y.; Li, Z.-Y., Size-dependence of surface plasmon resonance and oxidation for Pd nanocubes synthesized via a seed etching process. *Nano Letters* **2005,** *5* (7), 1237-1242.

185.   Xiong, Y.; Cai, H.; Wiley, B. J.; Wang, J.; Kim, M. J.; Xia, Y., Synthesis and mechanistic study of palladium nanobars and nanorods. *Journal of the American Chemical Society* **2007,** *129* (12), 3665-3675.

186.   Xiong, Y.; McLellan, J. M.; Chen, J.; Yin, Y.; Li, Z.-Y.; Xia, Y., Kinetically controlled synthesis of triangular and hexagonal nanoplates of palladium and their SPR/SERS properties. *Journal of the American Chemical Society* **2005,** *127* (48), 17118-17127.

187.   Rungtaweevoranit, B.; Baek, J.; Araujo, J. R.; Archanjo, B. S.; Choi, K. M.; Yaghi, O. M.; Somorjai, G. A., Copper nanocrystals encapsulated in Zr-based metal–organic frameworks for highly selective CO2 hydrogenation to methanol. *Nano letters* **2016,** *16* (12), 7645-7649.

188.   Vorlop, K. D.; Tacke, T., Erste Schritte auf dem Weg zur edelmetallkatalysierten Nitrat- und Nitrit-Entfernung aus Trinkwasser. *Chemie Ingenieur Technik* **1989,** *61* (10), 836-837.

APPENDIX

DEFECTS ENGINEERING IN UiO-66 STRUCTURE FOR ENHANCED ARSENIC REMOVAL FROM WATER
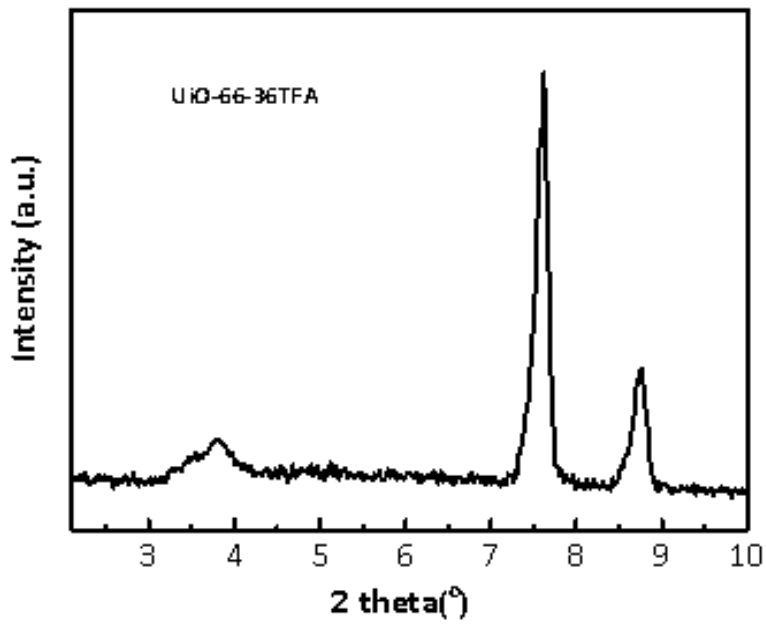
A. Annexe

Figure A.1. Short angle X-ray diffraction analysis of UiO-66-36TFA showing a broad peak at 3.8°
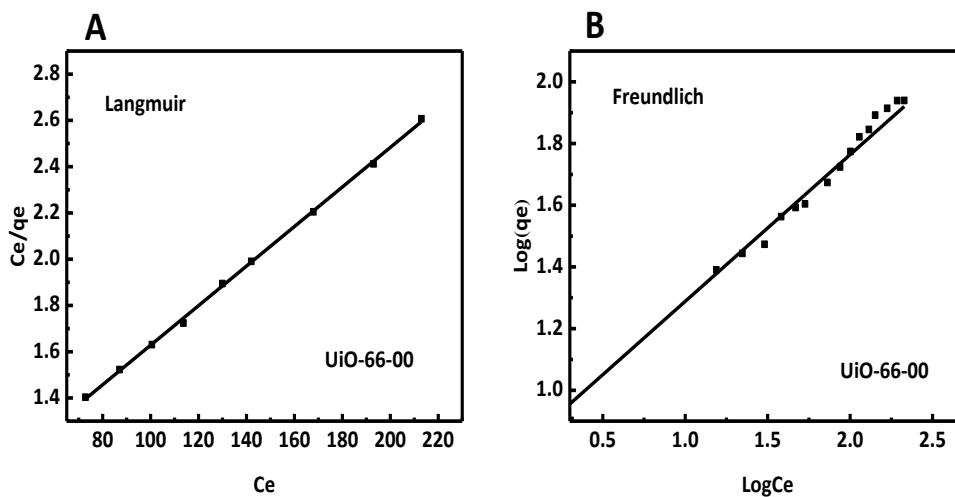
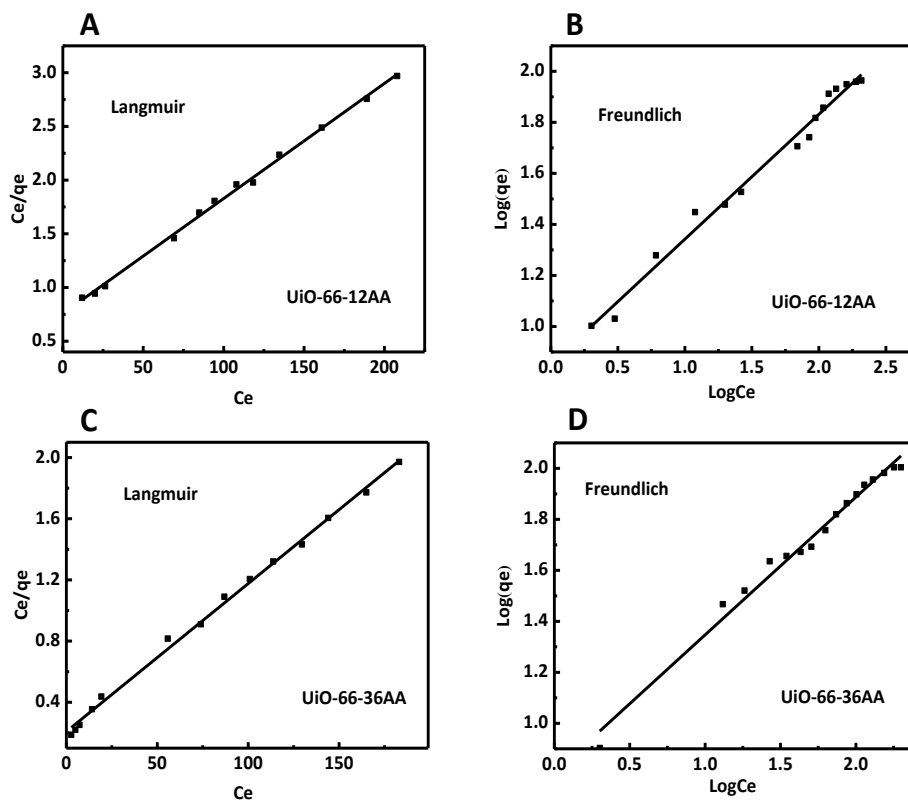Figure A.2. Data fitting using Langmuir (A) and Freundlich (B) models for the non-modulated UiO-66.

Figure A.3. Data fit for UiO-66-12AA Langmuir model (A) and Freundlich model (B) and for UiO-66-36AA Langmuir model (C) and Freundlich model (D).
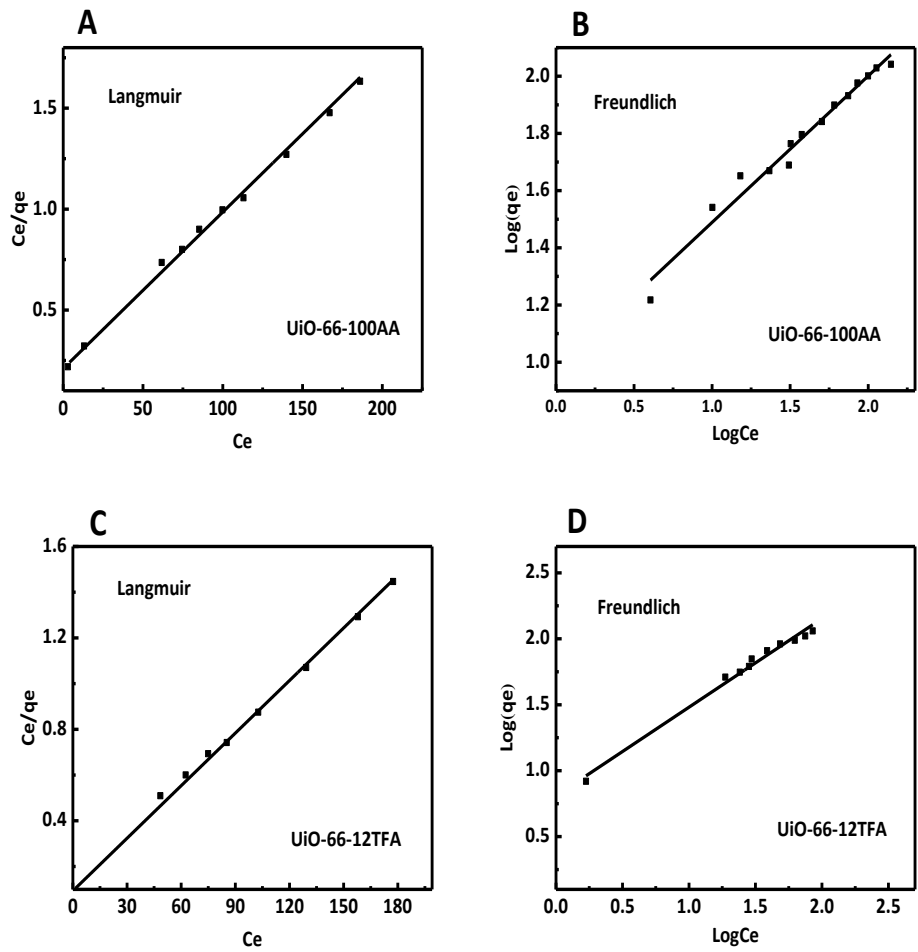
Figure A.4. Data fit for UiO-66-100AA Langmuir model (A) and Freundlich model (B) and for UiO-66-12TFA Langmuir model (C) and Freundlich model (D).

Table A.1. Langmuir and Freundlich parameters and correlation coefficients for As (V) adsorption onto the defected samples.

	Parameter	UiO-66-00	UiO-66-12AA	UiO-66-36AA	UiO-66-100AA	UiO-66-12TFA	UiO-66-36TFA
Langmuir	q_{max}	89.31	93.28	103.4	129.03	138.37	200
	k_L	0.01447	0.01416	0.046	0.037	0.0819	0.0905
	R^2	0.999	0.99766	0.9968	0.997	0.995	0.998
Freundlich	$\dfrac{1}{n}$	0.4756	0.4895	0.5403	0.512	0.672	0.60312
	k_F	6.4978	7.12	6.406	9.482	6.445	20.08
	R^2	0.960	0.987	0.985	0.9747	0.986	0.975
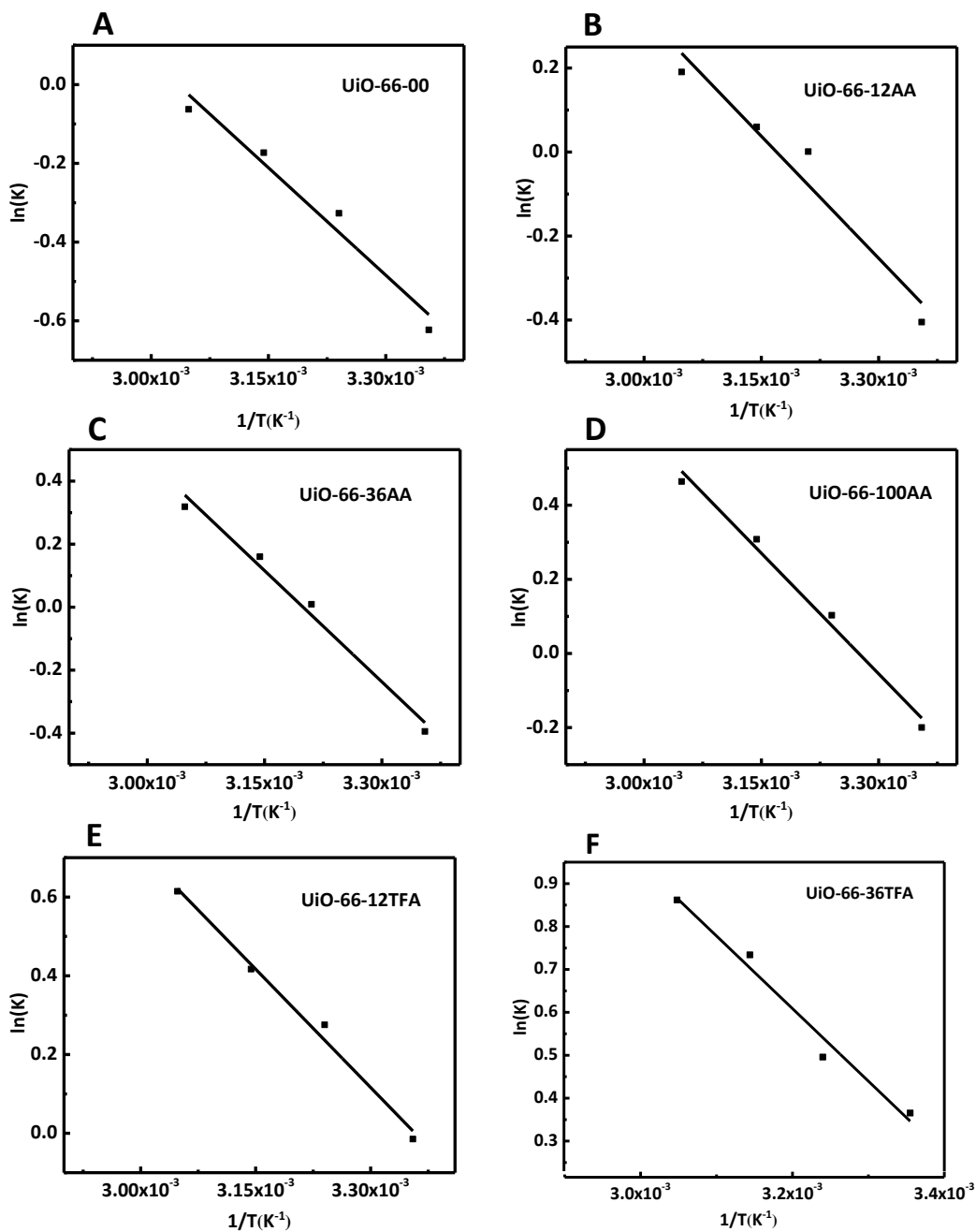
Figure A.5. Van't Hoff plot of ln(K) vs. 1/T for the various MOFs
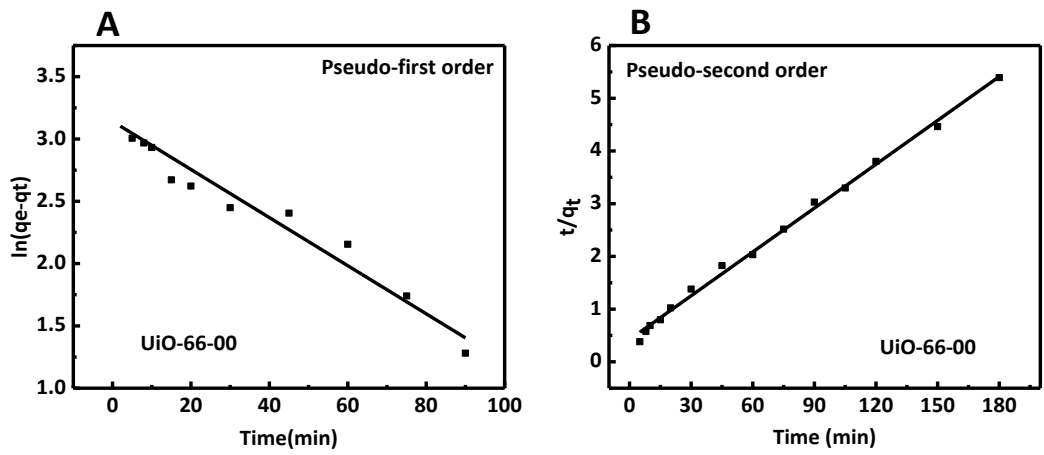
Figure A.6. (A) Pseudo-first-order fit for non-modulated UiO-66, (B) pseudo-second-order fit for non-modulated UiO-66.
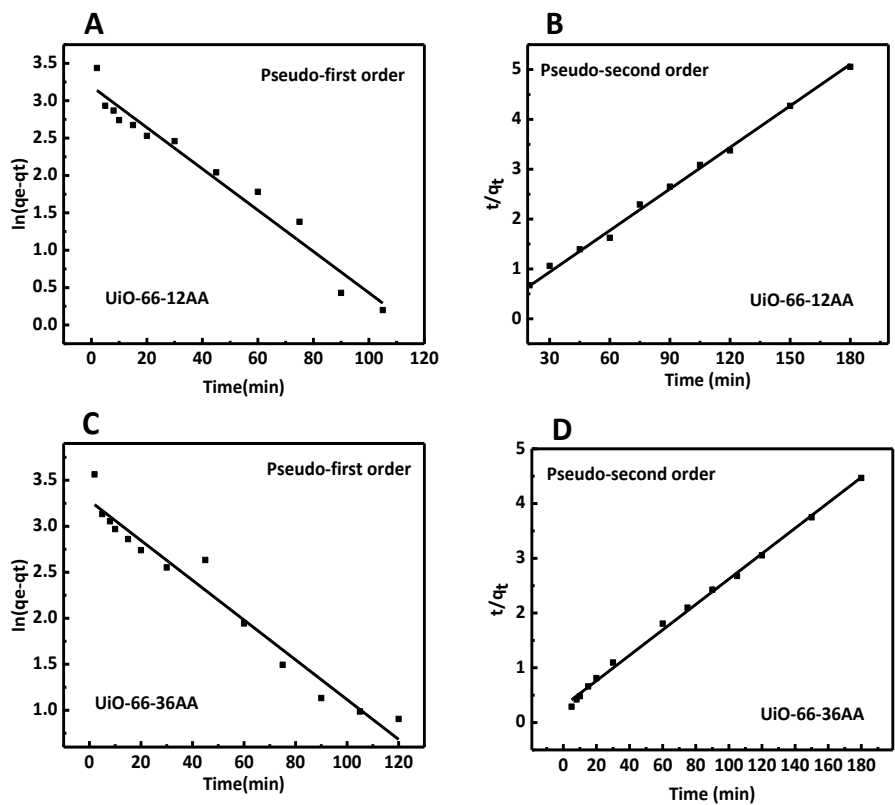

Figure A.7. (A) Pseudo-first-order fit for UiO-66-12AA, (B) pseudo-second-order fit for UiO-66-12AA, (C) Pseudo-first-order fit for UiO-66-36AA, (D) pseudo-second-order fit for UiO-66-36AA.
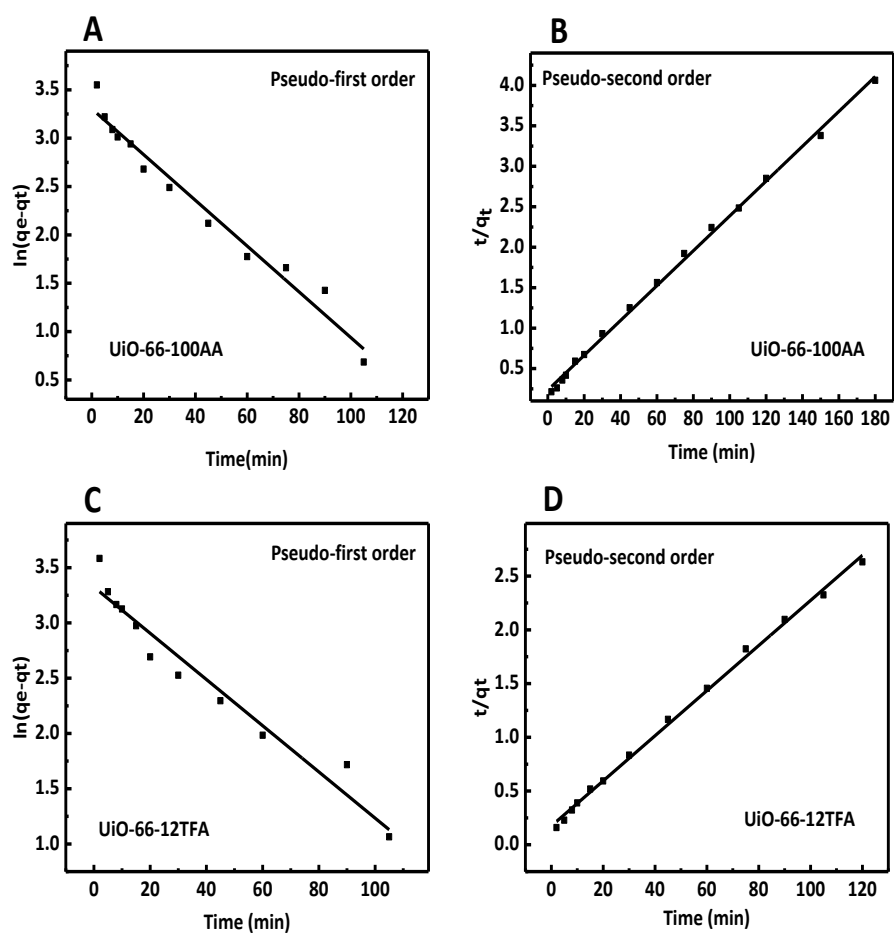
Figure A.8. (A) Pseudo-first-order fit for UiO-66-100AA, (B) pseudo-second-order fit for UiO-66-100AA, (C) Pseudo-first-order fit for UiO-66-12TFA, (D) pseudo-second-order fit for UiO-66-12TFA.

Table A.2. Parameters of As (V) Adsorption Kinetics by the MOF samples.

|	Parameter	UiO-66-00	UiO-66-12AA	UiO-66-36AA	UiO-66-100AA	UiO-66-12TFA	UiO-66-36TFA
pseudo-first order	q_e (mg·g^{-1})	23.10	24.366	26.522	27.224	27.78	32.1014
	k_1	0.01931	0.0276	0.0216	0.02366	0.0209	0.017
	R^2	0.944	0.964	0.962	0..9693	0.954	0.988
	q_e (mg·g^{-1})	36.07	35.99	43.04	46.446	47.64	60.20
pseudo-second order	K_2	1.82x10^{-3}	7.37x10^{-3}	1.8x10^{-3}	1.98x10^{-3}	2.52x10^{-3}	0.000151
	R^2	0.996	0.996	0.997	0.998	0.997	0.996
Intraparticle diffusion rate	1st slope	3.016	2.8264	3.508	3.953	3.992	6.4899
	2nd slope	2.75	1.93	2.324	2.6843	2.524	1.478
	3rd slope	0.1179	0.43788	0.158	0.16347	1.188	0.95329
Experimental q_e (mg·g^{-1})		33.3	35.5	40.20	44.29	48.49	58.37
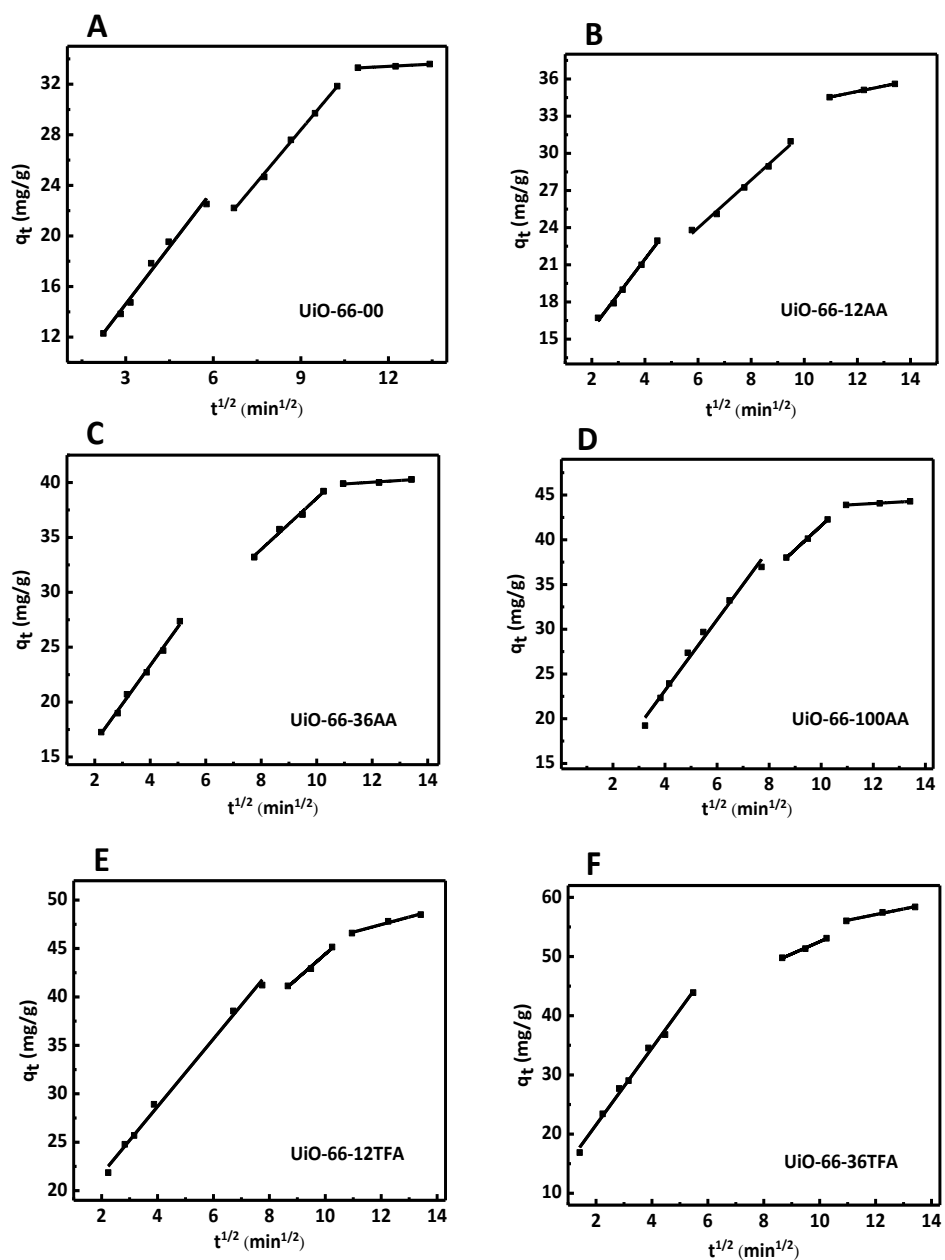
Figure A.9. Intra-particle diffusion models for (A) non-modulated UiO-66, (B) UiO-66-12AA, (C) UiO- 66-36AA, (D) UiO-66-100AA, (E) UiO-66-12TFA, (F) UiO-66-36TFA.
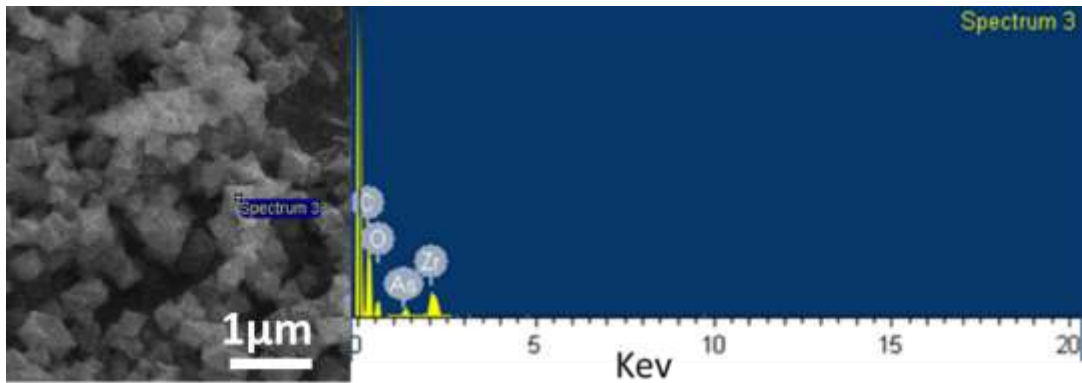
Figure A.10. SEM-EDX of UiO-66-36TFA after adsorption showing the presence of As on the surface of the MOF crystals
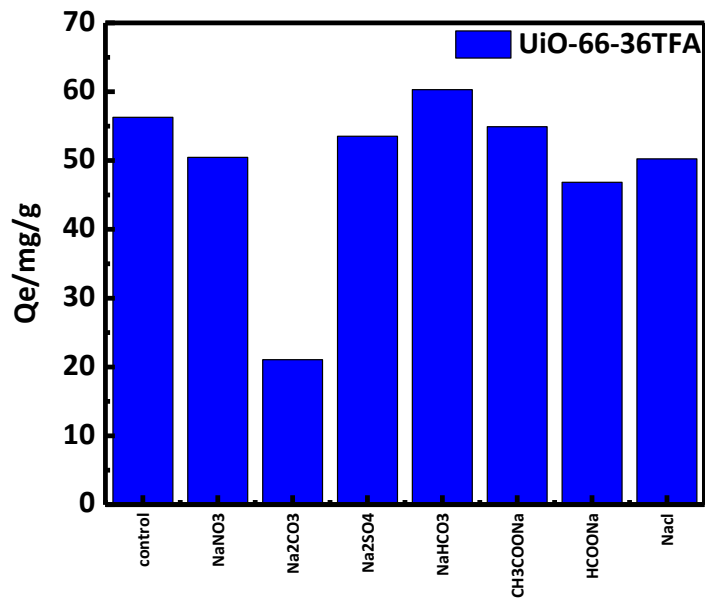

Figure A.11. Adsorption of arsenate by UiO-66-36TFA in the presence of anions. The control experiment was performed in the absence of anions.